THESIS FOR THE DEGREE OF DOCTOR OF PHILOSOPHY

Sorption of Cs, Ba, Ra, Co, Am, and Eu onto biotite: experiments and modelling

Pawan Kumar

Department of Chemistry and Chemical Engineering
CHALMERS UNIVERSITY OF TECHNOLOGY
Gothenburg, Sweden 2024

Sorption of Cs, Ba, Ra, Co, Am, and Eu onto biotite: experiments and modelling
PAWAN KUMAR
ISBN 978-91-8103-144-7

Doktorsavhandlingar vid Chalmers tekniska högskola
Ny serie nr 5602
ISSN 0346-718X

Department of Chemistry and Chemical Engineering
Chalmers University of Technology
SE-412 96 Gothenburg
Sweden
Telephone + 46 (0)31-772 1000

Cover:
Batch sorption experiment with biotite at three different ionic strengths (0.001M, 0.01M, and 0.1M), five pH values (5-9), and three temperatures (25, 40, and 60 ºC)

Chalmers Digitaltryck
Gothenburg, Sweden 2024

Sorption of Cs, Ba, Ra, Co, Am, and Eu onto biotite: A combined experimental and modelling study

Pawan Kumar
Department of Chemistry and Chemical Engineering
CHALMERS UNIVERSITY OF TECHNOLOGY
Gothenburg, Sweden 2024

Abstract

A solution to the problem of the highly radioactive waste that is generated by nuclear power is the construction of a final repository. In the Swedish concept for such a repository, the waste is protected by a multi-barrier system, which includes the granitic bedrock as the final barrier. In a worst-case scenario, where the initial barrier system fails, the waste can meet groundwater, and radionuclides may then start to migrate into the pore-system of the bedrock. Migration is highly dependent on the sorption of radionuclides on the minerals that constitutes granitic rock and radionuclide transport models depend on distribution coefficients, R_d (m^3/kg) values for each specific radionuclide. However, the values are conditional and cannot easily be predicted if the environmental conditions change.

In this investigation, the aim is to collect data for a predictive R_d model, based on surface complexation modelling of the sorption capacity of the mineral biotite, considered to have a high sorption capacity. A first series of batch sorption experiments were performed with a mixture of ^{134}Cs, ^{133}Ba, ^{60}Co and ^{152}Eu at tracer concentrations of approximately ~10^{-8} M, with three different ionic strengths of $NaClO_4$, three temperatures, and five different pH values under inert gas conditions ($[O_2]$ <1 ppm) for a duration of up to two months. The results show that the sorption of all four radionuclides was highly dependent on duration of experiment, pH, ionic strength, and temperature. A second series of batch sorption experiments was conducted using ^{226}Ra and ^{241}Am. Strong effects of the ionic strength and pH on the sorption of these two radionuclides were found. The titration experiment was performed with biotite suspensions to determine the pK_a values of the biotite mineral. Both sorption and titration data were modelled with a custom-made program package consisting of the PHREEQC geochemical modelling software and PYTHON shell with an error minimization routine. The sorption data for all metals was successfully modelled by considering one (2-pK_a) surface complexation site, presumably edge sites on the mineral, in combination with one ion-exchange site presumably on mineral basal plane. The optimized stability constants of Cs, Ba, Co, and Eu were used to evaluate the enthalpy (ΔH) and entropy (ΔS) of the sorption reactions from van't Hoff linear plots. For all the surface complexation species, the favorable entropy term was predominant over the unfavorable enthalpy term. On the other hand, for ion-exchange species, enthalpy was found to be favorable and predominant over an unfavorable entropy term.

Keywords: radionuclide sorption, biotite, surface complexation modelling, elevated temperature, enthalpy, and entropy

List of publications and manuscripts

This thesis is based on the following publication and manuscript.

Paper 1
S. Holgersson and P. Kumar, "A literature review on thermodynamic sorption models of radionuclides with some selected granitic mineral." Frontiers in Nuclear Engineering, **2**, 1222170 (2023).

Paper 2
P, Kumar, S. Holgersson, and C. Ekberg, "Cs, Ba, Co, and Eu sorption on biotite at pH 5-9 and varying ionic strength." (Submitted to Radiochimica Acta, under review)

Paper 3
P, Kumar, S. Holgersson, and C. Ekberg, "The influence of pH, ionic strength and temperature on Cs, Ba, Co, and Eu sorption on biotite: combined experimental and modelling study (Submitted to Journal of Contaminant Hydrology, under review)

Paper 4
P, Kumar, S. Holgersson, and C. Ekberg, "Ra and Am sorption on biotite at pH 5-9 and at varying ionic strength"(to be submitted to Journal of Radioanalytical and Nuclear Chemistry)

Abbreviations

ASD	Acidic Site Density
BET	Brunauer -Emmett-Teller; gas adsorption isotherm
BSM	Basic Stern Model
CA	Component Additive
CCM	Constant Capacitance Model
CD-MUSIC	Charge-Distribution Multi-Site Surface Complexation Model
CEC	Cation Exchange Capacity
DLM	Diffuse Layer Model or Double Layer Model
DFT	Density Functional Theory
EDL	Electric Double Layer
HTO	Tritium Water
OHP	Outer Helmholtz Plane
NEM	Non-Electrostatic Model
SCM	Surface Complexation Model
SSA	Specific Surface Area
TLM	Triple Layer Model
TSM	Thermodynamic Sorption Model
k	Surface Complexation Constant
k_{ex}	Selectivity Co-efficient
$pK_{a1,2}$	Acidity Constants

Table of Contents

1. Introduction

The current increasing electricity demand across the world (Fig. 1-1) has led to the continuous use of fossil fuels, resulting in a considerable rise in greenhouse gas emissions. These emissions contribute to climate change and global warming and presumably pose a serious threat to the environmental, economic and socio-political conditions of today. Therefore, it is crucial to reduce these harmful emissions to mitigate the severe effects of global warming [1]. One way of achieving this is by adopting more environmentally friendly sources of electricity production, such as wind, solar, biomass, and geothermal energy. These alternatives can potentially replace fossil fuels. However, it is important to note that these sources alone are insufficient in their capacity to fully meet the global electricity demand [2]. Hence, it is essential to also incorporate nuclear power to ensure a continuous and reliable energy supply.

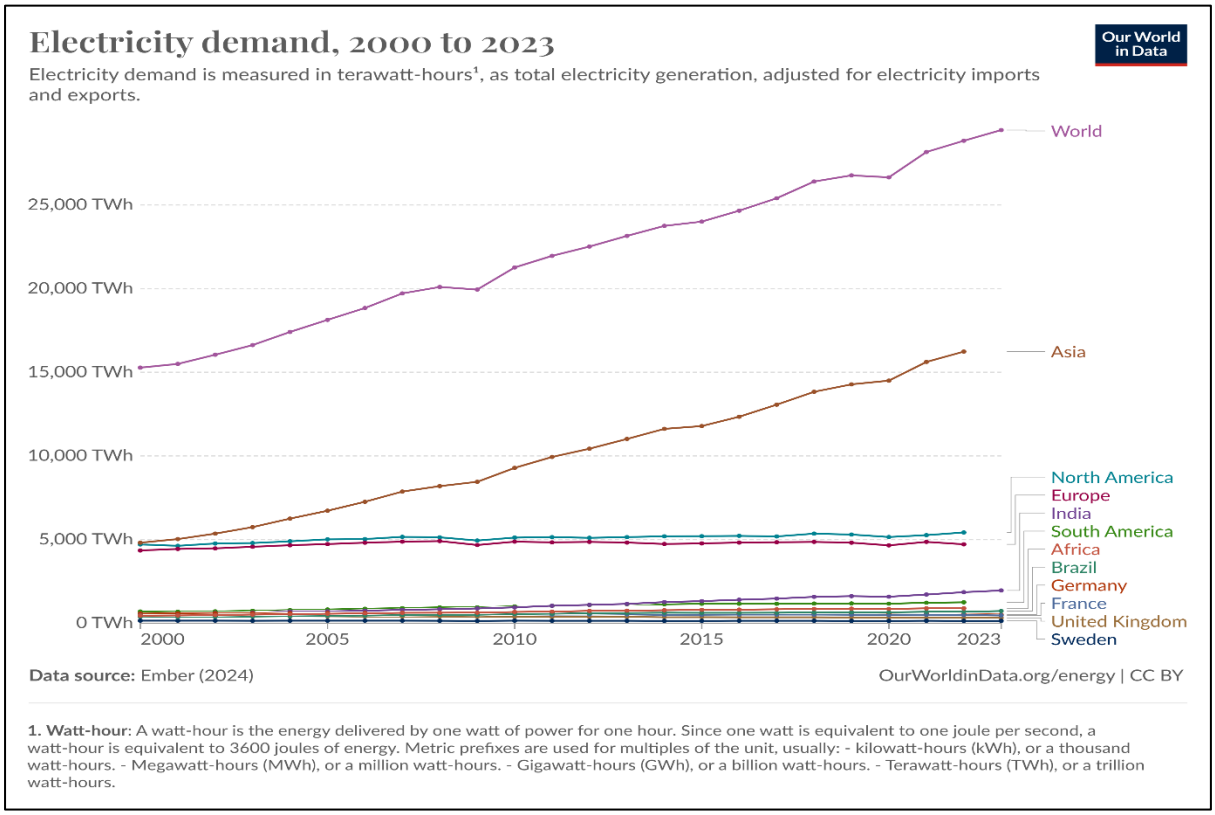

Fig. 1-1: The global electricity demand 2000-2023 [2]

Nuclear power plants (NPPs) have a global track record of nearly seven decades of operation, demonstrating their reliability as a carbon-free source of electricity. Despite the occurrence of some few severe accidents (i.e. Chernobyl in 1986 and Fukushima in 2011) during this period of operation, with the release of considerable amounts of radioactivity (mostly volatile I and Cs isotopes) to the environment, the overall environmental benefits that the low carbon emissions from nuclear power offers are immense compared with fossil fuel, both on local (soot particle emissions) and global (CO_2 emissions) scales. Numerous other advantages can be accounted for, including a cost-effective electricity production for the entire NPP lifespan, the ability to replace several coal plants with the installation of a single NPP, less land demand

than wind and solar facilities, and so on. On the other hand, obvious disadvantages of nuclear energy include a high initial capital cost investment, a necessity of rigorous adherence to operational safety protocols and the generation of highly radioactive waste.

The benefits of nuclear energy have been recognized worldwide, leading to a surge in interest in building more nuclear power plants to address the ever-increasing demand for electricity. Currently, 440 nuclear reactors operate across 33 countries, contributing to over 10% of the world's electricity supply, with approximately 60 additional reactors under construction, particularly in India, China, and the United Arab Emirates [3].

Sweden initiated its nuclear power journey in 1954 with the establishment of its first experimental nuclear reactor, R1, followed by the launch of a nuclear power program in 1956 for reactor-generated heat production. By 1980, the country had twelve commercially operational nuclear reactors and, together with hydro power, a CO_2 emission-free electricity production. However, due to short-sighted political issues, which led to the closure of half of these reactors [4] Sweden now operates three NPPs with six nuclear reactors, generating 30% of the nation's electricity. These reactors are scheduled to remain operational until 2040 [5].

When it comes to nuclear energy, the primary concern, both historically and at present, is the issue of radioactive waste. It is estimated that by the end of 2040, the existing nuclear facilities in Sweden will have produced approximately 12,000 tons of spent nuclear fuel [4]. The spent nuclear fuel is classified as long-lived radioactive high-level waste (HLW) and needs to be stored safely for an extended period, mainly due its content of long-lived actinide and trans-actinide radioisotopes with potential harmfulness to all forms of life [6] Therefore, this waste requires a special isolation technique, which makes the waste inaccessible to humans and the environment for a long time [7].

To address this issue, the Swedish Nuclear Fuel and Waste Management Company (SKB) has undertaken one of Sweden’s most significant environmental safety initiatives. Over the past four decades, SKB has sponsored and conducted a substantial research program to develop the so-called KBS-3 method for the final spent nuclear fuel repository. This method, or rather a concept, devises spent nuclear fuel to be encapsulated in sealed and corrosion-resistant copper canisters with steel inserts for mechanical reinforcement [8] [9] [10]. These canisters will then be placed in a tectonically stable zone of a granitic rock formation at depths ranging from 400 to 500 m. The canisters will be surrounded by bentonite clay to minimize the mobility of groundwater in the close vicinity of the canisters. Subsequently, the rock cavities will be backfilled and sealed. The entire disposal concept is shown in Fig. 1-2.

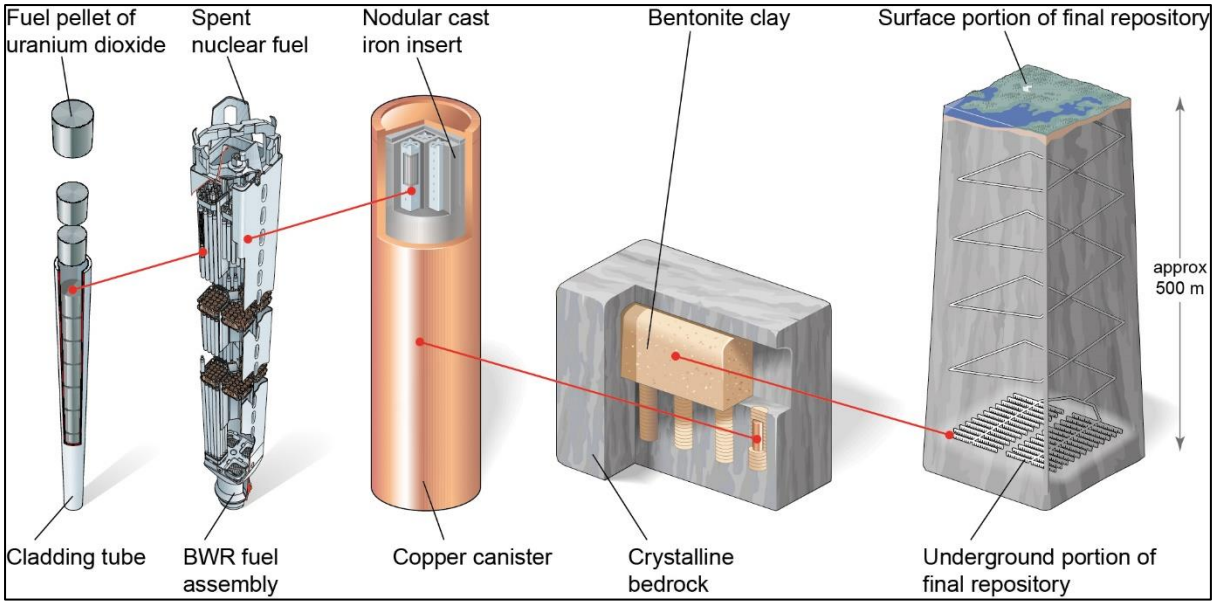

Figure 1-2: The KBS-3 method for disposal of spent nuclear fuel (Courtesy of SKB, Illustrator Mats Jerndahl)

The final repository for the Swedish spent nuclear fuel is planned to be located in the Forsmark area, not far from the NPP site in the municipality of Östhammar, about 150 km north of Stockholm. The repository is intended to store spent nuclear fuel for up to 10^5 years [7]. In Finland, the construction of a similar site by the POSIVA company has already begun.

In the event of a breach in a copper canister, which can result from several factors including unintentional damage during emplacement, creep due to unequal swelling of bentonite, or corrosion around cracks and welds, the spent nuclear fuel will be exposed to groundwater. This exposure can lead to the dissolution of radioisotopes in the spent fuel, thereby mobilizing them. However, the bentonite clay that covers the copper canister and fills the gap between the canister and the granite rock will act as a barrier to radioisotope migration, limiting the transport to diffusion only. The bentonite clay plays a crucial role for delaying the migration of radioactive materials from a defect canister to the surrounding granite rock.

However, due to the very long-time scales that are involved, the bentonite clay will subsequently be saturated to its maximum sorption capacity and migration will proceed into the host rock. Thus, the rock will serve as the final barrier to prevent radionuclide migration from reaching the biosphere. Therefore, understanding the characteristics of the granitic rock is very important for determining the overall safety of the repository.

In the context of typical Swedish bedrock conditions, the granitic bedrock at the Forsmark location is characterized by an exceptionally low occurrence of fractures, resulting in a notably diminished hydraulic conductivity.

The rock in Forsmark is a granodiorite, an igneous rock type closely related to granite, the main difference is a larger proportion of Ca-rich instead of Na-rich plagioclase minerals. The Forsmark rock is primarily composed of various feldspar minerals, particularly plagioclase and K-feldspar, alongside trace amounts of mica minerals such as biotite and chlorite [11] [12].

The latter two are considered to play a major part in providing a considerable sorption capacity for radionuclides. In addition, there are secondary minerals like calcite and clays to be found, mainly as fracture-filling materials.

The radionuclide sorption onto granitic rock and its constituent minerals has been extensively studied by both SKB and the Finnish nuclear waste management company POSIVA. The results from these studies are primarily reported as elemental sorption distribution coefficients (R_d-values) [13] [14] which quantifies the amount of element sorbed on a solid phase if the total amount dissolved element is known.

The distribution coefficients can be easily integrated into the transport models. However, they do have some limitations. That is, these distribution coefficients are only valid for a specific chemical condition. This implies that changes in groundwater conditions such as pH or ionic strength can have a major impact on these values. This necessitates adjusting distribution coefficients, which is often done through imprecise interpolation or extrapolation from existing data.

Therefore, to overcome this constraint, it has been suggested to predict the distribution coefficients with the use of Surface Complexation Modelling (SCM). In this methodology all chemical reactions that occur between a surface and the radionuclide are defined, including their reaction constants. By integrating such SCM with a geochemical speciation code like PHREEQC [15], the distribution coefficients can be calculated for any groundwater compositions. This integration enhances the reliability of predictions regarding radionuclide transport, particularly in environments where groundwater chemistry is subject to change over time, for example, during glaciation events with freshwater ingress or rising sea levels, with saline water ingress.

However, the implementation of SCM on complex materials like rock does have certain challenges. Firstly, the pure solid phases, in this case the individual minerals in granodiorite, have to be modelled separately. The individual SCMs are then to be combined to model the rock. This can be accomplished using the Component Additivity (CA) approach [16] [17].

Secondly, there's often a lack of existing studies that utilize SCM to interpret sorption distribution coefficients. Ideally, to have robust modelling, the SCM is based on sorption experiments performed with variations of a wide set of parameters, for example, pH, ionic strength and temperature, but also on the study of several different elements. Unfortunately, such comprehensive experimental studies are rarely found in existing literature.

The goal of this work is to generate a large dataset of distribution co-efficients for a single mineral. This data will then be used to build a SCM for the mineral to interpret and explain the radionuclide sorption behavior.

Moreover, the intention is that this study is the first step toward obtaining the necessary SCM parameters for various granitic minerals. These parameters will ultimately be used to model the radionuclide interaction for complex granitic rock formations.

The mineral choice for this work is biotite, one of the granitic minerals, which has been recognized for its strong sorption capacity for dissolved radioactive cations [18] [19] [20] [21]. Despite numerous investigations of radionuclide sorption onto biotite, only a limited number of researchers have employed SCM to analyse their sorption data and the parameter variations are often limited. One may say that this knowledge gap in understanding sorption on a reaction-mechanistic level extends not only to biotite itself but also to the overall sorption capacity of Forsmark granodiorite [22].

As previously stated, SCM involves assigning specific reactions to a surface of a specific and well-characterized solid phase. Aside from that, to develop a robust sorption model, based on experimental sorption data, a wide range of experimental conditions must be thoroughly investigated [23].

Therefore, this investigation aims to carry out batch sorption experiments with a well-characterized biotite with six different radionuclides, Cs(I), Ba(II), Ra(II), Co(II), Eu(III), and Am(III), at five different pH values (5,6,7,8,9) and three different (0.001, 0.01 and 0.1 M) ionic strengths of $NaClO_4$ at three different temperatures, 25, 40, and, 60ºC.

The results are to be modelled using a combination of surface complexation and ion-exchange reactions, with specific reactions defined and equilibrium constants optimized through a combination of PHREEQC [15] speciation calculations coupled with a parameter optimization routine written in PYTHON programming language. From the evaluated reactions and equilibrium constants at three different temperatures, it was also of interest to evaluate reaction enthalpies and entropies, to evaluate if the assumed surface reactions are distinct in the thermodynamic aspect.

2. Background

This section presents a concise overview of the main issues related to nuclear waste repositories and the mineralogical characteristics of the Forsmark site. It then introduces the biotite mineral, chosen for this investigation, and explains the Surface Complexation modeling (SCM) approach. Subsequently, a rationale is provided for the selection of radionuclides included in the study. The section concludes with a simplified summary of Paper I, which reviews previous SCM studies involving biotite.

2.1. Nuclear waste repository issues and the characteristics of host rock

The planned Swedish final repository for spent nuclear fuel, which uses the KBS-3 concept of fuel encapsulation in copper canisters and a backfill of bentonite clay in a granitic rock formation, have faced several significant technical and strategic challenges. While these challenges are considerable, they have been addressed through continuous research and international collaboration to ensure that the repository fulfils the required long-term safety and sustainability conditions.

One major concern is to manage thermal effects of spent nuclear fuel. The repository is designed to ensure that heat generated by radioactive decay is evenly distributed, preventing any rise in temperature within the nuclear waste repository during the placement of the disposal container [24]. Another issue is to ensure radiation safety during both construction and operation. The Swedish Radiation Safety Authority (SSM) closely monitors every step of the process, from waste encapsulation to long-term storage, to guarantee adherence to strict safety standards. Recently, a key area of debate in the scientific community involves the copper canisters for storing nuclear waste. Numerous studies, conducted by SKB, POSIVA and the corresponding authorities in respective country SSM and STUK, have initiated research in anaerobic copper corrosion where results are not entirely conclusive whether there is a potential for corrosion of copper canisters under the anticipated repository conditions or not [25]. Given that these canisters are expected to last for hundreds of thousands of years, ensuring their long-term durability is a crucial topic of ongoing research [26].

Additionally, the bentonite clay, used as a protective buffer around the copper canisters, is designed to swell when exposed to moisture, forming a tight seal. However, concerns remain about its long-term stability, particularly the risk of erosion from groundwater with very low ionic strength [27], which could weaken its ability to prevent water intrusion into the canisters. Another major challenge is to forecast the geological conditions over the next several hundred thousand years. Even small changes in groundwater chemistry, potentially caused by the intrusion of glacial meltwater or sea water [28] could affect the repository's safety. Since the bedrock serves as the repository’s final barrier this makes it crucial to study and understand the behavior of the surrounding granite rock formation at different conditions, especially the sorption capacity for radionuclides,

The site selected for the Swedish final repository of spent nuclear fuel is in the vicinity of the Forsmark NPP. The site was chosen for its tectonically stable bedrock and low hydraulic conductivity. The proposed repository area (SKB rock domain code RFM029) covers 84% of the site. The bedrock is largely medium-grained metagranite to granodiorite (SKB rock type code 101057), with smaller amounts of fine- to medium-grained granodiorite, granite, and tonalite (10%), amphibolite (3%), and a minor amount of pegmatite (2%) [29].

To analyze the composition of this metamorphic medium-grained metagranite to granodiorite rock, six thin sections were studied using a point-counting technique [12]. The results revealed the presence of various minerals, as illustrated in Table 2-1. Although, biotite has a lower mineral abundance compared to others (Table 2-1) it is known for its high capacity to retain radioactive cations [18] [19] [20] [21], because of this unique property, biotite was chosen as the focus of this study.

Table 2-1: *The amount and the formula of different mineral present in the granite rock**

Mineral	***Percentage***
Quartz	*26-39%*
Biotite	*3-12%*
K-feldspar	*14-29%*
Plagioclase	*27-41%*
Chlorite	*0-0.4%*
Muscovite	*0-1%*
Epidote	*0-1%*
Titanite	*0-1%*
Zircon	*0-0.2%*

* [12]

2.2. Structure of the biotite and its properties

Biotite is a dark, almost black, mica mineral. It is a sheet silicate that follows the Tetrahedral-Octahedral (TOT) plus cation (C) structural pattern that is common for all mica minerals. A schematic view of the structure is shown in fig. 2-1.

The T layers consist of one silicon and four oxygen atoms in a tetrahedral configuration, which can be represented as $Si_2O_5^{2-}$ units, where each Si has three shared ("basal") and one free ("apical") oxygen. In trioctahedral O layered micas, such as biotite, the O layers consist of divalent cations coordinated to six hydroxyl groups in an octahedral configuration, which can be represented as $M_3(OH)_6$, where each hydroxide is shared between three cations, in the O layer there is no "free" oxygen. There is also a variant of dioctahedral O layers which consist of trivalent cations, found in, for example, the muscovite mineral. T and O layers are bound together by replacing one OH group in the O layer with the apical O in the T layer. For bonding together one TOT layer, one can formally write:

$$2Si_2O_5^{2-} + M_3OH_6 \quad \Leftrightarrow \quad M_3Si_4O_{10}(OH)_2 + 4(OH)^- \qquad \text{(R2-1)}$$

Within the T layer, aluminum ions (Al^{3+}), or less commonly iron (Fe^{3+}) can partially replace the silicon ions (Si^{4+}). This substitution creates a negative electrical charge on the TOT layer which is balanced by the additional interlayer cation (C), typically by a potassium ion (K^+). A very rigid structure is formed due to the presence of non-hydrated K^+ ions between the two negatively charged TOT layers, which are bound together by electrostatic forces of attraction. The repetition of the TOT+C structure forms the biotite mineral, with a thickness ranging from 9.5 to 10Å [30].

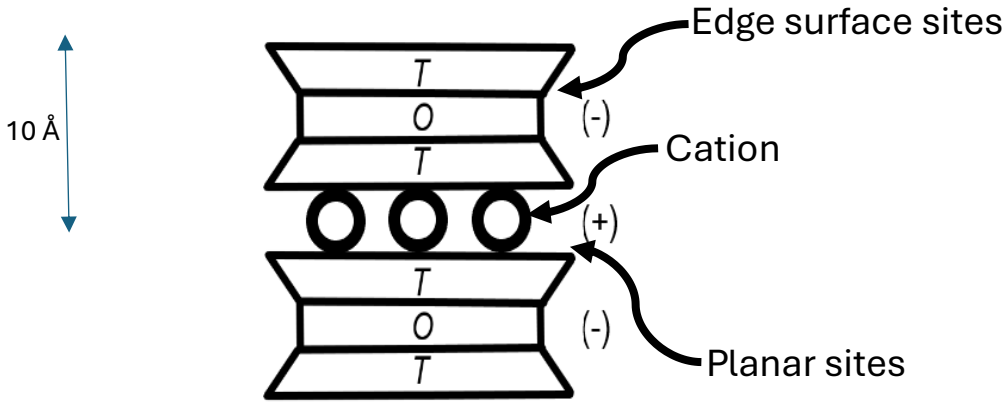

Figure 2-1: Schematic of biotite structure

On the surface of the biotite there are different sorption sites available, either edge sites of the type ≡SOH where S represents Si or Al, or basal plane "crevices" in the tetrahedral pattern. It can be assumed that cationic elements sorbs either by forming inner sphere complex or outer sphere complex with the former type of sites, or by engaging basal plane sites by a cation exchange mechanism [18] [31]. The interlayer K^+ cations are probably not accessible for ion exchange, unless the biotite is degraded, instead it is primarily the non-bound basal surfaces that engage in ion exchange.

In the literature study on dissolution and precipitation kinetics of sheet silicates [32], it was mentioned that the cation sorption onto the edge sites of the sheet silicate mainly occur due to the availability of two hydrated surface functional groups: aluminol (Al-O-H) and silanol (Si-O-H), which can become protonated according to the reactions (R2-2 to 4):

$$\equiv AlOH + H^+ \rightleftharpoons \equiv AlOH_2^+ \quad \text{(R2-2)}$$

$$\equiv AlO^- + H^+ \rightleftharpoons \equiv AlOH \quad \text{(R2-3)}$$

$$\equiv SiO^- + H^+ \rightleftharpoons \equiv SiOH \quad \text{(R3-4)}$$

Thus, the biotite edges can be characterized by having at least three surface acidity constants or pK_a values: two from the aluminol sites and one additional pK_a for the silanol sites.

Cations typically bind to these acidic/amphoteric sites through a so-called surface complexation mechanism. This mechanism can be categorized into two types. The first type involves the formation of a surface complex as an outer-sphere complex, where the hydration

shell remains intact. The second type involves the formation of a surface complex as an inner-sphere complex, where the hydration shell is displaced, and a chemical bond is formed between structural oxygen and cation.

The cavities on a basal plane, also known as ditrigonal siloxane cavities, are typically considered hydrophobic unless a negative charge develops due to isomorphic substitution of ions in the tetrahedral sheet. This charge is neutralized by cation sorption by an ion-exchange mechanism. This mechanism involves the replacement of one cation with another or by replacing several monovalent cations with a multivalent cation, if this can be considered as a viable exchange mechanism. The cation binding at this site, whether or not it retains its hydration shell, is purely electrostatic and depends on how well the cation fits into the surface cavity [33].

In the literature review on thermodynamic sorption models of radionuclides with selected granitic minerals [34], it was observed that the sorption of metals onto biotite often was modeled by considering at least one ion-exchange site and one surface complexation site. The latter was usually modeled using either by 1-pK_a (acidic) or 2-pK_a (amphoteric) edge sites. The location of the exchange sites, on the other hand, was not consistent, sometimes they were assumed to be edge sites, sometimes basal plane sites.

In some work a similar model has been implemented in a slightly more complex manner. In their approach, two different edge-type sites, "strong" and "weak," are considered [35]. The strong surface complexation sites are assumed to bind cations with a chemical bond, while the weak sites bind cations with their hydration shell intact, forming an electrostatic bond. Additionally, some studies also consider one extra ion exchange sites on the edges, commonly referred to in the literature as Frayed Edge Sites (FES). The latter is, however, thought to be formed only after a degradation of the biotite, where the interlayer edges are depleted of K^+ and replaced with other cations [36]. Contrary to K^+, the other cations are bound in a hydrated form, and this causes an expansion of the interlayer, also known as “flaring” or “fraying”. It is thought that this mechanism promotes further degradation of the biotite. In models, the FES have been shown to have very low capacity (few sites), albeit the binding can be strong, and it probably requires an initial proton attack on the edge groups to create FES. For pristine biotite at neutral conditions the FES can be assumed to be very few.

To conclude, according to literature, there are at least two mechanisms for sorption onto biotite: 1) surface complexation, presumably only with the edge sites, and 2) ion exchange, alternatively or simultaneously, with basal plane cavities and edge sites. To make matters more complex, both mechanisms seem to be able to engage in inner-sphere (ionic or covalent bond without hydration shell) and, also in outer-sphere (physical/electrostatic bond with hydration shell) binding types.

2.3. The selection of radionuclides in the batch sorption experiments

Approximately 49 “major” radionuclides have been identified in spent nuclear fuel [37]. From these, a shortlist of thirteen has been selected (Table 2-2) as particularly relevant for dose calculations, based on their high radiotoxicity and long-term risks [38]. according to the Swedish safety case evaluation. Consequently, the evaluation of the transport properties of these elements are crucial for the geological repository's safety assessment [39] [40].

In addition, long-lived daughter radionuclides have been included in Table 2-2 since they are part of the decay chains.

Table 2-2: *The list of radionuclides in spent fuel of particular interest for biosphere dose calculations* [38] *Additional daughters from these are marked with asterisk(*).*

Radionuclide	Comment
Am-241	In Np chain
C-14	Activation product
Cl-36	Activation product
Cs-137	Fission product
I-129	Fission product
Nb-94	Fission product
Pu-238	In U chain
Np-237*	In Np chain
Pa-231*	In Ac chain
Pu-239	In Ac chain
Pu-240	In Th chain
Pu-241	In Np chain
Ra-226*	In U chain
Sr-90	Fission product
Th-229*	In Np chain
Th-230*	In U chain
Th-232	In Th chain
U-234	In U chain
U-236*	In Th chain
U-238	In U chain

Six elements ^{134}Cs, ^{133}Ba, ^{60}Co, ^{226}Ra, ^{241}Am, and ^{152}Eu were selected for study in this work, either as primary (Cs, Ra, Am) or analogous (Ba, Co, and Eu) elements. Ba, an alkaline earth metal, shares similar properties with both Sr and Ra, due to their comparable outer electronic shells (s^2). Although Co is not part of spent nuclear fuel, it is included in this study because Ni is an activation product of steel and the elements can be seen as analogous to each other, due to their similar electronic configurations: [Ar]$3d^7s^2$ for Co and [Ar]$3d^8s^2$ for Ni. Long-lived Ni isotopes are found in a long-lived intermediate-level waste, which also raises concerns about

long-term radiotoxicity risks. Eu, finally, is mainly an analogue element for Am, since they have similar outer electronic structures ([Xe]$4f^7s^2$ vs [Rn]$5f^7s^2$).

All the six radionuclides that were selected for this study, ^{134}Cs, ^{133}Ba, ^{60}Co, ^{226}Ra, ^{241}Am, and ^{152}Eu have strong gamma-energy lines and are easily detected and can be quantified also in mixtures. Furthermore, all elements are redox insensitive and hence exist as defined redox states Cs(I), Ba (II), Ra(II), Co (II), Am (III) and Eu (III) under the repository conditions [13]. It was also of interest to include some assumed-to-be analogue elements to evaluate if these assumptions are actually valid for sorption onto biotite.

2.4. TSM of selected radionuclide on biotite: a literature review

2.4.1. Alkali metals

Only data for Cs was found in the literature. In case of alkaline and alkaline earth metals, it was observed that the sorption isotherm was the most commonly applied method for studying the sorption onto the biotite mineral [41] [42] [43] [21, 44]. However, these studies did not examine the effect of ionic strength on Cs sorption. Only in one study [42] the impact of electrolytic cations was studied.

The results indicate that Cs sorption is highly dependent on its concentration in the background electrolytic solution, suggesting that various sorption sites on the biotite surface are filled sequentially. To model sorption isotherm data, several researchers [44] [21] [42] used a surface complexation model (SCM) similar to the one applied to the clay mineral illite [45], which considers three different ion-exchange sites: basal plane, edge and frayed-edge sites (FES) on the biotite surface. The respective dominance of these sites depends on the range of cesium concentrations where the basal plane sites have the highest capacity (most abundant) but show weakest interaction. FES, on the other hand, have very low capacity, probably due to a low degradation state of the biotite used, but very high affinity for cations.

One study [41] used a single-site Langmuir isotherm. Based on the observed slow uptake time of Cs, the authors suggest that Cs sorption is due to the formation of both "strong" (chemical bond) and "weak" (electrostatic bond) surface complexes, which is probably not the cause of the delayed equilibrium, since the time for establishing equilibrium primarily depends on in-diffusion into the mineral porosity, and not on the presence of multi-sites.

In another work by [43], the Freundlich isotherm was fitted to the data. The Freundlich is an empirical isotherm, hence no surface reaction was assigned, but this isotherm should indicate the presence of at least two sites, contrary to the Langmuir isotherm which assumes one single site.

2.4.2. Alkaline earth metals

Biotite sorption data was found for the alkaline earths Ba, Ca and Sr. Ba sorption data for biotite is like Cs in so far that the sorption isotherm was the most common experimental method [46] [31]. However, only one study [31] examined the effect of background electrolyte concentration, and another [46] compared two different synthetic groundwater with different salinity. Also, like Cs, Ba sorption was found to be highly dependent on its concentration. Additionally, an increase in ionic strength or salinity significantly decreases Ba sorption, likely due to the increased competition for cation exchange sites. Typically, Ba sorption data was modelled using a similar approach as for Cs, based on a model for the illite mineral [45], with three different cation exchange sites: basal, edge and FES, with gradually decreasing uptake capacity. This model was also used for the single work that used Ca [31]. For Sr, the same three-site cation exchange model was used by [31].

To conclude, the models employed for Cs, Ca, Ba and Sr are similar for all metals, but the models themselves are different. In some case multi-site cation exchange is assumed, in some case single site surface complexation, although no pK_a values were assigned to the site. No studies were found that had systematically investigated the effects of pH, ionic strength, or temperature on the sorption.

2.4.3. Transition metals with oxidation state II

The only metal of this category studied is Ni and data was found in one work [47]. On the other hand, both pH and ionic strength were systematically varied while maintaining a fixed tracer concentration. The finding indicate that Ni(II) sorption is minimally affected by increased ionic strength. Instead, a clear sorption "edge" (the sorption increases steeply) for Ni was observed with pH variation (3-9.5), occurring around pH 7. A 1-pK_a (at 5.8) non-electrostatic surface complexation model in combination with one cation-exchange site was used, which adequately explained the Ni(II) sorption data. A residual sorption capacity in acidic range was assigned to cation exchange. In this pH range there was a small effect on Ni sorption, where 0.5M ionic strength ($NaClO_4$) seemed to suppress sorption when compared with 0.05M.

This suggests that Ni sorption is primarily controlled by surface complexation, with a small contribution from ion exchange, especially below the pK_a value of the surface complexation site.

2.4.4. Lanthanides/actinides with oxidation state III

Here, data was found only for lanthanide Eu. Two studies [20] [47] have examined Eu(III) sorption onto biotite both had systematic variations in pH and ionic strength at fixed tracer concentration, the latter stated as $9 \cdot 10^{-8}$M [47] and 10^{-5}M [20], The latter value is a high metal concentration if one would like to avoid hydroxide precipitation. The solubility of

$Eu(OH)_3(am)$ have been calculated to be below 10^{-5} M for pH<8 [48], however, in the study the pH range was not above pH 6 [20].

In both cases, the sorption outcomes showed that at a pH around neutral there is a sharp increase in Eu sorption, indicating the presence of at least one amphoteric/acidic surface site on the biotite surface. Interestingly, the position of the "edge" was widely different between the two studies: at pH 7 by [47] and pH 3 by [20]. This may indicate the presence of two surface complexation sites, then de-protonating at two different pK_a values.

In one study [47], the sorption data was modeled using a non-electrostatic model (NEM) that included one ion exchange site and a 1-pK_a surface complexation site, similar with the one used for Ni sorption. On the other hand, in the other study [20], a cation exchange model was selected instead, presumably due to that Eu sorption was found to be highly affected by change of ionic strength; 0.01, 0.1 and 1 M NaCl progressively suppressed Eu sorption to lower values, as measured above the sorption edge.

3. Theory

A basic description of the theoretical background of the investigated system is provided in this section. This comprises a brief summary of the sorption processes that are taking place on the mineral surface, the available surface complexation models, the batch sorption experiment and the various experimental techniques that are used to characterize biotite mineral.

3.1. Sorption on minerals and thermodynamic sorption models (TSM)

To gain a thorough understanding of the underlying reactions that occur at the solid-liquid interface, thermodynamic sorption models (TSMs), also known as surface complexation models (SCMs), are implemented. Strictly speaking, surface complexation is one specific mechanism for binding to the surface, so TSM is the more general term if one would like to include other sorption mechanisms, like ion-exchange, for example.

TSMs are powerful tools for enhancing our understanding of contaminant mobilization and its retention in the geological media (such as rocks, gravel, sand, and soils) in the environment. These models have been applied in various areas, including the evaluation of safety scenarios for nuclear waste repositories.

TSM involves the assumption of specific reactions between a surface and dissolved species in solution, which mostly results in the transfer of species from the aqueous to the solid phase. Usually, the transfer is considered reversible, that is, the species are adsorbed and not absorbed by the solid phase. The specific reactions assumed to take place depends on the solid characteristics, usually the capacity or number sorption sites per mass or per surface area and the type of surface functional groups present on the surface that constitutes these sites, and the species present in aqueous solution. This means that surface reactions can be coupled with solution reactions and that a speciation calculation for the whole system can be performed.

TSM is therefore usually performed as a reversed speciation calculation, the R_d values are known but the reaction constants are initially unknown. This requires an optimization routine, which minimizes the error sum of experimental and calculated R_d values, where the reaction constants are optimization parameters. The constants for these reactions are usually re-calculated for zero ionic strength.

There is a choice to include electrostatic effects in TSM which also considers the activity of surface species. This can be seen as analogous to the activity for solution species. Numerous TSMs, such as the Constant Capacitance Model (CCM), the Stern Model (also known as the Double Layer Model (DLM), the Triple Layer Model (TLM), and the Charge-Distribution Multi-Site Complexation Model (CD_MUSIC), have been thoroughly reviewed in a number of studies, including those by Davis et. Al., [49], Hayes et al., [50] and Koopal et. al. [51]. All these models take surface electrostatic accumulation effects into consideration. The Non-Electrostatic Model (NEM), in contrast, does not take these effects into account.

In general, the application of TSM is based on three assumptions:

1) Sorption can be formalized with mass balances and equilibrium constants of specific sorption reactions.

2) An inclusion of the electrostatic correction factor, also known as the coulombic effect, can be made to account for the influence of the electrostatic effect on the sorption reaction from ions attracted to the surface.

3) The amount of available sorption sites on the mineral surface are limited in number and this number can be quantified.

Of these, the assumption number 2 is not required for a Non-Electrostatic Model (NEM), which will be described next.

3.1.1. A basic TSM: the non-electrostatic model (NEM)

Ion sorption at the solid-liquid interface can occur through three distinct mechanisms [52] as listed below:

1) Inner Sphere Complexes: This involves the binding of ions to acidic or amphoteric surface sites through relatively short-range chemical bonds. These bonds can be either of the electron sharing (covalent) or electron-acceptor/donator (ionic) type.

2) Outer Sphere Complexes: Here, ions bind to acidic or amphoteric surface sites while retaining their hydration shell, which can be described as a formation of a longer-range electrostatic ("physical") bond.

3) Ion-Exchange Reactions: These reactions occur by an ion exchange mechanism that maintains site neutrality. It has been suggested that this mechanism involves not only an electrostatic binding on the surface but is also an ion solvation effect (a ion-dipole interaction) in solution. The latter effect means that "hydrophilic" ions prefer to stay in the aqueous phase, while the less hydrophilic ions are pushed to the solid-water interface. Also, the size of the ion can be of importance, since some elements fit better to the local structure of a specific exchange site than others and for this purpose, the hydration shell of the ion on an exchange site can be kept intact or be shed.

An example of the importance of size is the K^+ found in the interlayers of the biotite TOT structure, this cation is bound without any hydration shell. However, the exchange site can also bind hydrated ions, which then causes interlayer expansion, and ultimately, biotite degradation.

All these reactions can be described by the use of specific reaction constants and mass balances. However, in electrostatic models, there is an additional non-specific sorption of electrolyte ions

on the mineral surface, which is accounted for by including a diffuse layer model (see next section). In NEM, this type of non-specific attachment is not accounted for.

Consider a system where a solid with surface site, ≡S, is immersed in a liquid containing dissolved component A. The surface reaction between A and ≡S can be expressed as follows:

$$\equiv S + A \rightleftharpoons \equiv SA \qquad \text{(R3-1)}$$

For this reaction, the equilibrium constant, K, can be expressed as follows:

$$K = \frac{[\equiv SA]}{[A]\cdot[\equiv S]} \qquad \text{(Eq.1)}$$

Given that there is a finite number of surface groups $[\equiv S]_{tot}$. The Langmuir isotherm can be obtained by combining the mass balance for *S* with Eq. 1:

$$K = \frac{[\equiv SA]}{[A]\cdot([\equiv S]_{tot} - [\equiv SA])} \qquad \text{(Eq.2)}$$

The two constants K and the concentration of $[\equiv S]_{tot}$ define the isotherm and it is is one of the most basic type of TSM.

If one assumes that $[\equiv S]_{tot} >> [\equiv SA]$, signifying conditions far from saturation, the Eq. 2 can be written as :

$$K \cdot [\equiv S]_{tot} = \frac{[\equiv SA]}{[A]} \equiv K_d \qquad \text{(Eq.3)}$$

This is the linear sorption isotherm, defined by only one parameter, the distribution constant, K_d.

However, from an experimental point of view, what is commonly determined, particularly when A is a radioactive substance, is the distribution of all species that includes A at once, that is:

$$\frac{[A]_{sorbed}}{[A]_{aq}} = \frac{[\equiv SA]+[\equiv SAX]+[\equiv SAY]+\cdots.}{[A]+[AX]+[AY]+\cdots..} \equiv R_d \qquad \text{(Eq.4)}$$

The R_d -values, also known as the distribution coefficients, are usually determined from batch sorption experiments. In literature it is common that R_d is confused with the distribution constant, K_d.

However, unlike R_d, the K_d - values can rarely be measured directly and have to be calculated by fitting a basic Langmuir or linear isotherm model to the available experimental sorption data, which is obtained in terms of the distribution coefficient at different conditions, usually by varying pH, ionic strength or adsorbing element concentration.

The latter approach, where the initial concentration of the sorbing substance is varied, is called sorption isotherm measurements. This approach can be a method for determination of the number of sites involved in ion sorption, as each site is typically saturated at different $[A]_{tot}$ due to varying site densities. If the isotherm is used in linear form, this leads to lines with different slopes at different concentrations.

As described above in section 2.2, the silicate minerals typically have two surface groups: silanol and aluminol groups. Each of these have an ability to protonate and deprotonate, as shown in Reactions R2-2 to 4. Since protons compete with other cations for the sites, this implies that the R_d values are highly dependent on the pH of the solution. A typical "sorption edge" behavior, where R_d values significantly increase or decrease within a narrow pH range, is a clear indication of de-protonation reaction at a specific pK_a value of the surface site.

It must also be mentioned that the concentration of sorbed A, $[A]_{sorbed}$ in (Eq.4) is, unlike the concentration of A in solution $[A]_{aq}$, usually not directly measurable. Instead, it has to be calculated from the mass balance from a reference value of added A to the system, that is $[A]_{tot}$, and the measured value of $[A]_{aq}$:

$$[A]_{sorbed} = [A]_{tot} - [A]_{aq} \quad \text{(Eq.5)}$$

To model distribution coefficients with the NEM, it is essential to characterize the mineral to obtain specific surface characteristics, namely the pK_a values of the surface sites and the total site "densities" (sites/m^2). Both these characteristics can be determined by various experimental or theoretical methods. They can also be treated as fitting parameters, but this is usually not recommended since they tend to compensate for bad model assumptions and then are seldom constant.

The tritium exchange method [53] can be used to determine the total acidic site density (ASD). Titrations with electrodes on solid-phase suspensions are commonly used to evaluate the pK_a values for acidic surface sites from the titration curve. In addition, an ASD value can also be obtained in a titration as a fitting parameter. The cation exchange capacity (CEC) of the mineral is usually measured with the NH_4-acetate method [54].

The specific surface area (SSA) of the solid phase, measured in m^2/g, is typically determined with the BET gas adsorption method [55]. A value of SSA is not necessary to have if one works with only one size fraction of the same mineral specimen. However, for comparison of results between different size fractions and/or mineral specimen the SSA is a crucial normalization factor, since sorption capacity is related primarily to the surface area of the solid sample and not to its mass.

Examples of theoretical models that have been used for solid phase characteristics are the CD-MUSIC model, first presented by Hiemstra et al. [56] in 1989. It involves the use of spectroscopic or crystallographic data to explain pHpzc (point of zero charge), acidity constants, surface functional groups, and surface chemistry of minerals. Another theoretical

approach is based on the Density Functional Theory (DFT), which is a simplified approach of quantum calculations of the optimal geometry for minimizing the energy of a given system.

3.1.2. TSM with the electrostatic effect

The NEM is the foundation also for electrostatic models, with features added for the consideration of the build-up of surface charge and the associated effects on the subsequent sorption of ions with the same charge. This surface charge can therefore be viewed as the cause of non-ideal effects which requires an introduction of an activity coefficient for surface sites/species.

In solution thermodynamics, the activity coefficient is the correction factor to the concentration, which is used to compensate for interaction of charges between the dissolved species and bulk electrolyte solution in a non-ideal solution. Thus, the activity coefficient reduces the effective concentration, which is known as the activity, compared with the concentration as determined from the mass balance. In case of the ideal conditions, in this case a dilute solution, the activity coefficient is equal to one. The activity coefficients decrease with increasing ionic strength and charge of the involved species.

The activity coefficient y_i for a dissolved species i with charge z_i can be calculated with different models, one commonly used model for low to intermediate ionic strength (I<0.5M) is the Davies model:

$$\log y_i = -0.5 \cdot (z_i)^2 \left(\frac{\sqrt{I}}{1+\sqrt{I}} - 0.3 \cdot I\right) \qquad \text{(Eq.6)}$$

In the description below of the most common electrostatic models for the solid-solution interface the terminology used in reference [57] is adapted.

The first basic model of electric charge buildup at the solid-solution interface was proposed by Helmholtz in 1853 [58] , who considered the interface to consist of a fixed plane of charge on solid and a fixed plane of opposite charge in liquid. This constitutes the first of examples given here of an Electrical Double Layer (EDL) model, in this case it is characterized by a constant capacitance *C* (C/V) or (F) that may be formulated as a parallel plate capacitator:

$$C = \frac{\varepsilon_0 \cdot \varepsilon \cdot A}{d} = \frac{\sigma \cdot A}{\Psi_0} \qquad \text{(Eq.7)}$$

Here $\varepsilon_0 = 8.85 \cdot 10^{-12}$ $C \cdot V^{-1} \cdot m^{-1}$ is the permittivity of vacuum, ε=78.5 is the relative permittivity of the solution, *A* (m^2) is the plate area, *d*(m) is the distance between the two plates and Ψ_0(V) is the surface potential. The distance *d* is usually measured to the plane consisting of the outer radii of adsorbed and hydrated electrolyte ion (<1 nm) which is also called the Outer Helmholtz Plane (OHP). This type of EDL model is called a Constant Capacity Model (CCM) and is usually only applicable to high electrolyte concentrations (>0.01M). The relationship with the conditional surface site density σ(C/m^2) is:

$$\sigma = C \cdot \Psi_0 \cdot m^{-1} \cdot SSA^{-1} \quad \text{(Eq.8)}$$

Here *m*(kg) is the solid mass(kg) and SSA(m^2/kg) is the specific surface area. For minerals with acidic/amphoteric sites the conditional surface site density depends on the corresponding pK_a values of the surface sites and the total surface site density σ_{tot} through a mass balance [57].

However, it was subsequently found out that the capacitance varies with surface potential and also with the electrolyte concentration and another formulation of an EDL model was made by Gouy [59] and Chapman [60] [61] who assumed a diffuse layer of ions in thermal equilibrium with surrounding solution and hence distributed according to a Boltzmann-distribution:

$$c(x) = c_{bulk} \cdot e^{\left(-\frac{ZF\Psi_0}{RT}\right)} \quad \text{(Eq.9)}$$

Here $c(x)$ and c_{bulk} are electrolyte concentrations at a close distance x from the solid interface and in bulk solution, respectively. As the distance from the surface increases the localized high concentration of ions decreases and approaches the bulk concentration. This layer of concentration gradient of ions near the surface is known as a diffuse layer and the model is called Gouy-Chapman Diffuse Layer Model (DLM). The concept is similar to the Debye-Huckel theory of an ionic "atmosphere" around an ion in solution. The charge density at distance x is assumed to follow the Poisson equation:

$$\sigma_d(x) = -\varepsilon \cdot \varepsilon_0 \frac{d^2\Psi}{dx^2} \quad \text{(Eq.10)}$$

Based on Eqs. (9 -10), the relationship between the surface potential for the diffuse layer, Ψ_d and the surface charge density of the diffuse layer σ_d(C/m^2) of a 1:1 electrolyte can be derived as:

$$\sigma_d = -(8RT\varepsilon\varepsilon_0 c \cdot 10^3)^{0.5} \cdot sinh\left(\frac{Z\Psi_d F}{2RT}\right) \quad \text{(Eq.11)}$$

Here, c(M) is the electrolyte concentration and *Z* is the ionic charge of electrolyte. Inserting the constants values yields:

$$\sigma_d = -0.1174c^{0.5} \cdot sinh(Z\Psi_d \cdot 19.46) \quad \text{(Eq.12)}$$

The DLM requires that the potential and charge density at the interface between the solid and the diffuse layers must be balanced:

$$\Psi_0 = \Psi_D \quad \text{(Eq.13)}$$
$$\sigma = -\sigma_D \quad \text{(Eq.14)}$$

This means that the potential at the surface Ψ_0 can be calculated for a given conditional charge density at the surface σ. This can be compared with the corresponding relationship for CCM (Eq.8), where also a value for the capacitance *C* must be known to calculate the potential at the surface. There is no means to measure *C* directly, so it should be treated as a fitting parameter. However, in (Eq.8), there are physical constraints of values for ε and *d* so that the fitted value of C/A should be in the range of 0.1-2.0 F/m^2 [50]. Also, in CCM, a separate *C* must be fitted for each ionic strength.

Knowledge of the potential at the surface Ψ_0 is essential for calculating the surface site activity factors, which will soon be described below.

The original DLM assumes that the point charges of ions can reach the inner surface without physical limitations, which at high ionic strengths can lead to very high and unrealistic capacitance values for the diffuse layer. An updated version of the model combines the CCM and DLM into a composite model, known as the Basic Stern Model (BSM) [62], which addresses this issue. Stern proposed that ions have a finite size, which restricts how close they can get to the surface similar to the CCM. As a result, there is a layer of physically bound ions of finite size on a finite number of sorption sites in the OHP. Beyond this the diffuse layer, as described by the DLM, begins.

One may note that chemical-bond sorption can be described with all models via the conditional surface charge density, which is formally a surface property, and the electrostatic effect of electrolyte ions in the solution is treated by the outer layers. However, only the BSM so far describes electrostatically adsorbed electrolyte ions on specific sites in an intermediate layer, allocated inside a separate plane in the solution (often called the Stern plane). The BSM is sometimes described as a Double Layer Model, a term to avoid here to not confuse it with the Diffuse Layer Model described above. Hence, there is a separate surface charge density σ_s for the Stern plane, so that:

$$\sigma + \sigma_s + \sigma_d = 0 \qquad \text{(Eq 15)}$$

$$\sigma = C_s \cdot (\Psi_0 - \Psi_d) \qquad \text{(Eq.16)}$$

The σ_d term in (Eq.15) can be substituted with (Eq.13) to calculate Ψ_d from the knowledge of the two conditional charge densities: σ of the chemically adsorbed ions (depending on assigned reaction constants and the mass balance) and σ_S of the physically adsorbed electrolyte ions, depending on assigned reaction constants and the mass balance. It can be assumed that both of these surface charge densities can be related to the same surface site mass balance, that is, the sites hold either a chemically sorbed species or a physically sorbed species:

$$\sigma_{tot} = \sigma + \sigma_s \qquad \text{(Eq.17)}$$

However, just as for the CCM, a capacitance, C_s must be fitted. The BSM can be described as a double layer sorption model, if one considers the Stern plane as site-specifically electrostatically sorbed ions in addition to chemically bound species at the surface.

Even more elaborate models, such as the Triple Layer Model (TLM) [63] which separates the solution near the surface into three distinct layers: 1) 0-plane or first Stern plane, this time for chemically bonded ions, 2) β-plane or second Stern plane for electrostatically bond ions and 3) the d-plane of the diffuse layer. The TLM can be seen as the chemically bonded interactions have been lifted from the surface into a separate layer in order to give this layer a separate capacitance value, which can be used as an additional fitting parameter. However, it is not entirely clear if the protonation of the surface should be lifted out to the inner plane as well. If these too are lifted out, what remains is a constant negative potential on the surface. Our interpretation of TLM is that protonation reactions remain on surface and only metal/ligand interactions with chemical bonds is lifted out to the 0-plane.

For the overall mass balance, a similar reasoning as for the BSM can be made also for the TSM: no matter the plane, all species have to share the same surface sites (i.e. one cannot have an outer and an inner complex at the same surface site). There are now two capacitances to consider, one for the 0-plane and one for the β-plane in the fitting of parameters.

One may note that ion-exchange reactions are not considered in electrostatic models, which may be reasonable since the surface charge is always balanced by the exchanged ions. This is often noticed empirically as the uptake of ions are not influenced by surface charge (i.e. solution pH) unless at very acidic conditions were protons compete also for the exchange sites. To implement these electrostatic solid-solution interface models for calculating activity factors one can consider the energy of interaction between surface and solution species as consisting of two parts:

$$\Delta G_{tot} = \Delta G_{int} + \Delta G_{coul} = \Delta G^*_{int} - \Delta Z \cdot F \cdot \Psi_0 \qquad \text{(Eq.18)}$$

Where the second, coulombic part comes from the Nernst equation. What is constant here is the internal ΔG_{int}, hence:

$$\Delta G_{int} = \Delta G_{tot} - \Delta G_{coul} = \Delta G^*_{int} + \Delta Z \cdot F \cdot \Psi_0 \qquad \text{(Eq.19)}$$

Consider the sorption reaction R3-1 above. The reaction constant can then be written as:

$$K_{int} = \frac{[\equiv SA]}{[A]\cdot[\equiv S]} \cdot e\left(\frac{-\Delta Z F \Psi_0}{RT}\right) = K_{app} \cdot e\left(\frac{-\Delta Z F \Psi_0}{RT}\right) \qquad \text{(Eq.20)}$$

In (Eq.19) K_{app} is the apparent equilibrium constant which varies depending on the value of the surface potential Ψ_0. The exponential term in (Eq.19) may therefore be seen as an activity coefficient for a charged surface species. The factor depends on the sign and the integer size of ΔZ and also the sign of the potential Ψ_0 in a way that may not be intuitive.

How this work is best demonstrated by examples. If we consider the second pK_a for an amphoteric site, ΔZ=+1 because by the protonation the surface charge increases by one, and a negative potential is associated with the negatively charged site, hence:

$$K_{a2}^{-1} = \frac{[\equiv SOH]}{[H^+]\cdot[\equiv SO^-]} \cdot e\left(\frac{\Delta ZF|\Psi_0|}{RT}\right) = \frac{[\equiv SOH]}{[H^+]\cdot[\equiv SO^-]\cdot e\left(\frac{-\Delta ZF|\Psi_0|}{RT}\right)} \cdot = \frac{[\equiv SOH]}{[H^+]\cdot[\equiv SO^-]\cdot\delta_1} \qquad \text{(Eq.21)}$$

Here we have introduced δ_1 as the activity factor for single- charged surface species. Since δ_1<1, this promotes the formation of charged ≡SO^- groups through the mass balance action on the expense of non-charged ≡SOH groups. This is reasonable, since the EDL builds up a positive charge on a negative surface and thereby screens the surface from incoming protons, hence the relative amount of ≡SOH should decrease by the EDL effect.

If instead the first pK_a for an amphoteric site is considered, then again ΔZ=+1 but the potential is positive from positively charged surface sites, and one gets:

$$K_{a1}^{-1} = \frac{[\equiv SOH_2^+]}{[H^+]\cdot[\equiv SOH]} \cdot e\left(\frac{-\Delta ZF|\Psi_0|}{RT}\right) = \frac{[\equiv SOH_2^+]\cdot\delta_1}{[H^+]\cdot[\equiv SOH]} \qquad \text{(Eq.22)}$$

Here the activity factor also promotes the formation of the charged complex over the neutral one, which is reasonable since in this case the EDL builds up a negative charge on a positive surface, thus electrostatically attracting protons to the surface. Such reasoning can be made also for surface complexes with multivalent metal cations, which may give ΔZ >1 and then will introduce higher order (δ_2, δ_3…) surface activity coefficients.

Finally, one may note that the surface site activity factor is related to a pair of surface species and not to a single species, hence the use of ΔZ as it describes the transfer of surface charge between the two surface species.

3.2. Determination of enthalpy and entropy using vant's Hoff equation

The traditional approach for evaluating the effect of temperature on any chemical reaction involves the determination of the thermodynamic parameters of enthalpy and entropy of reaction with the van`t Hoff equation:

$$Log\ K = \frac{\Delta S^o}{R} - \frac{\Delta H^o}{RT} \qquad \text{(Eq. 23)}$$

where T is the absolute temperature, R is the gas constant, and $\Delta H^o$and ΔS^o are the enthalpy and entropy of reaction, in this case of this work, the ion-exchange and surface-complexation reactions.

When the equilibrium constant is plotted against the inverse of the temperature, a straight line is usually obtained, if the temperature variation is in a limited interval, with the slope representing ($-\Delta H^o/R$) and the intercept corresponding to ($\Delta S^o/R$).

A reaction is considered endothermic when heat is absorbed for bond breaking, resulting in a net positive enthalpy change, which contributes with a non-favorable term for ΔG. In an exothermic reaction, heat is released, leading to a net negative enthalpy change, which contributes to a favorable ΔG for the reaction. A positive ΔS, on the other hand, contributes to a favorable ΔG, since an increase in entropy is always a spontaneous process. Thus, depending on the size of the respective contributions to a favorable negative Gibbs energy for a reaction, one can have reactions that are dominated by enthalpy (bond formation) or by entropy (bond breaking).

3.3. The BET isotherm

A short introduction to the so-called BET theory [55] for gas molecule adsorption on surfaces is given here, since it was used in this work for determining the specific surface area of biotite. The BET theory describes a multilayer sorption of gas molecules on a surface by considering the condensation and evaporation rates. It can be considered as a multi-layer version of the Langmuir isotherm for gases:

$$V_a = \frac{V_m \cdot b \cdot P}{1 + b \cdot P} \qquad \text{(Eq.24)}$$

(Eq.24) is equivalent to (Eq.2), the Langmuir isotherm for a dissolved species in solution in contact with a solid. The reaction constant is replaced with the constant *b*, and concentration of sorbing species (gas molecules) is replaced with pressure *P*, assuming an ideal gas. V_a and V_m are the number of occupied and total sites, respectively.

The BET isotherm takes the form:

$$V_a = \frac{V_m \cdot C \cdot P}{(P_0 - P)\left[1 + (C-1)\cdot\frac{P}{P_0}\right]} \qquad \text{(Eq.25)}$$

Where *C* is constant. In the application for the determination of the volume of one monolayer of gas V_m, (Eq.25) is linearized:

$$\frac{P}{V_a \cdot (P_0 - P)} = \frac{1}{C \cdot V_m} + \frac{C-1}{C \cdot V_m} \cdot \frac{P}{P_0} \qquad \text{(Eq,.26)}$$

By adding precise volumes V_a of adsorbing gas and by measuring the pressures *P* and P_0, the constants V_m and *C* can be determined. The specific surface area can then be calculated by knowledge of the mean area occupied by one gas molecule, 16.2 $Å^2$ and 21.0 $Å^2$ are values normally used for N_2 molecule and Kr atoms, respectively. One may note that the precision of

measurement increases with decreasing saturation pressure P_0, where P_0 for Kr gas is 300 times lower than for N_2,

3.4. Determination of point of zero charge (pH_{pzc})

The point of zero charge, often denoted as pH_{pzc}, refers to the pH at which a solid surface has no net electrical charge. At this specific pH, the number of positively charged sites on the surface is equal to the number of negatively charged sites, resulting in a neutral overall charge.

The pH_{pzc} for the biotite mineral was determined using equation given below:

$$\Delta H^+ = [H^+]_t - [H^+] + \frac{Q_w}{[H^+]} \quad \text{(Eq.27)}$$

Where, Q_w is the water dissociation constant, ΔH^+ is the difference between the total and free H^+concentration (mol/l), $[H^+]_t$ is the total proton concentration and $[H^+]$ is the free proton concentration.

4. Materials and Methods

4.1. Origin and preparation of the biotite sample

This study uses a biotite specimen with origin from Risör, Norway**.** Its chemical composition has been analyzed to $K_{1.1}(Mg_{0.7}Mn_{0.1}Ti_{0.2}Fe(II)_{1.9}Fe(III)_{0.1})Fe_{0.1}Al_{1.3}Si_{2.6}O_{10}(OH)_2$ with 99.99% mineral purity [64]. The mineral density has been determined to 3.10kg/m^3 [65].

For sample preparation, the biotite was initially crushed using a knife grinding machine (IKA model M20) for 1 to 2 minutes. The crushed material was then sieved in two fractions: 0.25-0.5mm and 0.063-0.125mm using Retsch stainless steel sieves, assisted by a shaking machine (Retsch AS200). The sieving process, which lasted approximately 1.5 hours, was conducted in two stages: 30 minutes at high amplitude followed by 1 hour at low amplitude. Following sieving, the biotite was repeatedly washed with 90% ethanol until the wash solution became clear. The cleaned biotite was then dried in a vacuum chamber (Vacucell, MMM Group) at room temperature for one week at a pressure below 30 mmHg.

4.2. Measurement of the specific surface area

Prior to analyzing the specific surface area, the biotite mineral was dried for 24 hours at a pressure of approximately 10 µm Hg at the drying station of a gas adsorption instrument (Micromeritics ASAP2020). The specific surface area (SSA) of triplicate samples was then measured with this instrument through krypton (Kr) gas adsorption, with the data analyzed using the BET isotherm [55] via the instrument's software.

4.3. Determination of the cation exchange capacity (CEC)

The cation exchange capacity (CEC) of the biotite mineral was determined by the use of the ammonium acetate method [54]. Triplicate samples of 1 gram of biotite were placed in a 50 ml polypropylene centrifuge tube (Oak Ridge, Thermo Scientific) containing 30 ml of 1M ammonium acetate solution (Sigma-Aldrich, 99.99%). Sampling was conducted at six intervals over 1, 2, 4, 8, 16, and 32 days. For each sampling, the samples were centrifuged (Beckman Coulter, Avanti J26S XP) for 30 minutes at 20,000 rpm. The supernatant was then filtered through a 0.45 µm polypropylene filter, diluted tenfold with 0.5M nitric acid, and analyzed using Inductively Coupled Plasma Optical Emission Spectroscopy (ICP-OES) (Thermo, iCAP XP Pro). The mathematical expressions used to calculate the CEC are detailed in the attached manuscript 2.

4.4. Conditioning of the biotite sample

Impurities such as Ca^{2+} and K^{+} are commonly present on the surface of biotite, potentially affecting the accuracy of sorption experiments. To reduce these surface impurities and convert the biotite to its Na form, a conditioning experiment was conducted on a portion of the biotite mineral. Three $NaClO_4$ (Merck, 98%) solutions (0.001M, 0.01M, and 0.1M) were prepared using ultrapure water (MilliQ, Merck) with a pH of approximately 7. The biotite was mixed with the solutions at a solid-to-liquid ratio of 1:50 in 10 ml polypropylene tubes (Sarstedt). The experiment lasted about 1.5 months to maximize sodium exchange on the biotite surface. During this time, the electrolytic solution was replaced three times, and the supernatant was analyzed for exchangeable cations using ICP-OES (Thermo iCAP Pro XP Duo). The results are shown in the table below:

Ionic Strength	Amount (cmolc/kg)	Percentage
0.001 M	$5.22.10^{-2}$	5.17%
0.01M	$1.04.10^{-1}$	10.29%
0.1M	$3.22.10^{-1}$	31.91%

4.5. Determination of the biotite acidic site density (ASD)

The acidic site density (ASD) of the biotite was determined with the tritium exchange method [53]. Following this method, a tritium water (HTO) solution of 53 MBq/mL was prepared. In a 50 mL centrifuge tube (Oak Ridge 3119-0050, Thermo Scientific), 5 grams of crushed biotite mineral was dispersed in 20 mL of 52 MBq/mL HTO solution. A total of five tubes were prepared: three containing biotite and two without the mineral, serving as blanks. The tubes were conditioned for three months. After this period, the two phases were separated by centrifugation at 20,000 rpm for 30 minutes, and the HTO solution was removed. The open tubes containing wet biotite were transferred to a fume hood to dry and subsequently placed in a vacuum chamber (Vacucell, MMM Group) for 100 hours at room temperature. The complete dryness of the biotite was confirmed by progressively measuring the weight of the tubes until no further reduction of weight was observed.

Next, the dried mineral was transferred into new tubes, and a specific amount of alkaline solution (pH ~11) made with ultrapure water was added. These samples were then placed in an ultrasonic bath for 2 minutes and subsequently on a shaking machine. This process aimed to extract the radioactive protons bound to the mineral surface to solution. Sampling was conducted periodically over ~57 days, following centrifugation at 20,000 rpm for 30 minutes. In each sampling, a 1 mL aliquot was taken and measured using a Liquid Scintillation Counter (LSC). The experiment assumed that all radioactive protons attached to the mineral surface were detached or exchanged with non-radioactive protons. The amount of extracted or exchanged acidic protons per surface area, N_H (mol/m^2), was calculated as follows:

$$N_H = \frac{A_t}{A_L S_{BET} M} moles\ m^{-2} \quad \text{(Eq.28)}$$

Where A_L is the specific activity of HTO in the starting solution (cpm/mol HTO), S_{BET} is the BET surface area (m^2/g) and M represents the mass of biotite in gram, and A_t is the total specific activity of HTO in the new added water (cpm).

4.6. Titration on biotitie for acidditiy constants (pK_a)

The acid-base properties of the biotite mineral were investigated using continuous titration method at temperatures of 25, 40, and 60 °C. The titration was conducted with standard solutions of 0.01M HCl and 0.1M NaOH (both Titrisol, Merck), prepared within a glovebox under a controlled nitrogen atmosphere.

The titration was performed using an automatic titration system (905 Titrando, Metrohm) and controlled by a computer program (Tiamo v2.2, Metrohm) that managed the timing and volume of reagent addition. A glass electrode (6.0250.010, Metrohm) was used to monitor H^+ concentration throughout the process. A fixed time interval of 15 minutes between each addition was selected based on the stability of the signal, as this interval was deemed optimal to avoid mineral dissolution while allowing sufficient time for the system to reach equilibrium, as recommended by references [66] [67].

Prior to each titration, the electrode was calibrated for [H^+] using the Gran titration method [68]. Three titrations were conducted at each temperature, with each titration involving 0.5 g of biotite mixed with 50 mL of 0.01 M $NaClO_4$ (98%, Merck) in a double-walled titration vessel with magnetic stirrer, water circulation and lid. To protect the solution from CO_2 ingress, inert gas was bubbled through the solution. For adjusting the initial pH to approximately 3, 2.5 to 3 mLs of 0.01 M HCl were added. The suspension was then titrated with a fixed volume of 4 µl per addition at 25 °C [66] [67], and 8 µl per addition at 40 and 60 °C using 0.1 M NaOH. The temperature was controlled by the help of a water circulation bath (TC120, Grant).

4.7. Batch sorption experiments

The objective of this experiment was to determine R_d values for the selected radionuclides sorption onto biotite, across a wide range of conditions. To this end, two successive experimental campaigns for the sorption experiments were prepared. The first consisted of a mixture of Cs(I), Ba(II), Co(II), and Eu(III) radioactive tracers, while in the second campaign Ra(II) and Am(III) radiotracers were mixed. Both campaigns used Na-converted biotite with varying ionic strengths, 0.001 M, 0.01 M, and 0.1 M $NaClO_4$, five different pH, 5, 6, 7, 8, and 9, and at three different temperatures, 25, 40, and 60 °C.

Solutions were prepared by dissolving $NaClO_4$ (98%, Merck) to 0.001 M, 0.01 M, and 0.1 M concentration, respectively. Each of these was divided into five solutions, which were then

buffered to the target pH values using specific buffers: pH 5 with 1,4-Diethylpiperazine (DEPP, Alfa Aesar, 89%), pH 6 with 2-(N-Morpholino) ethanesulfonic acid (MES, Sigma-Aldrich, 99%), pH 7 with 3-(N-Morpholino) propanesulfonic acid (MOPS, Sigma-Aldrich, 99.5%), pH 8 with 1,4-Piperazinebis (propanesulfonic acid) (PIPPS, Merck, 98%), and pH 9 with DEPP. These buffers were chosen for their non-metal-complexation properties [69]. The pH of these solutions was measured using a pH electrode (pHC3006-9, PHM240, Radiometer) and adjusted with 0.1 M NaOH or $HClO_4$ as needed. For the 0.001 M $NaClO_4$ solutions, the buffer concentration was 0.5 mM, while for the 0.01 M and 0.1 M $NaClO_4$ solutions, the buffer concentration was 5 mM. Any contribution of the buffers to the ionic strength was found negligible by analyses of these solutions for Na, K, Mg and Ca with ICP-OES.

Each of the fifteen solutions was spiked with a mixture of radioactive Cs, Ba, Co, Eu (for the first experimental campaign) and Ra^{2+}, Am^{3+} (for the second campaign) in a concentration of approximately 10^{-8}M except Ra which was 10^{-13}M. The pH of each solution was again adjusted using either 0.1 M NaOH or 0.1 M $HClO_4$. The specifications for the radionuclides were: ^{134}Cs (CsCl in 0.1 M HCl), ^{133}Ba ($BaCl_2$ in 0.1 M HCl), ^{60}Co ($CoCl_2$ in 0.1 M HCl), ^{152}Eu ($EuCl_3$ in 0.5 M HCl), ^{241}Am ($AmCl_3$ in 1 M HCl), all were 10 μg/mL in carrier isotopes (Eckardt & Ziegler). For ^{226}Ra a carrier-free solution of $RaNO_3$ with 0.1MBq/mL ($1 \cdot 10^{-10}$ M) dissolved in 1 M HCl was used. For both campaigns, the procedure described which follows, were the same.

The sorption experiment was conducted in triplicates at temperatures of 25, 40, and 60 °C, the latter two series by the use of dry heating blocks (Isotemp, Fisherbrand). The experiments were carried out inside a nitrogen-filled glovebox (MBraun InLab) to minimize oxygen exposure and prevent carbonate formation. 0.1 g portions of Na converted biotite (particle size range of 0.250-0.500 mm) were equilibrated for 1 month in 5 mL of respective 0.001, 0.01 and 0.1 M $NaClO_4$ neutral solutions in PP centrifugation tubes (OakRidge 3119-0010, Thermo). Then, after centrifugation at 45000 g for 30 mins.with centrifuge (Avanti J26S, BeckmanCoulter), almost all supernatants were removed and replaced with 5 ml of spiked, pH-buffered $NaClO_4$ solution of corresponding concentration to the removed solutions, resulting in a solid-to-liquid ratio of 1:50. Additionally, 30 (duplicates) blank samples without biotite were prepared for the assessment of wall sorption, and also 15 (one for each stock solution) acidic reference samples were prepared to measure the concentration of the added reference radioactivity.

Sampling for the sorption experiment occurred at intervals of 2, 14, 30, and 60 days. Prior to each sampling, the tubes were centrifuged for 30 mins at 45 000 g. Except for the final sampling, where 0.5 ml was pipetted, an aliquot of 0.1 ml (2% of vol.) from the supernatant was collected to 6 mL PP tubes and mixed with 0.4 mL of 1M HCL buffer solution. Using an HPGe detector (GammaAnalyst with DSA2000 MCA and Genie2000 v.3.4.1 software, Canberra/Mirion), calibrated to the same geometry, the gamma activity of the radionuclides in the aqueous phase was measured.

Based on the mass balance formula for a batch experiment [70] the R_d - values were determined as:

$$R_d = \left(\frac{\bar{C}\cdot V_{ref}\cdot V_{out,n}}{A_{out,n}} - \left(V_0 - \sum_{i=1}^{n-1} V_{out,i}\right) - L_d - \frac{V_{out,n}\cdot\sum_{i=1}^{n-1} A_{out,1}}{A_{out,n}}\right)\cdot\frac{1}{m} \qquad \text{(Eq.29)}$$

Where V_{ref} (L) is the volume of the radioactive solution added initially, $\bar{C}$ (cpm/L) is the average measured reference concentration taken from the acidic references, and $V_{out,n}$ (L) and $A_{out,n}$ (cpm) are the volume and measured activity of sample n of the one to n successive samples. The batch's initial liquid volume, or V_0(L), comprises V_{ref} and any leftover liquid from the preconditioning. The mass of the material in the sorption experiment is represented by m(g), and the factor correcting for wall sorption is L_d (L), which is measured in a separate blank series of batch experiment. In (Eq 29) the two summation terms are derived from an overall mass balance and account for the quantities and radioactivity extracted in the subsequent samplings: the first term accounts for reference, the second term for batch experiments.

Essentially the same formula is used to compute the wall sorption factor; however, since the mass involved in wall sorption is unknown, the wall sorption factor L_d (L) is defined as:

$$R_{d,wall}\cdot m_{wall} = \left(\frac{\bar{C}\cdot V_{ref}\cdot V_{out,n}}{A_{out,n}} - \left(V_0 - \sum_{i=1}^{n-1} V_{out,i}\right) - \frac{V_{out,n}\cdot\sum_{i=1}^{n-1} A_{out,1}}{A_{out,n}}\right) \equiv L_d \qquad \text{(Eq.30)}$$

4.8. Modeling methods

The titration data was modelled by including the following reactions:

$$NaX + H^+ \rightleftharpoons HX + Na^+ \qquad \text{(R4-1)}$$

$$\equiv SOH \rightleftharpoons \equiv SO^- + H^+ \qquad \text{(R4-2)}$$

$$\equiv SOH_2 \rightleftharpoons \equiv SOH + H^+ \qquad \text{(R4-3)}$$

$$\equiv SO^- + Na^+ \rightleftharpoons \equiv SONa \qquad \text{(R4-4)}$$

$$\equiv SOH + Na^+ \rightleftharpoons SOHNa^+ \qquad \text{(R5-5)}$$

The reactions consider, in turn, ion-exchange on basal planes between protons and cation of electrolyte (R4-1), protonation of edge surface (R4-2 and 3) and a strong (R4-4) and a weak (R4-5) surface complex with cation, in this case from electrolyte. The corresponding selectivity co-efficient for ion-exchange K_{NaX} is defined by:

$$\mathrm{K}_{EX} = \frac{[HX]\{Na^+\}}{[NaX]\{H^+\}} \qquad \text{(Eq. 31)}$$

The surface acidity constants K_{a1} and K_{a2} are defined as

$$K_{a1} = \frac{[\equiv SOH]\{H^+\}}{[\equiv SOH_2]} \quad \text{(Eq.32)}$$

$$K_{a2} = \frac{[\equiv SO^-]\{H^+\}}{[\equiv SOH]} \quad \text{(Eq. 33)}$$

The surface complexation constants for the reactions (R4-4) and (R4-5) are

$$K_{SONa} = \frac{[\equiv SONa]}{[\equiv SOH]\{Na^+\}} \quad \text{(Eq.34)}$$

$$K_{SOHNa} = \frac{[\equiv SOHNa^+]}{[\equiv SOH]\{Na^+\}} \quad \text{(Eq.35)}$$

Where, the symbol [] indicates the concentration is given in unit mol/L. For the titration data the model was fitted by minimizing the error sum

$$\sum_{i=1}^{n} abs(\{H^+\}_{exp,i} - \{H^+\}_{calc,i}) \quad \text{(Eq.36)}$$

In (Eq.36) *n* is the number of steps in the titration curve, $\{H^+\}_{exp,i}$ is the measure proton activity at point *i* and $\{H^+\}_{calc,i}$ is the calculated proton activity according to the mass balances:

$$\frac{V_{HCl} \cdot C_{HCl} - V_{NaOH} \cdot C_{NaOH}}{V_{tot,i}} = [H^+] - [OH^-] + [HX] + [\equiv SOH] + 2 \cdot [\equiv SOH_2] - [NaX] \quad \text{(Eq.37)}$$

$$\frac{CEC \cdot m_{biotite}}{V_{tot,i}} = [HX] + [NaX] \quad \text{(Eq.38)}$$

$$\frac{ASD \cdot m_{biotite}}{V_{tot,i}} = [\equiv SO^-] + [\equiv SOH] + [\equiv SOH_2] + [\equiv SONa] + [\equiv SOHNa^+] \quad \text{(Eq. 39)}$$

$$\frac{[Na^+]_{NaClO4} \cdot V_{NaClO4} + [Na^+]_{NaOH} \cdot V_{NaOH,i}}{V_{tot,i}} = [Na^+] + [NaX] + [\equiv SONa] + [\equiv SOHNa^+] \quad \text{(Eq.40)}$$

Here *CEC* and *ASD* are the measured cation exchange capacity and acidic site density in moles/g, respectively. $m_{biotite}$ is the mass of biotite in the titration and $V_{tot,i}$ is the total volume at titration point *i*. This equation system, with the four "master species" H^+, Na^+, HX and $\equiv SO^-$ as variables together with (Eqs. 31-35) is solved for each titration point with the PHREEQC software [71]. The initial contribution of H^+ and Na^+ from the biotite itself to (Eq. 37) and (Eq.40), respectively, were judged to be negligible compared with the amounts added as solutions at the start of titration.

The optimization of the model was accomplished by coupling the PHREEQC [71] chemical speciation software with a PYTHON optimization routine through an integration code [72] [73]. This code is a Microsoft COM (component object model) version of PHREEQC called

IPHREEQC and facilitates a link to communicate and interchange the data between PHREEQC and other software like Excel, MATLAB and programming languages such as PYTHON, and Visual Basic. The optimization parameters are the assumed reaction constants and selectivity coefficients, as defined in (Eqs 31-35). One may also note that these are treated in PHREEQC as valid at zero ionic strength and that activity coefficients are applied to all dissolved species by the program, according to the given ionic strength.

With several parameters fixed from modelling of titration, that is, the equilibrium constants and coefficients in (Eqs. 31-35), a similar model was fitted to the radionuclide distribution coefficients R_d obtained from modelling radionuclide in-diffusion into biotite particles, as described in previous section, in the batch sorption experiments.

$$\sum_{i=1}^{n} abs(R_{d,exp,i} - R_{d,calc,i}) \quad \text{(Eq.41)}$$

Here *n* denotes the number of batch experiments for one radiotracer at a specific temperature, which were 45 in total (5 pH, 3 ionic strengths, triplicates). Similar reactions for ion exchange (R4-1) and surface complexation (R4-4 and 5) were used for the radiotracer cations. However, here also hydroxide complex formation had to be considered. The hydroxide complexes included in the model are shown in Table 4-1, below.

Table 4-1: Thermodynamic data of aqueous hydroxide complexes of Ba, Ra, Co, Am, and Eu used in sorption modeling.

Reaction	**log_β**
$Ba^{2+} + H_2O = Ba(OH)^+ + H^+$	0.65[a]
$Co^{2+} + H_2O = Co(OH)^+ + H^+$	4.39[b]
$Co^{2+} + 2H_2O = Co(OH)_2 + 2H^+$	8.23[b]
$Co^{2+} + 3H_2O = Co(OH)_3^- + 3H^+$	10.0[b]
$Eu^{3+} + H_2O = Eu(OH)^{2+} + H^+$	6.4[b]
$Eu^{3+} + 2H_2O = Eu(OH)_2^+ + 2H^+$	12.3[b]
$Eu^{3+} + 3H_2O = Eu(OH)_3^0 + 3H^+$	17.1[b]
$Ra^{2+} + H_2O = Ra(OH)^+ + H^+$	0.51[c]
$Am^{3+} + H_2O = Am(OH)^{2+} + H^+$	6.8[b]
$Am^{3+} + 2H_2O = Am(OH)_2^+ + 2H^+$	12.9[b]
$Am^{3+} + 3H_2O = Am(OH)_3^0 + 3H^+$	15.8[b]

[a]PHREEQC database MINTEQ, [b] [48], [c]PHREEQC database ThermoChimi

Some hydroxide complexes of radiotracers were allowed to form surface complexes, and, in some cases, exchange species and corresponding reactions and reaction constants were defined according to same formalism as for the cations. The hydroxide surface species are described further in the results.

Mass balances for the batch sorption modelling were also similar to those shown for titration modeling, except that both volume and pH were assumed to be constants. The latter condition means that a mass balance for protons (Eq.37) was not necessary to include in model.

5. Results and Discussion

A comprehensive explanation of all experimental and modeling results can be found in the publications at the end of this thesis. This section highlights key results from the sorption experiments, modeling, and time-dependent studies as an example. Detailed sorption data and modeling results are available in Appendices A and B, respectively.

5.1. Characterisation of biotite mineral

The specific surface area (SSA) of crushed biotite was determined for the 0.25-0.5 mm particle fraction to 0.47±0.01 m^2/g. In comparison, a Finnish biotite specimen of exactly the same particle size range reported by [42] had a surface area of 0.83 m^2/g. Several factors could explain this discrepancy. For example, measuring surface area with different gases can yield different results. The Kr-BET method used here is 300 times more precise than the N_2-BET method due to differences in saturation pressures. Other possible reasons include variations in crushing and cleaning techniques, as well as inherent differences in the biotite samples.

The Cation Exchange Capacity (CEC) of the biotite crystal was found to be 1.03±0.03 $cmol_C/kg$. This measured value can be compared to CEC values for other biotite specimens reported in the literature: 16.3$cmol_C/kg$ [42] and 1.26$cmol_C/kg$ [35]. According to the study by Puukko et al. [47], the CEC values for three Finnish biotite specimens of non-specified size fractions fall between 1.3-1.7$cmol_C/kg$. In general, the CEC values for the various biotite specimens appear to be quite consistent, except for the value determined by [42].

A review of the thermodynamic sorption model of radionuclide with some selected granitic minerals reveals that acidic site density (ASD) is often evaluated either through modeling titration data or by molecular-level modeling using density functional theory. Literature experimental data for biotite seems to be non-existent.

In this study, a tritium exchange method [53] was employed to determine ASD of biotite at neutral pH to minimize its dissolution. This method has been previously used to estimate the site density of various mineral oxides. The time-dependent results are shown in fig. 5-1, indicate that already within the first few days of the experiment, most of the protons on the biotite surface were exchanged with tritium protons. Following this initial period, the exchange rate decreased significantly and eventually stabilized. The results from this experiment suggest that the biotite ASD is $3.14 \pm 0.6 \cdot 10^{-6}\ mol/g$. This finding is consistent with the results obtained by theoretical value of $7.6 \cdot 10^{-6}$ mol/g calculated with density functional theory [35].

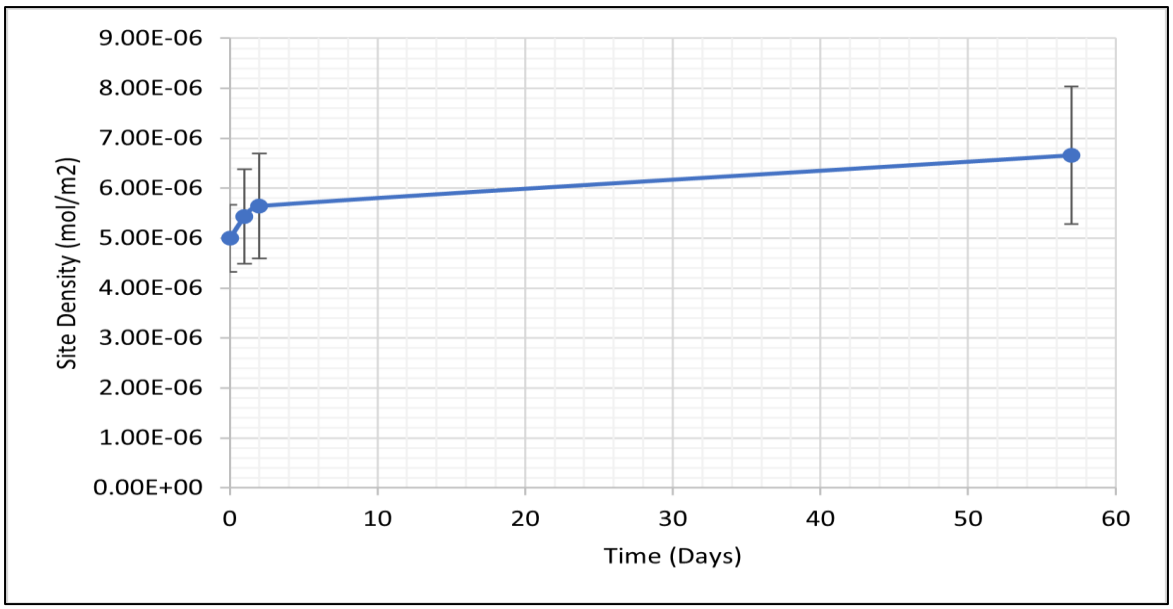

Figure 5-1: Results for acidic site density measurements, evaluated with the help of tritium exchange method.

5.2. Titration Results

Figure 5-2 presents the modeled and experimental titration results for a 0.01 M background electrolyte at 25, 40, and 60 °C. The titration curves at all three temperatures exhibit a typical S-pattern with inflexion points between pH 6 and 7, indicating the presence of at least one acidic site on the mineral surface. Consequently, both a 1-pK_a and a 2-pK_a models were applied to fit the data using the PHREEQC geochemical speciation program [71] coupled with a PYTHON optimization routine. The results gave a better fitment with a 2-pK_a model, which is also consistent with previous studies [32]. The optimization process included not only site protonation/deprotonation, but also proton and Na exchange on separate exchange sites and Na sorption reactions on the acidic sites. The modeling results for all temperatures are detailed in Table 5-1. The optimized acidity constants at 25 °C shown in Table 5-1 are consistent with previous findings (for example, pK_{a1} = -4.6, pK_{a2} = -6.4) [74]. There is no comparative data for the higher temperatures available.

The pK_a values were found to be affected by an increase in temperature. It was observed that as the temperature increased from 25 to 60 °C, the constants for the formation of charged species $\equiv SO^-$ and $\equiv SOH_2^+$ increase on the expense of the neutral species ≡SOH. This is probably not an electrostatic effect since the surface activity factor is exponentially proportional to temperature (Eq. 20).

Similarly, the stability constant for the hydrated Na^+ ion (“outer sphere”) surface complex also increased with temperature, indicating that higher temperatures enhance Na^+ sorption on the biotite surface. However, the impact of temperature on the selectivity coefficient for the H^+ and Na^+ exchange reaction seems not to be affected by the increased temperature.

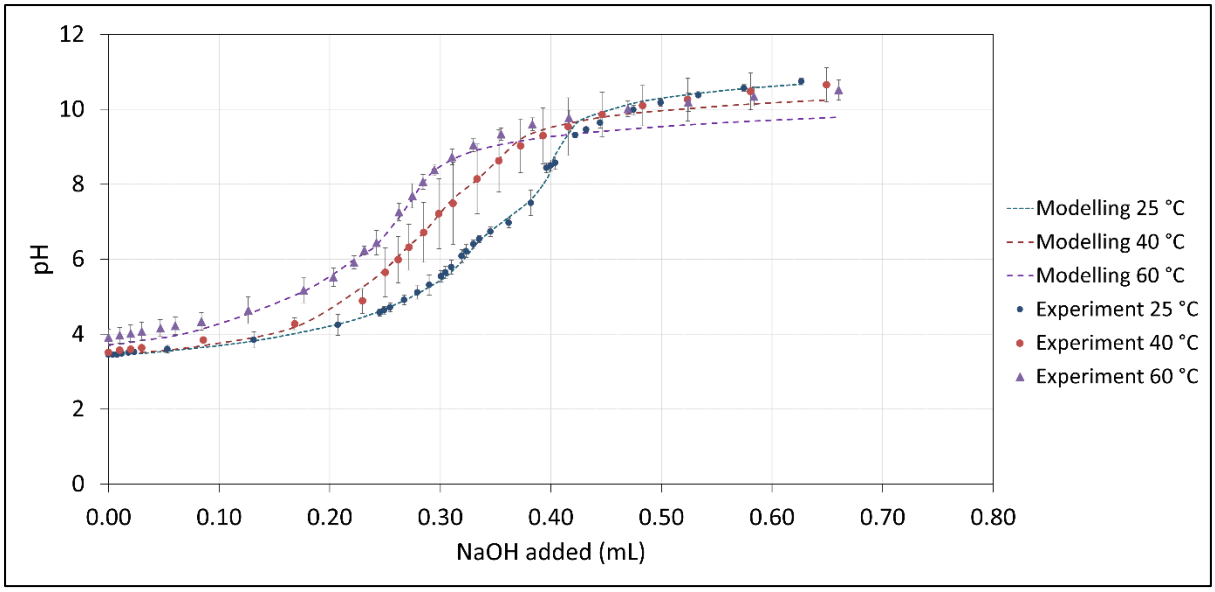

Figure 5-2: Experimental and modelled titration results onto biotite suspension in 0.01 M $NaClO_4$ at 25, 40, and 60 ºC

Table 5-1 Optimized protonation ($\equiv SOH_2$), deprotonation ($\equiv SO^-$), sodium inner ($\equiv SONa$) and outer ($\equiv SOHNa^+$) sphere complex and cation exchange (X) reaction constants along with the site density and CEC for biotite in 0.01 M $NaClO_4$ at 25, 40, and 60 ºC

Reactions	**Constant or coefficient at 25 ºC**	**Constant or coefficient at 40 ºC**	**Constant or coefficient at 60 ºC**
$\equiv \mathrm{SOH_2^+} \rightleftharpoons \equiv \mathrm{SOH} + \mathrm{H^+}$	-4.9 ± 0.1	-5.0 ± 0.2	-5.3 ± 0.1
$\equiv \mathrm{SOH} \rightleftharpoons \equiv \mathrm{SO^-} + \mathrm{H^+}$	-7.1 ± 0.2	-7.0 ± 0.3	-6.9 ± 0.2
$\equiv SO^- + \mathrm{Na^+} \rightleftharpoons \equiv \mathrm{SONa}$	1.6 ± 0.1	2.0 ± 0.4	3.2 ± 0.1
$\equiv \mathrm{SOH} + \mathrm{Na^+} \rightleftharpoons \equiv \mathrm{SOHNa^+}$	0.5 ± 0.1	2.0 ± 0.8	2.3 ± 0.2
$NaX + H^+ \rightleftharpoons HX + Na^+$	3.0 ± 0.2	2.9 ± 0.2	2.9 ± 0.1
Sorption site densities (mol/g)			
Acidic Site density (optimized)			$1.7 \pm 0.1.10^{-5}$
Cation Exchange Capacity (optimized)			$2.6 \pm 0.4 .10^{-5}$

To improve the model fitment to the titration data, the acidic site density (ASD) and cation exchange capacity (CEC) were also allowed to be optimized. The optimized ASD is a factor of 5.32, and the CEC is a factor of 2.6 times higher than the experimentally obtained values. The discrepancy in ASD may arise due to the fact that both the tritium exchanges were conducted at a neutral pH, where silanol groups may not be protonated. Correcting with a factor of 3 for silanol groups gives an experimental ASD value of $9.5 \cdot 10^{-6}$ mol/g, which is much closer to the optimized value. Also, one cannot exclude that the rather vigorous stirring of the biotite suspension during titrations may have created some fine particles that may have enhanced both ASD and CEC. However, the reaction constant and coefficients should not be affected by such a possible artifact.

The results of the potentiometric titration of a biotite suspension in a 0.01 M $NaClO_4$ solution at 25, 40, and 60 °C are also presented in Fig 5-3 as a traditional delta H^+ plot versus pH. The graph depicts the net amount of protons consumed at these three temperatures. The intersection point of the titration curves at all three temperatures is around a pH value of 5.8 which indicates

that the biotite surface in solution is neutral at this pH. This point is also known as the point of zero charge (pH_{pzc}). A similar value of pH_{pzc} at about 6 for biotite suspension in 0.1 M $NaClO_4$ has been reported [47].

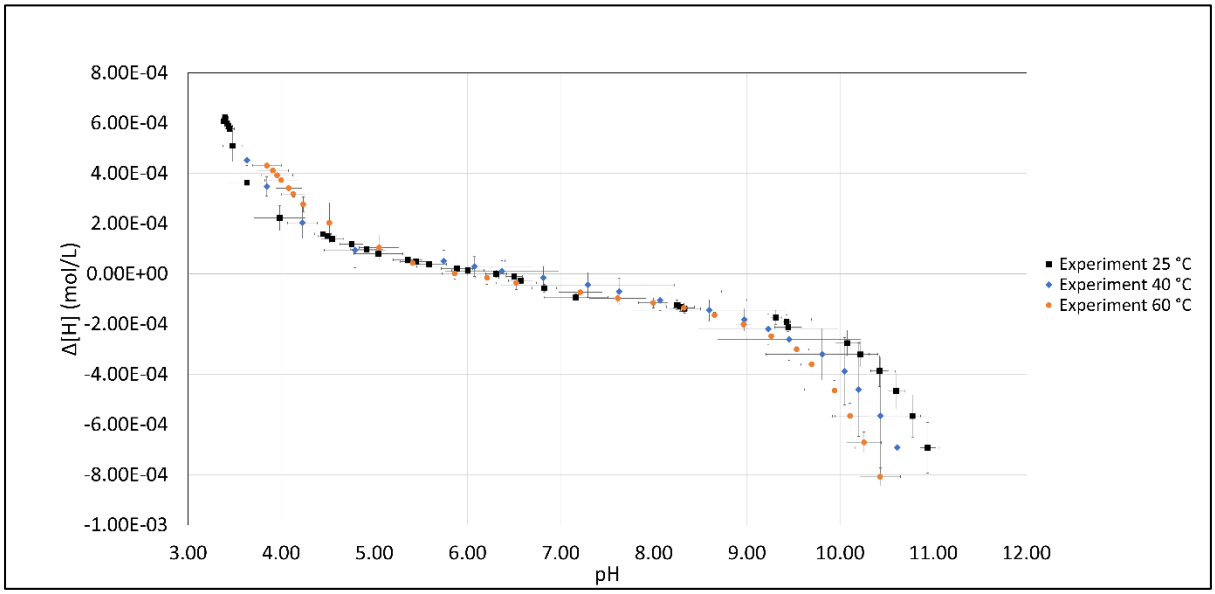

Figure 5-3: Potentiometric titration results for biotite in 0.01 M $NaClO_4$ solution at 25, 40, and 60 °C

5.3. Sorption and modelling results

5.3.1. Time dependent results

The batch sorption studies were conducted over a period of approximately two months. During this time, the apparent distribution coefficients (R_d) were anticipated to progressively increase due to the in-diffusion transport process into the porous biotite grains, which the experimental data also confirm.

For all radionuclides, this time-dependent results were consistent. Therefore, Fig. 5-4 presents the time-dependent sorption data for Ba and Co at an ionic strength of 0.01 M and temperatures of 25, 40, and 60 °C as an illustrative example. The complete set of time-dependent R_d-values is available in Appendix A and the modelled equilibrium R_d values for Cs, Ba, Co and Eu are presented in Paper 2 and the following Tables. At the time of writing this Thesis, the modelled equilibrium R_d values were not available for the Ra and Am in-diffusion data, hence the apparent R_d at final sampling occasions are presented instead.

The results indicate that equilibrium for radioactive sorption was achieved within about one month. There was no significant increase in sorption beyond this point; in fact, there was a slight decrease, which may be attributed to partial dissolution of biotite, especially at high pH values. Thus, by extracting equilibrium R_d values from an in-diffusion model to all the data points rather than to just take the final data point may compensate for a certain dissolution of biotite during the final stage of the experiments. The initial rapid increase in radionuclide sorption suggests that a significant number of active sites were available on the biotite surface.

Additionally, the recorded time-evolution of the apparent R_d values indicates that temperature had little effect on the time required to achieve equilibrium.

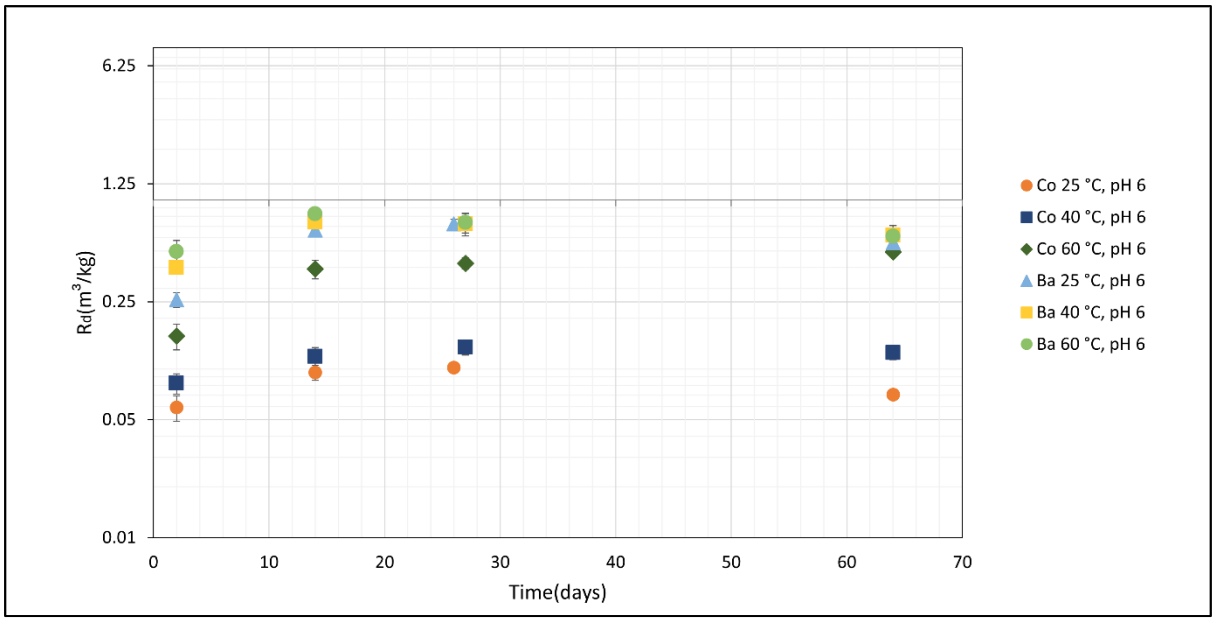

Figure 5-4: An illustration to show effects of contact time on Ba (II) and Co(II) sorption onto the Na converted biotite in 0.01 M $NaClO_4$ solution at pH 6 for 25, 40, and 60 °C

5.3.2. Sorption modelling results of Cs at 25, 40, and 60 °C

Figs. 5-5 (25°C), 5-6 (40°C), and 5-7 (60°C) illustrate the experimental and modelling outcomes for Cs sorption onto biotite for all ionic strengths and pH values. The complete sorption dataset for Cs is given in Appendix A.

The experimental results indicate that Cs sorption is significantly influenced by all three investigated conditions: ionic strength (0.001M, 0.01M, 0.1M), pH (5, 6, 7, 8, and 9), and temperature (25°C, 40°C, and 60°C).

It was observed that at all three temperatures, the R_d values decrease as the background electrolytic concentration increases from 0.001 to 0.1 M, which is likely due to the competition from Na^+ ion for the sorption sites as the ionic strength increases.

Additionally, pH was found to have a significant impact on the Cs distribution coefficients on biotite, with sorption gradually increasing with the increase in pH at all three temperatures However, at the lowest ionic strength (0.001M) and at temperatures of 25, 40, and 60°C, a slight decrease in sorption was observed when pH varied from 7 to 9 (Figs 5-5 (25 °C), 5-6 (40 °C) and 5-7 (60 °C)), but this is possibly within the error margin. Otherwise, there can be an increased sorption at around pH 7 for Cs at lowest ionic strength, but why this should be the case is not clear since the aqueous speciation for Cs is very simple with just the species Cs^+.

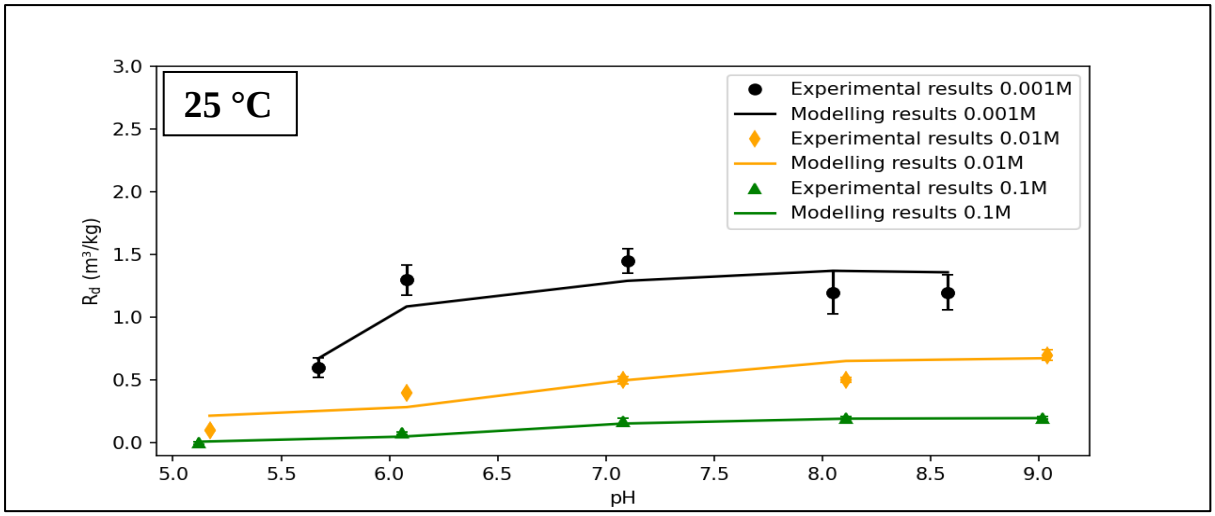

Figure 5- 1: Cs sorption experimental (symbol) and modelling (line) results onto biotite at 25 °C in 0.001M, 0.01M, and 0.1M $NaClO_4$ solution as a function of pH.

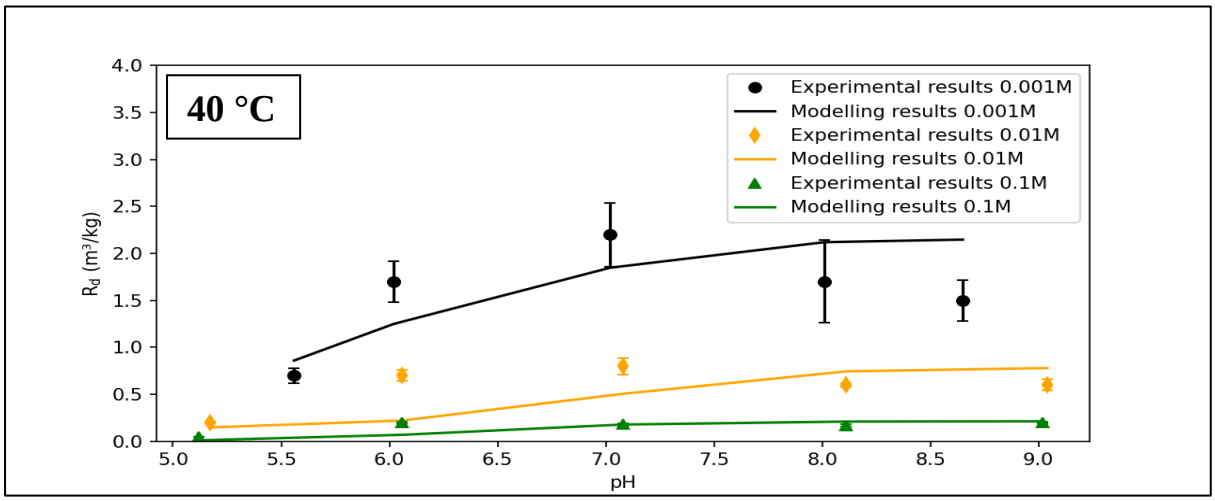

Figure 5-6: Cs sorption experimental (symbol) and modelling (line) results onto biotite at 40 °C in 0.001M, 0.01M, and 0.1M $NaClO_4$ solution as a function of pH.

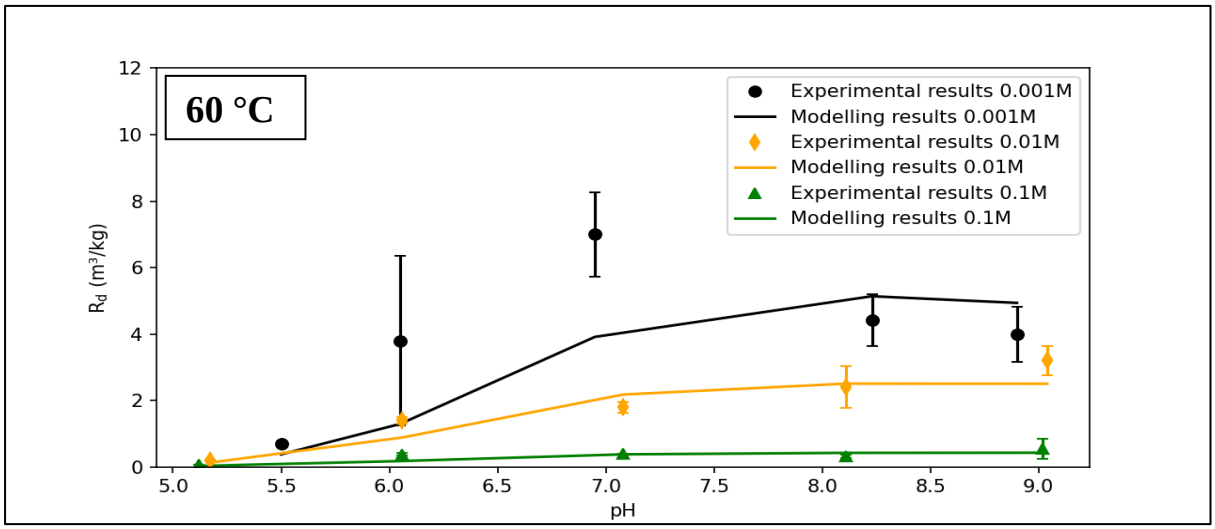

Figure 5-7: Cs sorption experimental (symbol) and modelling (line) results onto biotite at 60 °C in 0.001M, 0.01M, and 0.1M $NaClO_4$ solution as a function of pH.

Furthermore, the experimental findings suggest that the temperature significantly affects Cs sorption, especially at a concentration of 0.001M, where the Cs distribution coefficient increases from 0.6 to 7.8 m^3/kg. For the other two ionic strengths (0.01M and 0.1M), the temperature effect is less pronounced but still detectable.

To model the Cs sorption data, three Cs surface species were used: one ion exchange species, CsX, one surface complexation species, ≡SOCs, a "strong" inner-sphere complex, and one "weak" outer-sphere surface complex, $\equiv SOHCs^+$. However, the weak surface complex $\equiv SOHCs^+$ was later removed from the model since it had a negligible contribution to model fitting to the Cs sorption data.

The modeling speciation results for the lowest background concentration (0.001M) are shown in Figs. 5-8 (25 °C), 5-9 (40 °C), and 5-10 (60 °C), as examples. The outcomes for the other two ionic strengths (0.01M and 0.1M) are detailed in Appendix B.

At all three temperatures, the contribution of Cs sorption from the ion-exchange species was highest at lower temperatures (Fig. 5-8). As the temperature increased from 25°C to 60°C, the contribution of ion exchange decreased, and surface complexation became the dominant sorption mechanism, as illustrated in Figs. 5-8 (25°C), 5-9 (40°C), and 5-10 (60°C).

A similar effect was observed with the increase in ionic strength from 0.001M to 0.1M at all three temperatures. The ion-exchange species had a very high contribution at 0.001M, which decreased to low at 0.01M and became negligible at 0.1M $NaClO_4$, as shown in Appendix B for 25 40 and 60°C. A summary of the implemented surface reactions at the investigated conditions in the modeling are provided in Table 5-2.

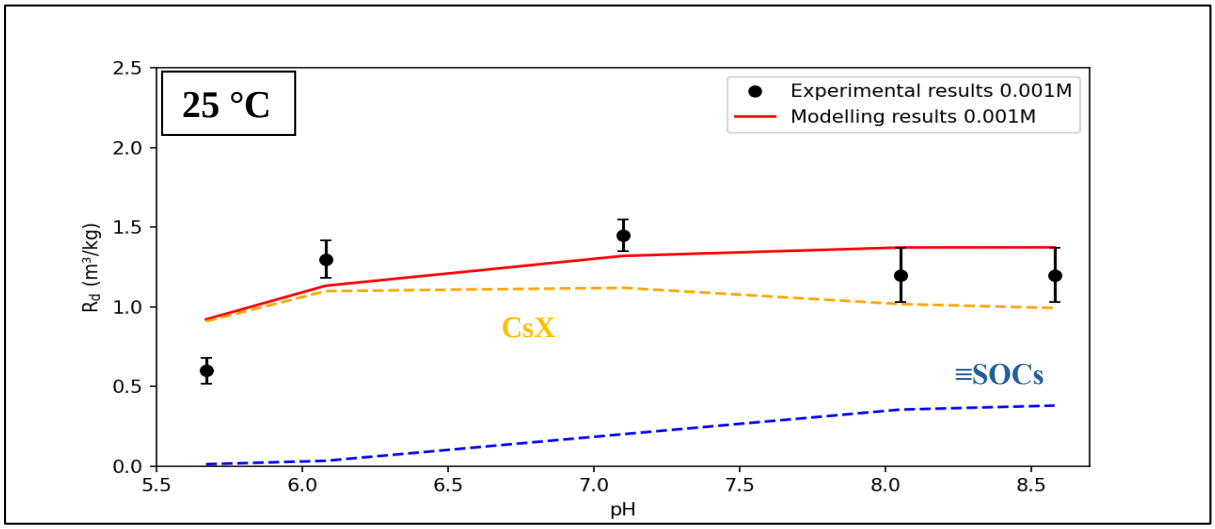

Figure 5-8: An example experimental (symbols) and modelling (continuous lines) results for Cs sorption onto biotite mineral at 25ºC in 0.001 M $NaClO_4$ solution showing the contribution of different Cs species in its sorption: (A: yellow line) CsX; (B: blue line) ≡SOCs

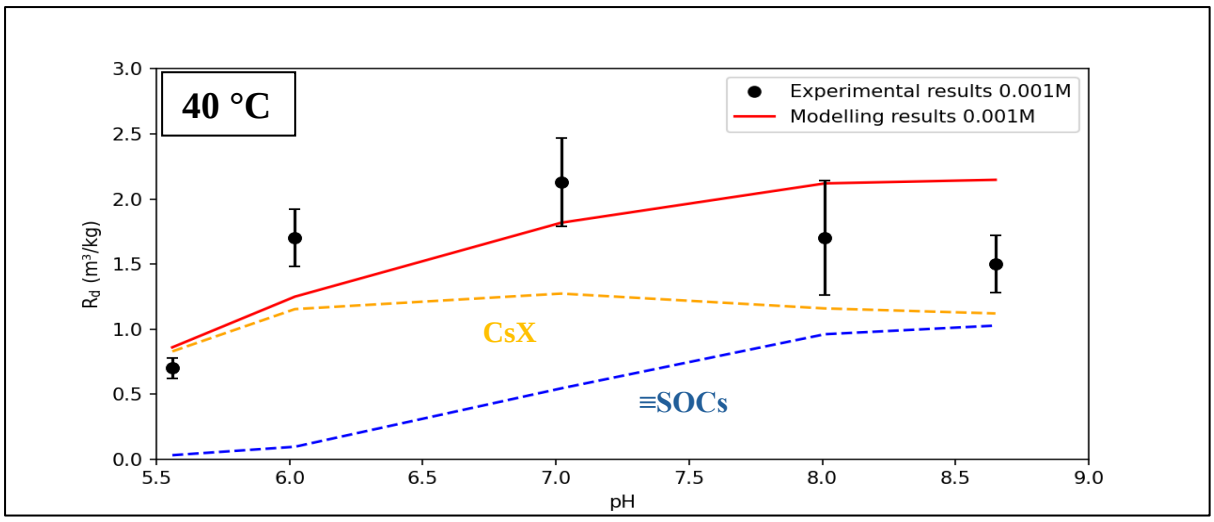

Figure 5-9: An example experimental (symbols) and modelling (continuous lines) results for cesium sorption onto biotite mineral at 40 ºC in 0.01 M $NaClO_4$ solution showing the contribution of different Cs species in its sorption: (A: yellow line) CsX; (B: blue line) ≡SOCs

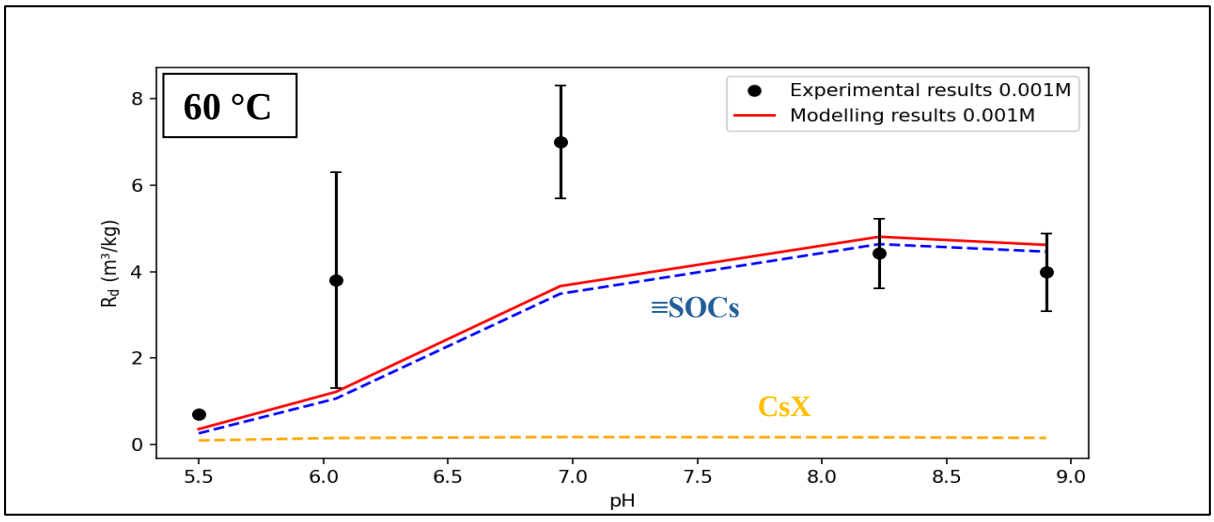

Figure 5-10: An example experimental (symbols) and modelling (continuous lines) results for cesium sorption onto biotite mineral at 60ºC in 0.1 M $NaClO_4$ solution showing the contribution of different Cs species in its sorption: (A: yellow line) CsX; (B: blue line) ≡SOCs

Table 5-2: Modelled surface complexation reactions and associated constants (log k) at zero ionic strength and ion-exchange reactions with selectivity coefficients (log k_{ex}) for Cs at 25, 40, and 60 °C

Reactions	**Log k (25 °C)**	**Log k (40 °C)**	**Log k (60 °C)**
$\equiv SO^- + Cs^+ \rightleftharpoons \equiv SOCs$	4.6 ± 0.2	5.0 ± 0.2	6.2 ± 0.2
$\equiv SOH + Cs^+ \rightleftharpoons \equiv SOHCs^+$	Not significant	Not significant	Not significant
$Cs^+ + NaX \rightleftharpoons CsX + Na^+$	**Log k_{ex}(25 °C)**	**Log k_{ex}(40 °C)**	**Log k_{ex}(60 °C)**
0.001M	1.7	1.8	0.9
0.01M	2.0	1.7	1.0
0.1M	1.5	1.0	0.8

The selectivity coefficients (log k_{ex}) for cation exchange reactions at 25, 40, and 60°C for background electrolytic concentrations of 0.001M, 0.01M, and 0.1M are presented in Table 5-2. Previous studies have shown that the selectivity coefficient changes with ionic strength.

However, the modeling results in this work indicate that the average log k_{ex} values for all ionic strengths are 1.7±0.4 at 25°C, 1.5±0.4 at 40°C, and 0.9±0.1 at 60°C, which means that they are within an acceptable range of standard deviation and thus seemingly independent on ionic strength.

5.3.3. Sorption modelling results for Ba at 25, 40, and 60 °C

Figures 5-11 (25°C), 5-12 (40°C), and 5-13 (60°C) present both experimental and modeling results that illustrate the influence of temperature, ionic strength, and pH on Ba sorption. Detailed Ba sorption data for all three temperatures are provided in the tables in Appendix A.

The experimental findings show that Ba uptake is strongly influenced by both pH (5, 6, 7, 8, and 9) and ionic strength (0.001 M, 0.01 M, and 0.1 M). Similar to Cs, it was observed that at all three temperatures, the amount of Ba sorbed onto the biotite surface decreases as the $NaClO_4$ concentration increases (Figs. 5-11, 5-12, and 5-13). This trend is attributed to the increased competition from Na^+ for sorption sites as ionic strength rises.

Additionally, Ba sorption increases with increased pH across all ionic strengths and temperatures. However, unlike Cs, the temperature was found to have a minimal effect on Ba R_d values, as evidenced by the comparisons in Figs. 5-11 (25°C), 5-12 (40°C), and 5-13 (60°C).

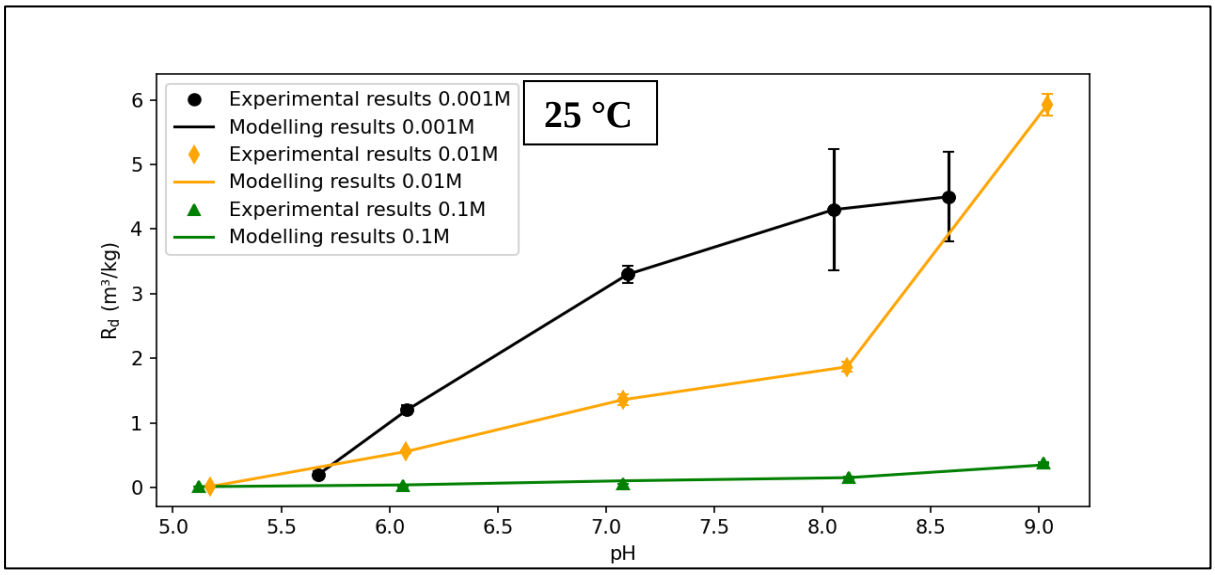

Figure 5-11: Ba(II) sorption experimental (symbol) and modelling (line) results onto biotite at 25 °C in 0.001M, 0.01M, and 0.1M $NaClO_4$ solution as a function of pH.

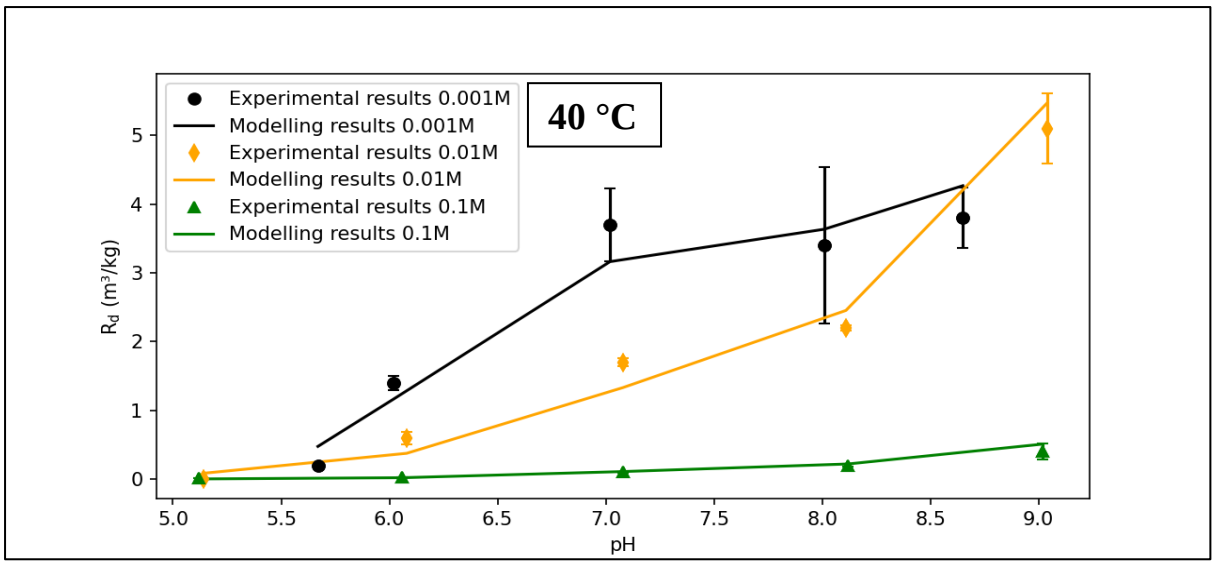

Figure 5-12: Ba(II) sorption experimental (symbol) and modelling (line) results onto biotite at 40 °C in 0.001M, 0.01M, and 0.1M $NaClO_4$ solution as a function of pH.

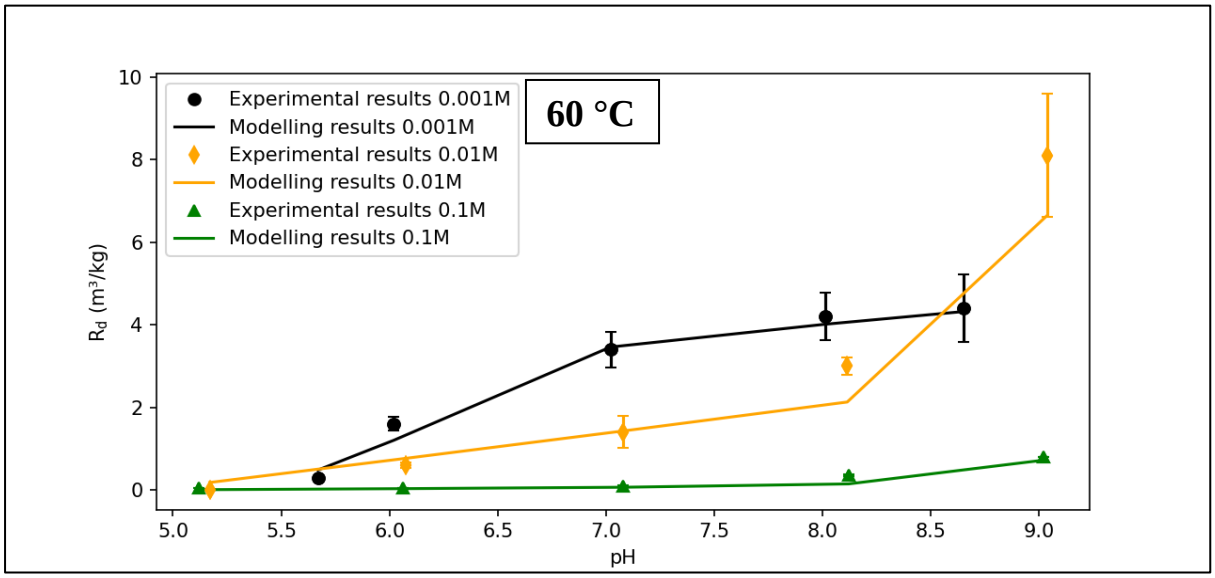

Figure 5-13: Ba(II) sorption experimental (symbol) and modelling (line) results onto biotite at 60 °C in 0.001M, 0.01M, and 0.1M $NaClO_4$ solution as a function of pH.

.

The modeling speciation findings for the lowest ionic strength (0.001M) are presented in an example Figs. 5-14 (25°C), 5-15 (40°C), and 5-16 (60°C). The results for the other two background electrolytic concentrations (0.01M and 0.1M) are available in Appendix B.

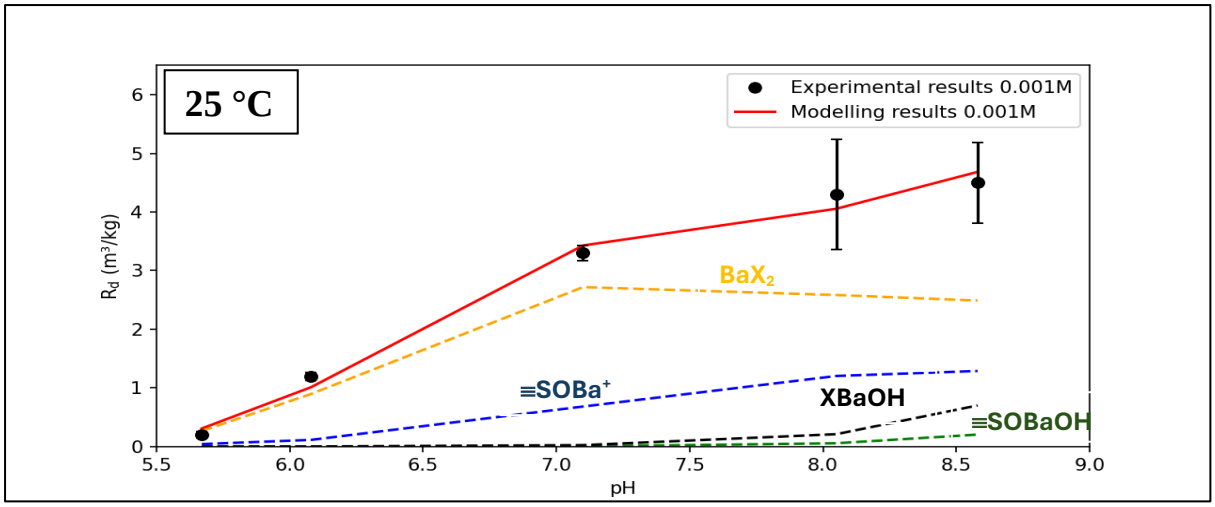

Figure 5-14: An example experimental (symbols) and modelling (continuous lines) results for barium sorption onto biotite mineral at 25ºC in 0.001 M $NaClO_4$ solution showing the contribution of different Ba species in its sorption:(A: Yellow line) BaX_2; (B: Blue line) ≡$SOBa^+$; (C: Green line)) ≡SOBaOH; (D: Black line) XBaOH.

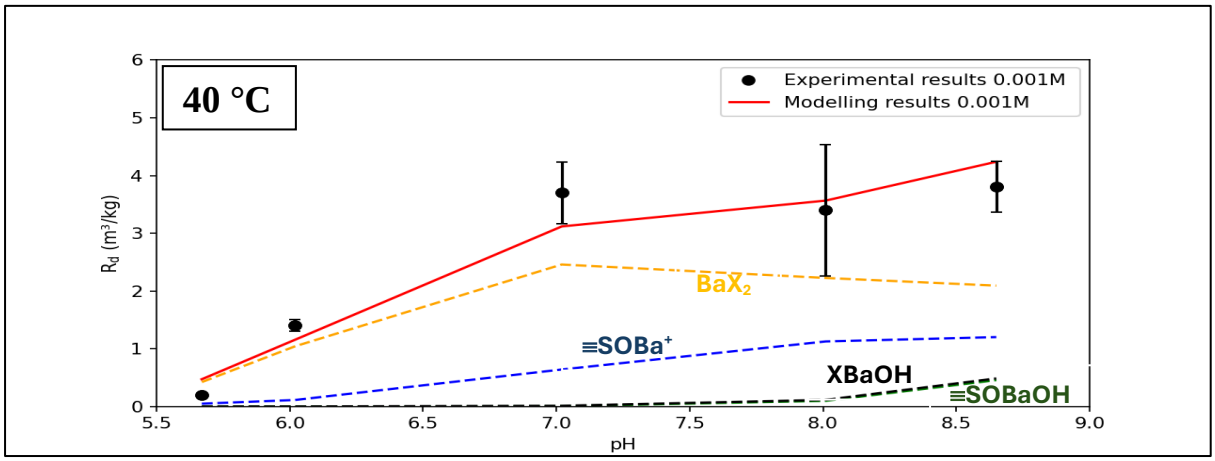

Figure 5-15: An example experimental (symbols) and modelling (continuous lines) results for barium sorption onto biotite mineral at 40ºC in 0.01 M $NaClO_4$ solution showing the contribution of different Ba species in its sorption:(A: Yellow line) BaX_2; (B: Blue line) ≡$SOBa^+$; (C: Green line)) ≡SOBaOH; (D: Black line) XBaOH.

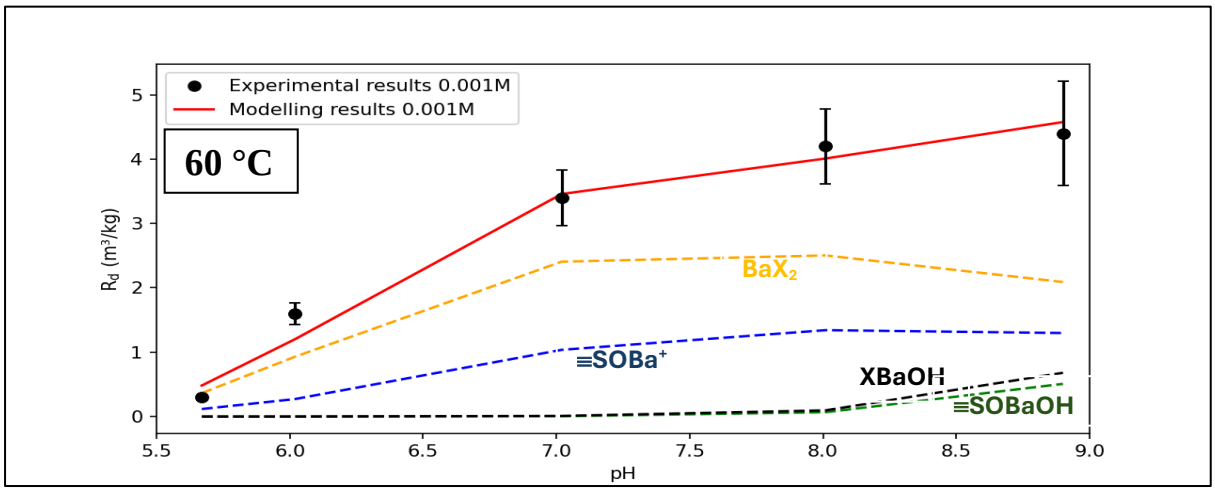

Figure 5-16: An example experimental (symbols) and modelling (continuous lines) results for barium sorption onto biotite mineral at 60ºC in 0.1 M $NaClO_4$ solution showing the contribution of different Ba species in its sorption:(A: Yellow line) BaX_2; (B: Blue line) ≡$SOBa^+$; (C: Green line)) ≡SOBaOH; (D: Black line) XBaOH.

To replicate the Ba sorption data, five surface species were initially included in the model: the ion-exchange species BaX_2 and ≡XBaOH and the surface complexes ≡SOBa$^+$ ("strong" complex), ≡SOHBa^{2+} ("weak" complex), and ≡SOBaOH (a hydrolyzed Ba species). However, just like the case with the Cs sorption modelling, the "weak" surface complex was later removed from the model, as its inclusion did not improve the fit of the sorption data.

The hydrolyzed ion-exchange species, ≡XBaOH, and the surface complex species, ≡SOBaOH, contribute to Ba sorption only at pH levels ranging from 8 to 9. Details of the reactions used in the modeling, along with their corresponding selectivity coefficients and surface complexation constants, are provided in Table 5-3.

As illustrated in Figs. 5-14 (25°C), 5-15 (40°C), and 5-16 (60°C), the ion-exchange species BaX_2 remains the dominant species across the entire pH range (5 to 9) at all three temperatures. It also suggests that Ba sorption on biotite is largely temperature independent, apparently due to that the ion-exchange reaction is dominating sorption at the lowest ionic strength. In contrast, for Cs, the surface complex species ≡SOCs become increasingly dominant as the temperature rises from 25 to 60°C. Based on the modeling results for these two metals together, it can be inferred that ion exchange is not influenced by temperature, whereas surface complexation is temperature dependent.

However, the modeling results also indicate that as the ionic strength increases from 0.001 M to 0.1 M, the contribution of Ba sorption via the ion-exchange mechanism begins to diminish, with surface complexation emerging as the primary mechanism controlling Ba uptake. This shift is likely due to the increased competition from Na^+ ions for sorption sites, as previously explained. This is also reflected in a certain temperature dependency of Ba sorption at the highest ionic strength.

Table 5-3: Modelled Surface complexation reactions and their associated constants (log k) at zero ionic strength and ion-exchange reactions with selectivity coefficients (log k_{ex}) for Ba at 25, 40, and 60 °C

Reaction	**Log k (25 °C)**	**Log k (40 °C)**	**Log k (60 °C)**
$\equiv SO^- + Ba^{2+} \rightleftharpoons \equiv SOBa^+$	5.0 ± 0.2	5.3 ± 0.3	5.9 ± 0.4
$\equiv SO^- + Ba(OH)^+ \rightleftharpoons \equiv SOBaOH$	9.2 ± 0.2	9.3 ± 0.3	9.7 ± 1.1
$\equiv SOH + Ba^{2+} \rightleftharpoons \equiv SOHBa^{2+}$	Not significant	Not significant	Not significant
$Ba^{2+} + 2NaX \rightleftharpoons BaX_2 + 2Na^+$	**Log k_{ex} (25 °C)**	**Log k_{ex} (40 °C)**	**Log k_{ex} (60 °C)**
0.001 M	-0.4	-0.5	-0.6
0.01 M	**0.5**	**0.3**	**0.5**
0.1 M	0.4	-0.5	-1.7
$NaX + BaOH^+ \rightleftharpoons BaOHX + Na^+$	**Log k_{ex} (25 °C)**	**Log k_{ex} (40 °C)**	**Log k_{ex} (60 °C)**
0.001 M	6.5	5.8	5.0
0.01 M	**7.7**	6.7	5.1
0.1 M	7.4	6.0	5.6

In modeling the Ba sorption data, the selectivity coefficients for non-hydrolyzed cation exchange were allowed to vary across all ionic strengths. The optimization results yielded Ba selectivity coefficients with large relative standard deviations, indicating that these coefficients should not be treated as constant over the range of ionic strength investigated. The average log k_{ex} values for ion exchange species BaX_2 at 25, 40, and 60°C are 0.2 ± 0.5, -0.3 ± 0.4, and -0.6 ± 1.1, respectively.

5.3.4. Sorption modelling results for Co at 25, 40, and 60 °C

Figures 5-17 (25°C), 5-18 (40°C), and 5-19 (60°C), present the experimental and modeling results for $NaClO_4$ concentrations of 0.001 M, 0.01 M, and 0.1 M at five different pH values. The complete data sets of R_d values for Co are provided in Appendix A.

The experimental results indicate that Co uptake is significantly influenced by change in pH. However, the effect of ionic strength on Co sorption was found to be minimal, especially when compared to Cs and Ba. At all three temperatures and ionic strengths, the R_d values for Co decreased as the pH decreased, a pattern similar to that observed for Cs and Ba. This behavior is likely due to the increased competition for sorption sites from H^+ ions at lower pH levels. The minimal impact of ionic strength suggests that Co may be sorbing onto the biotite surface primarily through surface complexation, where Na^+ can be expected to not compete.

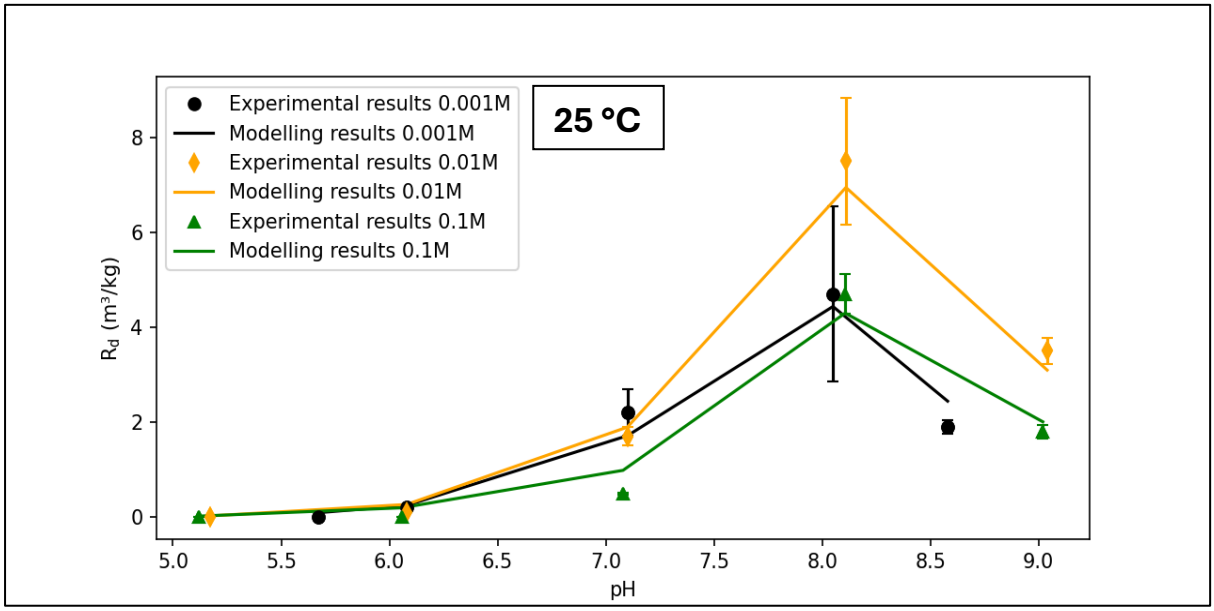

Figure 5-17: Co(II) sorption experimental (symbol) and modelling (line) results onto biotite at 25 °C in 0.001M, 0.01M, and 0.1M $NaClO_4$ solution as a function of pH.

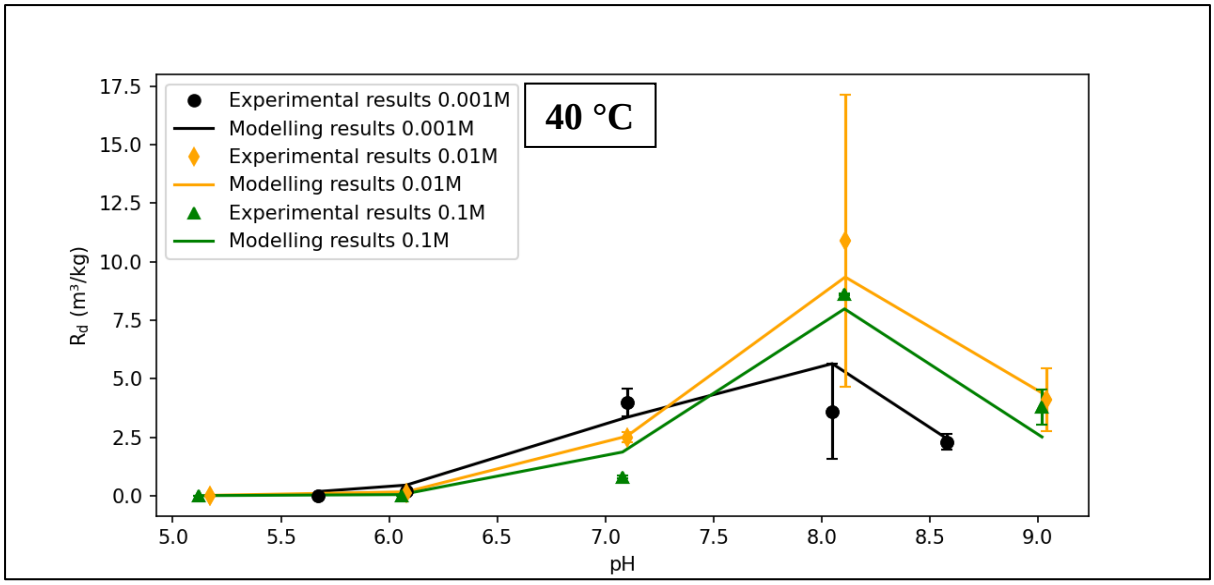

Figure 5-18: Co(II) sorption experimental (symbol) and modelling (line) results onto biotite at 40 °C in 0.001M, 0.01M, and 0.1M $NaClO_4$ solution as a function of pH.

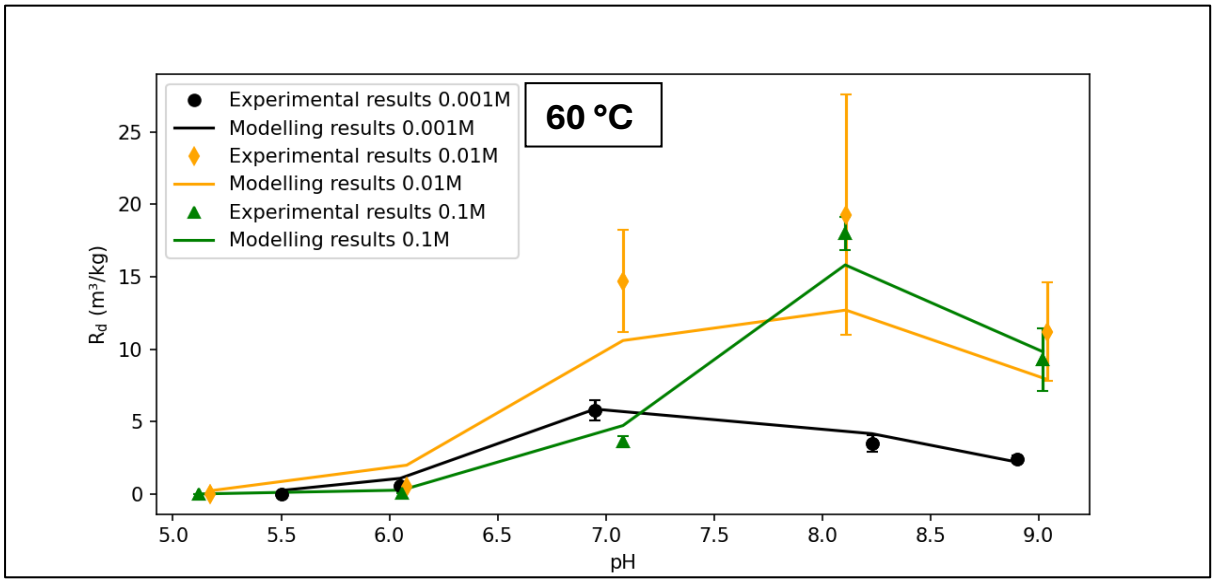

Figure 5-20: Co(II) sorption experimental (symbol) and modelling (line) results onto biotite at 60 °C in 0.001M, 0.01M, and 0.1M $NaClO_4$ solution as a function of pH.

For all temperatures and background electrolyte concentrations, Co uptake increased from pH 6 to 8 and then decreased from pH 8 to 9, as shown in Figs. 5-17, 5-18, and 5-19. The distinct sorption "edge" between pH 6 and 8 indicates that Co uptake is primarily controlled by surface complexation, owing to the abundance of deprotonated sites. Titration results for biotite at 25, 40, and 60°C suggest that the pK_{a2} value is approximately 7 (Table 5-1), where these deprotonated sites becomes more prevalent and thus significantly influence Co sorption at a pH value of around 7.

The similar observations were made in the study by [75] in their work of the effects of ionic strength on cation sorption onto oxide. The sharp increase in sorption signifies that surface complexation, rather than ion exchange, is responsible for Co sorption. However, the decrease in Co sorption at pH values above 8 is likely due to the increased tendency of Co to form

aqueous hydroxide complexes, which, to a certain extent, remain in solution rather than sorbing to the biotite surface. A very strong effect of temperature in Co sorption was seen. The Co R_d values was increasing from 1.86 to 19.3 m^3/kg (for 0.1M $NaClO_4$ see Appendix) with the increase in temperature (from 25 to 60 °C).

Figures 5-20 (25°C), 5-21 (40°C), and 5-22 (60°C) show the modeling speciation results for 0.001 M ionic strength, as an example. Appendix B has a complete summary of the remaining modelling results for the other two ionic strengths (0.01M and 0.1M).

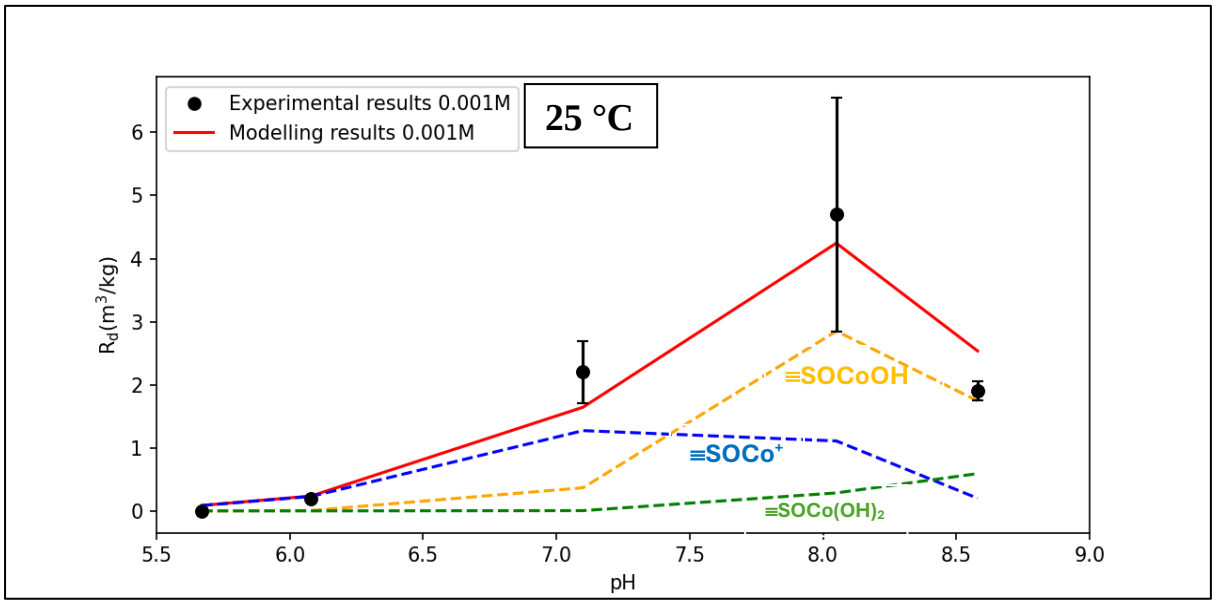

Figure 5-20: An example experimental (symbols) and modelling (continuous lines) results for cobalt sorption onto biotite mineral at 25ºC in 0.001 M $NaClO_4$ solution showing the contribution of different Co species in its sorption: (A: Blue line)≡$SOCo^+$; (B: yellow line)≡SOCoOH; (C: green line) ≡ $SOCo(OH)_2^-$.

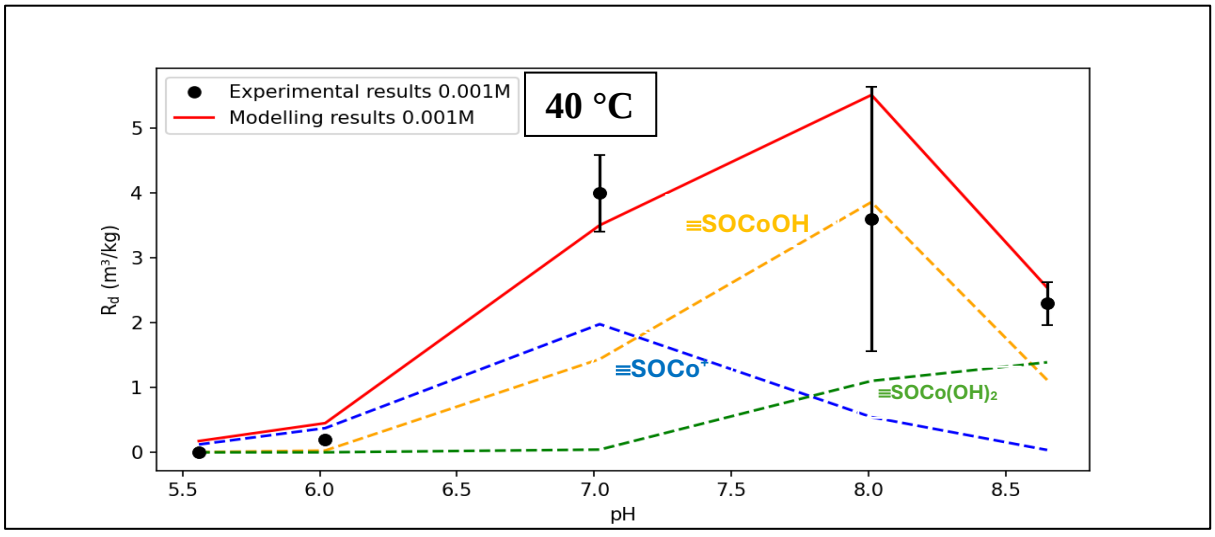

Figure 5-21: An example experimental (symbols) and modelling (continuous lines) results for cobalt sorption onto biotite mineral at 40ºC in 0.01 M $NaClO_4$ solution showing the contribution of different Co species in its sorption: (A: Blue line)≡$SOCo^+$; (B: yellow line)≡SOCoOH; (C: green line) ≡ $SOCo(OH)_2^-$.

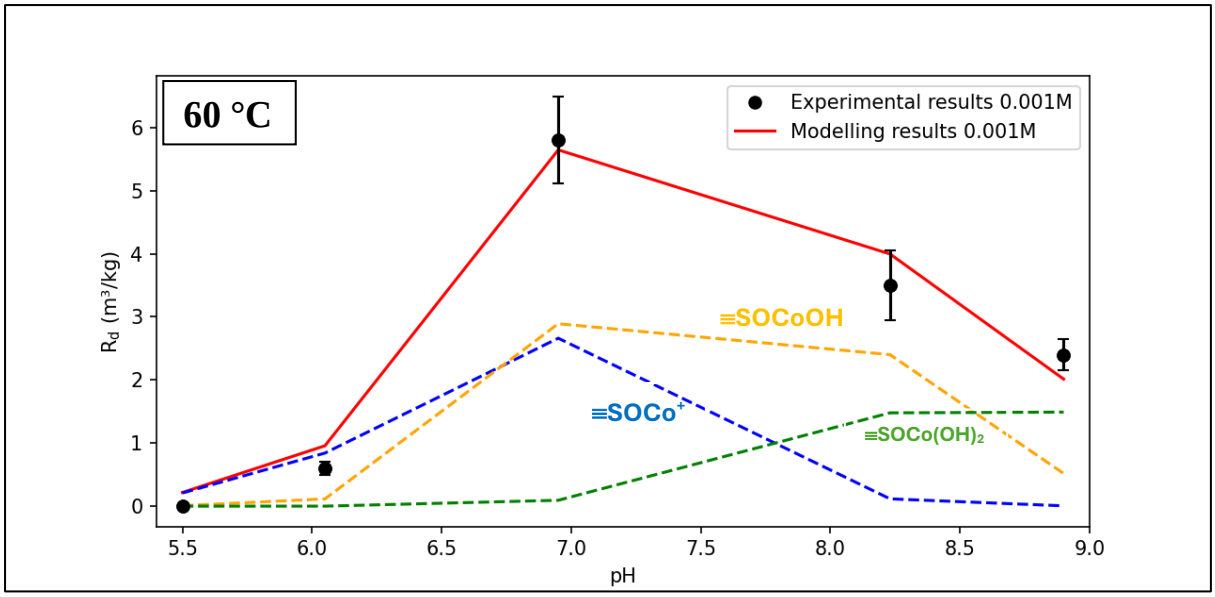

Figure 5-22: An example experimental (symbols) and modelling (continuous lines) results for cobalt sorption onto biotite mineral at 60ºC in 0.1 M $NaClO_4$ solution showing the contribution of different Co species in its sorption: (A: Blue line)≡$SOCo^{+}$; (B: yellow line)≡SOCoOH; (C: green line) ≡ $SOCo(OH)_2^-$.

The modeling of Co sorption data was successfully achieved using three surface complexes (≡$SOCo^{+}$, ≡SOCoOH, ≡$SOCo(OH)_2^-$) and one ion-exchange species (CoX_2). However, both the weak surface complex ≡$SOHCo^{2+}$ and ion-exchange species (CoX_2) were later excluded from model because it did not contribute to improving the model fitment to Co sorption.

The modelling results confirm that surface complexation is the predominant mechanism that governs the Co uptake at all investigated conditions (Figs. 5-20 (25°C), 5-21 (40°C), and 5-2 (60°C)). Which was expected to be the case as explained above for the case of Cs and Ba uptake regarding the correlation between the temperature and its strong influence on surface complexation mechanisms.

The surface complexation constants for the reactions studied at various temperatures and ionic strengths are listed in table 5-4. The optimized constants for these surface complexation reactions were found to be temperature-dependent, increasing with rising temperature. This effect is attributed to the formation of surface complexes (≡$SOCo^{+}$, ≡ SOCoOH, and ≡ $SOCo(OH)_2^-$).

Table 5-4: Modelled Surface complexation reactions and their associated constants (log k) at zero ionic strength for Co at 25, 40, and 60 °C

Reaction	**Log k (25 °C)**	**Log k (40 °C)**	**Log k (60 °C)**
≡ $SO^- + Co^{2+} \rightleftharpoons$ ≡ $SOCo^{+}$	5.4 ± 0.2	5.6 ± 0.4	6.4 ± 0.4
≡ $SO^- + Co(OH)^{+} \rightleftharpoons$ ≡ SOCoOH	7.3 ±0.5	8.0 ±0.7	8.3 ± 1.0
≡ $SO^- + Co(OH)_2 \rightleftharpoons$ ≡ $SOCo(OH)_2^-$	4.8 ±0.3	5.7 ±0.6	6.7 ±1.3
≡ SOH + $Co^{2+} \rightleftharpoons$ ≡ $SOHCo^{2+}$	Not significant	Not significant	Not significant
$Co^{2+} + 2NaX \rightleftharpoons CoX_2 + 2Na^{+}$	Not significant	Not significant	Not significant

5.3.5. Sorption modelling results for Eu at 25, 40, and 60 °C

The Figs. 5-23 (25°C), 5-24 (40°C), and 5-25 (60°C) display the experimental and modeling results for the background electrolytic concentration of 0.001, 0.01, and 0.1 M at 25, 40, and 60 ºC. The complete dataset for all three temperatures and ionic strength are shown in Appendix A.

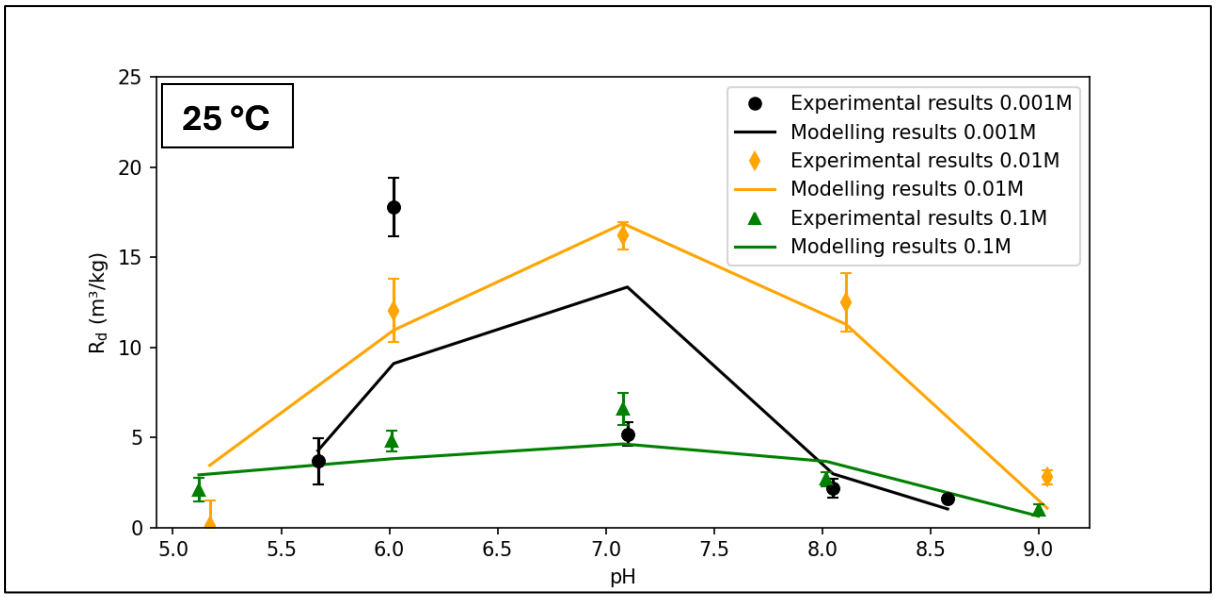

Figure 5-23: Eu(III) sorption experimental (symbol) and modelling (line) results onto biotite at 25 °C in 0.001M, 0.01M, and 0.1M $NaClO_4$ solution as a function of pH.

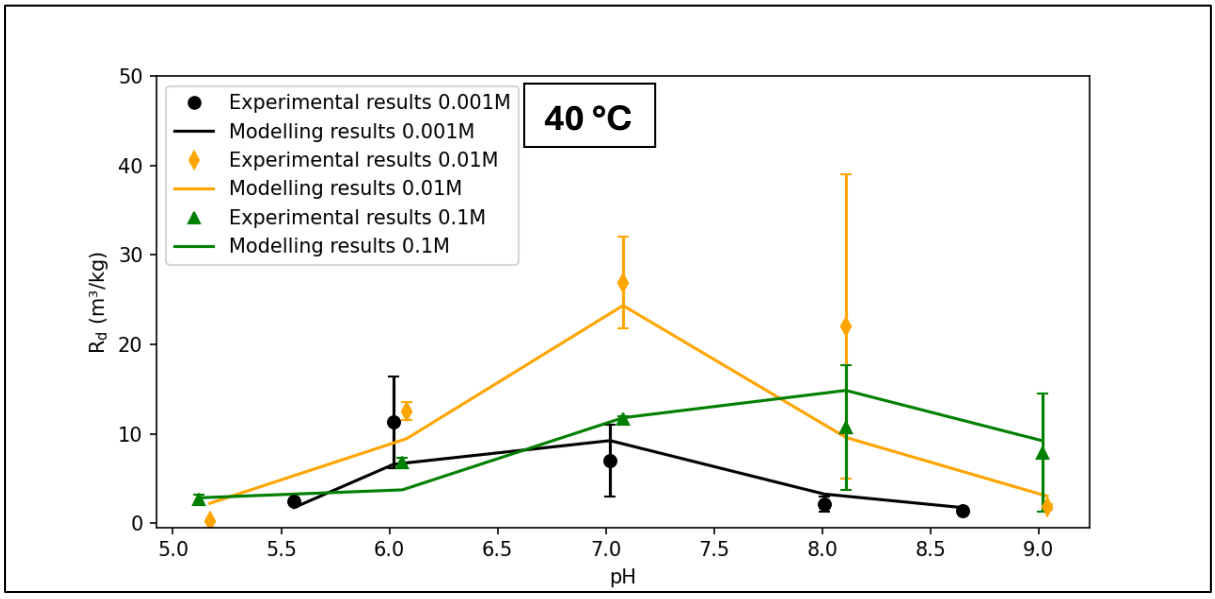

Figure 5-24: Eu(III) sorption experimental (symbol) and modelling (line) results onto biotite at 40 °C in 0.001M, 0.01M, and 0.1M $NaClO_4$ solution as a function of pH.

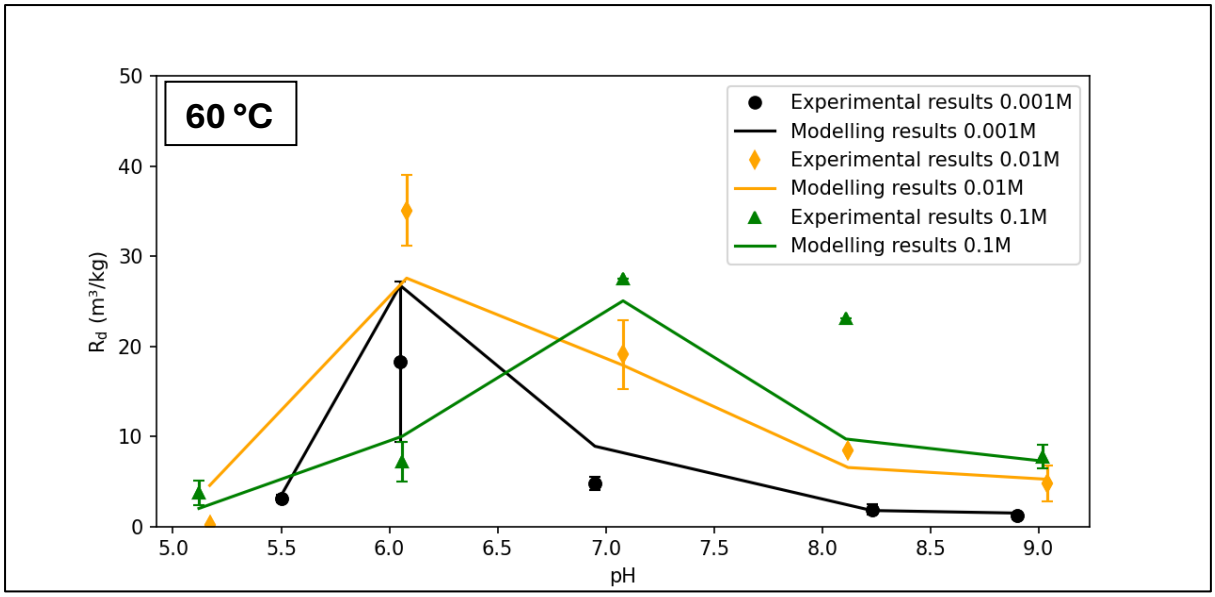

Figure 5-25: Eu(III) sorption experimental (symbol) and modelling (line) results onto biotite at 60 °C in 0.001M, 0.01M, and 0.1M $NaClO_4$ solution as a function of pH.

Similar to Co, Eu sorption was found to be strongly influenced by both pH and temperature variation. However, a certain influence of ionic strength was also seen on Eu sorption, especially at 40 and 60°C, as indicated in the corresponding figures.

The experimental and modeling results show that Eu uptake increases gradually from pH 5 to 7 at 25°C for 0.01 M and 0.1 M $NaClO_4$ (see Appendix), at 40°C across all ionic strengths, and at 60°C for the highest concentration (0.1 M). A similar increase from pH 5 to 6 was observed at 25°C for the lowest ionic strength and at 60°C for 0.001 M and 0.01 M $NaClO_4$. However, beyond pH 7, Eu uptake begins to decline as pH rises to 9 under all conditions. This decline is likely due to Eu's tendency to form aqueous hydrolysis complexes.

The temperature significantly enhances Eu sorption, increasing the R_d value from approximately 2.76 to 35.1 m^3/kg in a 0.01 M $NaClO_4$ solution. Given the pronounced effect of temperature and the limited impact of ionic strength, the results of Eu sorption, when compared to those of the other three elements, indicate that Eu is likely to be sorbing mainly through surface complexation. However, at the lowest ionic strength and temperature some contribution from ion exchange of Eu can be expected.

Figures 5-26 (25°C), 5-27 (40°C), and 5-28 (60°C) show the modeling speciation results for 0.001 M ionic strength, as an example. Appendix B has a complete summary of the remaining modelling results for the other two ionic strengths (0.01M and 0.1M).

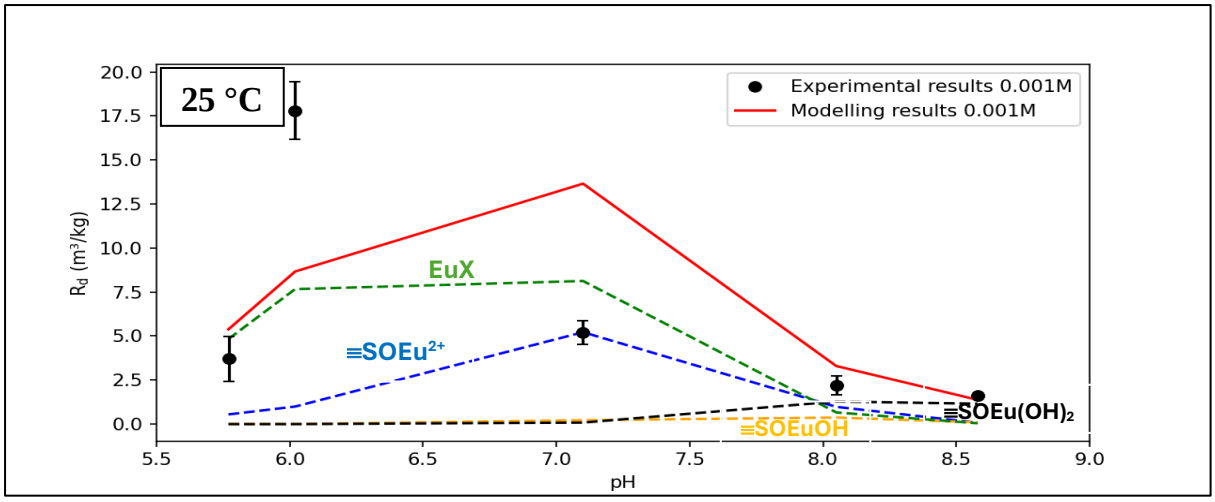

Figure 5-26: An example experimental (symbols) and modelling (continuous lines) results for europium sorption onto biotite mineral at 25ºC in 0.001 M $NaClO_4$ solution showing the contribution of different Eu species in its sorption: (A: blue line) ≡ $SOEu^{2+}$; (B: yellow line) ≡ $SOEu(OH)^{+}$; (C: green line) EuX_3; (D: black line) ≡ $SOEu(OH)_2$

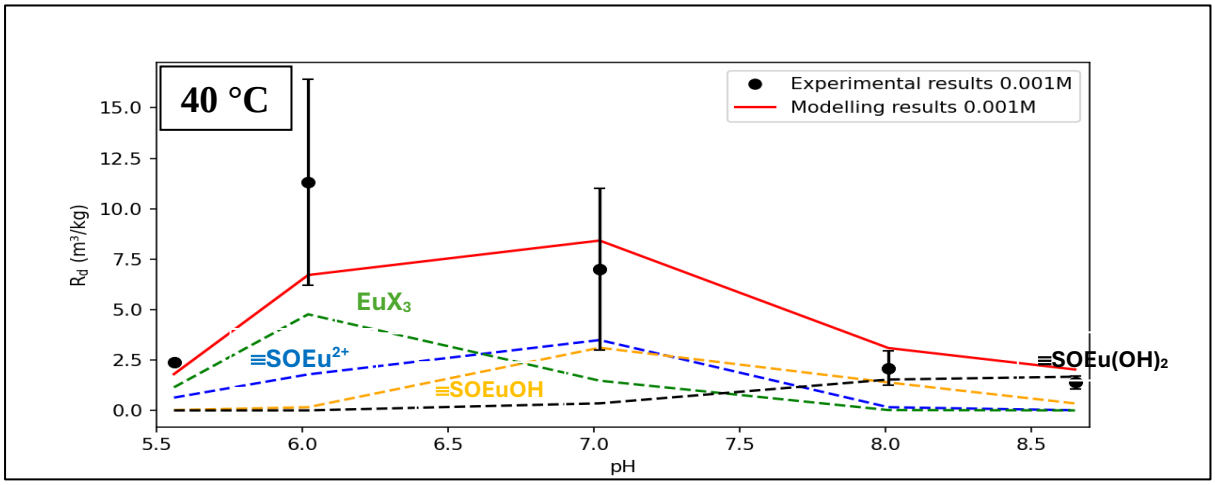

Figure 5-27: An example experimental (symbols) and modelling (continuous lines) results for europium sorption onto biotite mineral at 40ºC in 0.01 M $NaClO_4$ solution showing the contribution of different Eu species in its sorption: (A: blue line) ≡ $SOEu^{2+}$; (B: yellow line) ≡ $SOEu(OH)^{+}$; (C: green line) EuX_3; (D: black line) ≡ $SOEu(OH)_2$

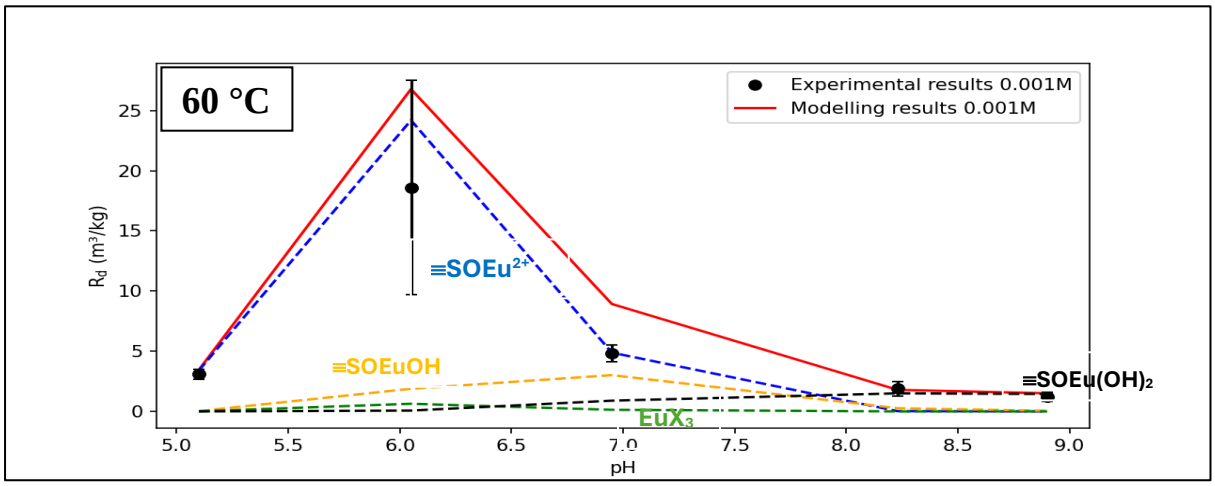

Figure 5-28: An example experimental (symbols) and modelling (continuous lines) results for europium sorption onto biotite mineral at 60ºC in 0.1 M $NaClO_4$ solution showing the contribution of different Eu species in its sorption: (A: blue line) ≡ $SOEu^{2+}$; (B: yellow line) ≡ $SOEu(OH)^{+}$; (C: green line) EuX_3; (D: black line) ≡ $SOEu(OH)_2$

To fit the Eu sorption data across all three temperatures (25°C, 40°C, and 60°C) and ionic strengths (0.001 M, 0.01 M, and 0.1 M), three surface complexation species were considered: $\equiv SOEu^{2+}$, $\equiv SOEu(OH)^{+}$, $\equiv SOEu(OH)_2$, and the exchange species EuX_3.

Although a weak surface complex ($\equiv SOHEu^{+}$) was also considered, it was excluded from the modeling due to its negligible effect on data fitting.

Modeling results indicate that at 25°C (Fig. 5-26) and for all ionic strengths, Eu sorption is primarily dominated by the ion-exchange species EuX_3 from pH 5 to 6. Around pH 7, both the ion-exchange species EuX_3 and the surface complex $\equiv SOEu^{2+}$ influence the sorption. Beyond pH 7, the sorption is mainly controlled by the surface complex $\equiv SOEu(OH)^{+}$.

At higher temperatures the ion exchange species gradually diminishes in importance and surface complexation dominates sorption.

At 60°C (Fig. 5-28), Eu uptake around pH 6 is predominantly due to the surface complex $\equiv SOEu^{2+}$, which appears to be favored over other surface species at this elevated temperature. Table 5-5 presents the surface complexation constants and selectivity coefficients for the four species: $\equiv SOEu^{2+}$, $\equiv SOEu(OH)^{+}$, $\equiv SOEu(OH)_2$, and EuX_3. The increase in surface complexation constants with temperature indicates a greater favorability of these surface complexes at higher temperatures. The selectivity coefficients were allowed to vary with changes in ionic strength and temperature. As with Ba, these coefficients were not constant over the ionic strength range investigated and the average values exhibited a large standard deviation.

Table 5-5: Modelled Surface complexation reactions and their associated constants (log k) at zero ionic strength and ion-exchange reactions with selectivity coefficients (log k_{ex}) for Eu at 25, 40, and 60 °C

Reaction	**Log k (25 °C)**	**Log k (40 °C)**	**Log k (60 °C)**
$\equiv SO^- + Eu^{3+} \rightleftharpoons \equiv SOEu^{2+}$	6.2 ± 0.2	6.5 ± 0.8	8.1 ± 0.2
$\equiv SO^- + Eu(OH)^{2+} \rightleftharpoons \equiv SOEu(OH)^{+}$	6.2 ± 0.9	6.9 ± 1.3	8.1 ± 1.2
$\equiv SO^- + Eu(OH)_2^{+} \rightleftharpoons \equiv SOEu(OH)_2$	5.3 ± 0.3	5.6 ± 1.2	6.6 ± 1.2
$\equiv SOH + Eu^{3+} \rightleftharpoons \equiv SOHEu^{2+}$	Not significant	Not significant	Not significant
$Eu^{3+} + 3NaX \rightleftharpoons EuX3 + 3Na^{+}$	**Log k_{ex} (25 °C)**	**Log k_{ex} (40 °C)**	**Log k_{ex} (60 °C)**
0.001M	-2.6	-2.7	-2.9
0.01M	0.5	0.3	-0.2
0.1M	3.3	3.3	2.1

5.3.6. Sorption modelling results for Ra at 25°C

Figure 5-29 shows the experimental and modeling results for Ra sorption onto biotite. The data demonstrated that pH and ionic strength had a substantial influence on Ra sorption. Ra sorption was found to rise continuously from pH 5 to pH 8, regardless of background electrolytic concentration. At pH values greater than 8, Ra sorption increased significantly, most likely due

to the formation and sorption of Ra hydroxyl species (Fig. 5-29). Ra's sorption behavior was discovered to be comparable to that of Ba, as seen above.

There was, however, some difference in R_d-values between Ra and Ba since it was observed that. Ra distribution co-efficient at 0.001M was found to be nearly twice as large as that for Ba ($R_{d\ Ba} = \sim 4$ and $R_{d\ Ra} = \sim 8$). Similar results were reported in [31] a study on the sorption of alkaline earth metals onto biotite. One possible reason is that Ra has a slightly lower hydration energy, and a larger ionic radius (152 Å) compared to Ba (135 Å) [76], which may account for Ra's greater sorption affinity relative to Ba.

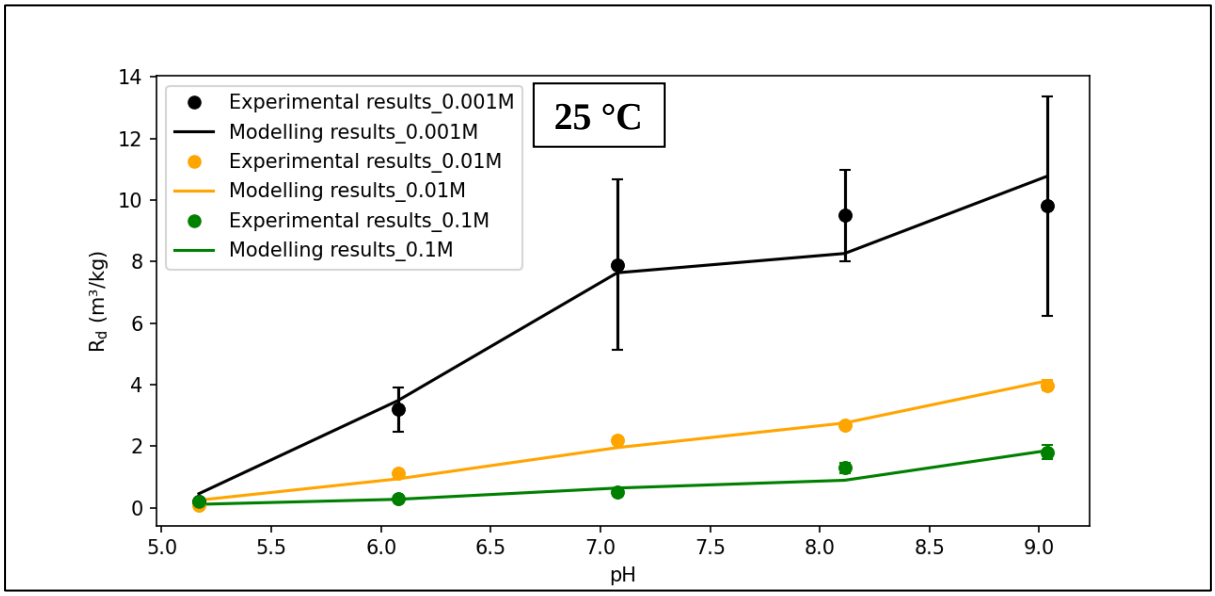

Figure 5-29: An example of Ra(II) sorption experimental (symbol) and modelling (line) results onto biotite at 25 °C in 0.001M, 0.01M, and 0.1M $NaClO_4$ solution as a function of pH.

Similar to Ba, the Ra sorption data was modeled by implementing three surface complexes (≡SORa$^+$, ≡SORaOH, and ≡SOHRa^{2+}) and two cation exchange (RaX_2 and RaOHX) species as depicted in an example Fig. 5-30. The ≡SOHRa^{2+} weak surface complex was initially included in the model but was later removed as it had no significant impact on the fit. The modeling results indicate that Ra sorption is primarily governed by ion exchange (RaX_2) across the pH range of 5 to 9 at a background electrolyte concentration of 0.001 M, with some contribution from the ≡SORa$^+$ surface complex. On the other hand, both RaOHX and ≡SORaOH surface species seem to be involved in Ra sorption at higher pH levels (8 to 9). This behavior is similar to what was found for Ba sorption.

Furthermore, the modeling suggests that as the background electrolytic concentration increases from 0.001 M to 0.1 M, surface complexation took over as a dominant mechanism governing Ra sorption, as shown in Fig. 13 in Appendix B. The corresponding reactions and their constants are provided in Table 5-6.

Table 5-6: Modelled Surface complexation reactions and their associated constants (log k) at zero ionic strength and ion-exchange reactions with selectivity coefficients (log k_{ex}) for Ra at 25, 40, and 60 °C

Reaction	**Log k (25 °C)**
$\equiv SO^- + Ra^{2+} \rightleftharpoons \equiv SORa^+$	5.4 ± 0.2
$\equiv SO^- + Ra(OH)^+ \rightleftharpoons \equiv SORaOH$	9.4 ±0.5
$\equiv SOH + Ra^{2+} \rightleftharpoons \equiv SOHRa^{2+}$	Not significant*
$Ra^{2+} + 2RaX \rightleftharpoons RaX_2 + 2Na^+$	**Log k_{ex} (25 °C)**
0.001 M	-0.1
0.01 M	1.0
0.1 M	2.4
$NaX + RaOH^+ \rightleftharpoons RaOHX + Na^+$	**Log k_{ex} (25 °C)**
0.001 M	6.5
0.01 M	7.0
0.1 M	7.7

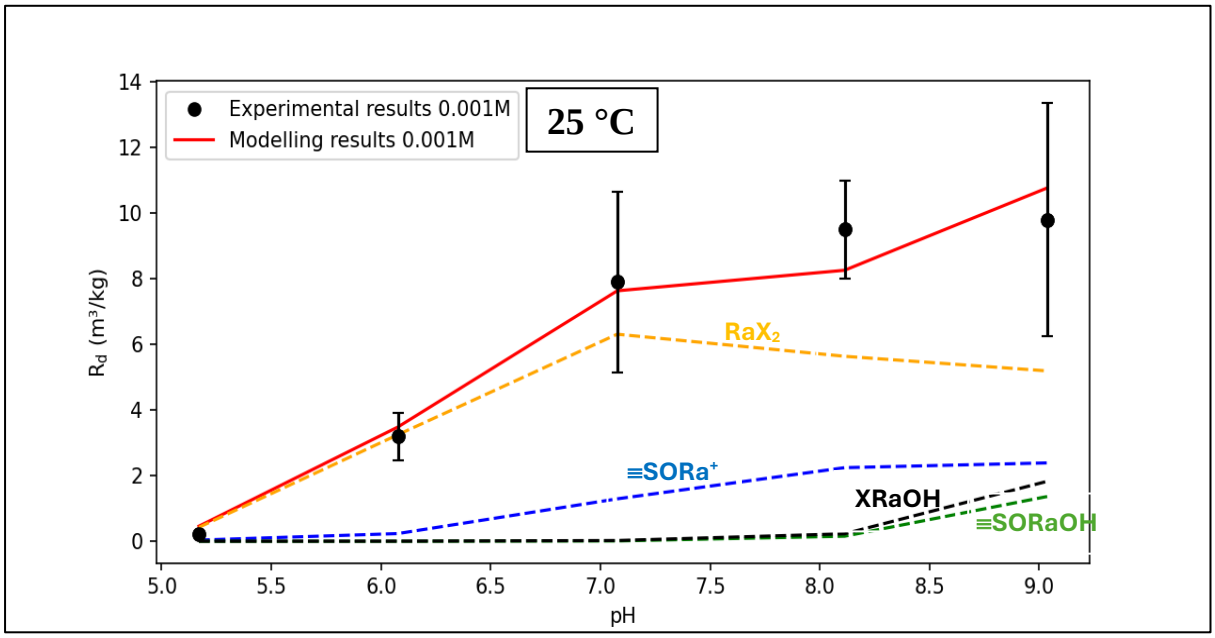

Figure 5-30: An example of Experimental (symbol) and modelling (continuous line) results for Ra sorption onto biotite in 0.001 M $NaClO_4$ solution at 25 °C. The contribution of different Ra(II) species in its sorption is represented by different curves:(A: Yellow line) RaX_2; (B: Blue line) $\equiv SORa^+$; (C: Green line)) ≡SORaOH; (D: Black line) XRaOH

5.3.7. Sorption modelling results for Am at 25°C

The results of the Am(III) sorption experiments at 25°C and modeling are shown in Fig. 5-31.

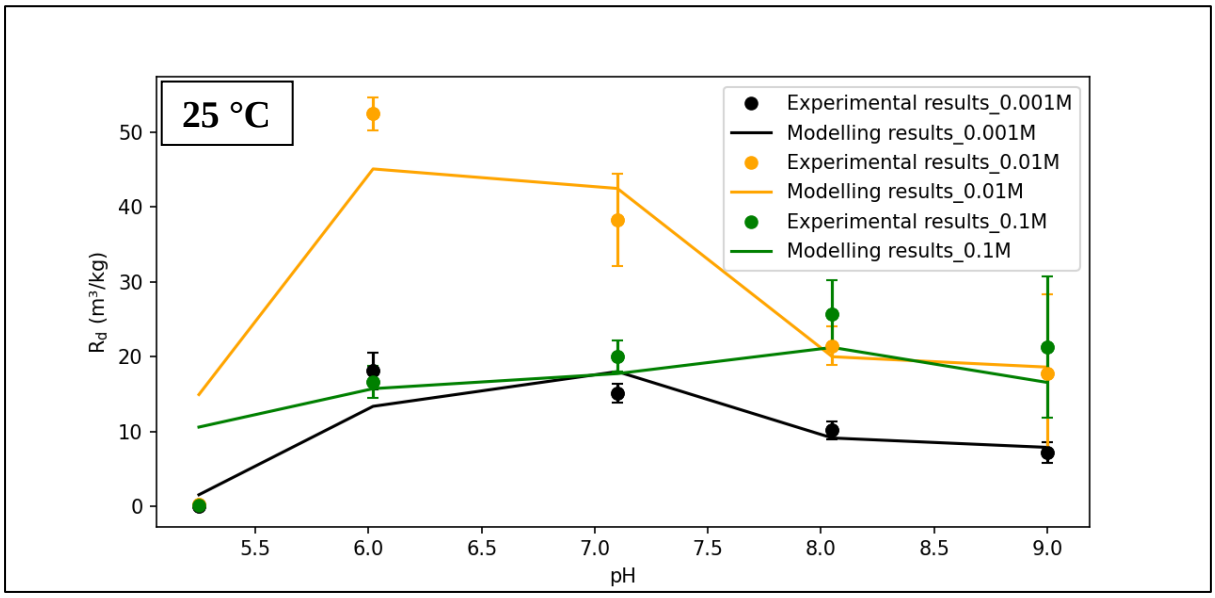

Figure 5-31: Am(II) sorption experimental (symbol) and modelling (line) results onto biotite at 25 °C in 0.001M, 0.01M, and 0.1M $NaClO_4$ solution as a function of pH.

The results show that Am sorption is strongly pH-dependent but also influenced by ionic strength. For the middle ionic strength sorption increased sharply between pH 5 and 6, followed by a gradual decline as pH rose to 9. This decrease in sorption at higher pH levels (above pH 6) is likely due to the formation of aqueous Am hydroxide complexes, a behavior that is consistent across all ionic strengths tested (0.001 M, 0.01 M, and 0.1 M). The sorption behavior of Am(III) closely resembles that of Eu(III), as depicted earlier in Fig. 5-23 at 25°C. This similarity can be attributed to their comparable ionic radii (Am^{3+} = 98 pm, Eu^{3+} = 94.7 pm) and analogous electronic configurations (Am: [Rn] $5f^7$ $7s^2$ and Eu: [Xe] $4f^7$ $6s^2$).

There was one notable difference in the R_d-values between Am and Eu however, since Am showed maximum R_d-values approximately three times higher (52.3 m^3/kg) than Eu (18.5 m^3/kg). One may also note that sorption is strongest for the middle ionic strength for both Eu and Am.

A previous study on Am sorption onto biotite [77] reported R_d-values comparable to this work around 10-30 m^3/kg at pH 6-7. This is consistent with the present study.

Am, like Eu, forms several hydrolysis products within the pH range of 5 to 9, as shown in Figure 5-32. Below pH ~7, the dominant species is Am^{3+}. However, at pH levels above ~7, Am^{3+} undergoes hydrolysis, leading to the formation of $AmOH^{2+}$ and $Am(OH)_2^+$ aqueous species. These hydrolyzed species must be considered during the optimization process, particularly when modeling sorption behavior in the pH range between 5 and 9.

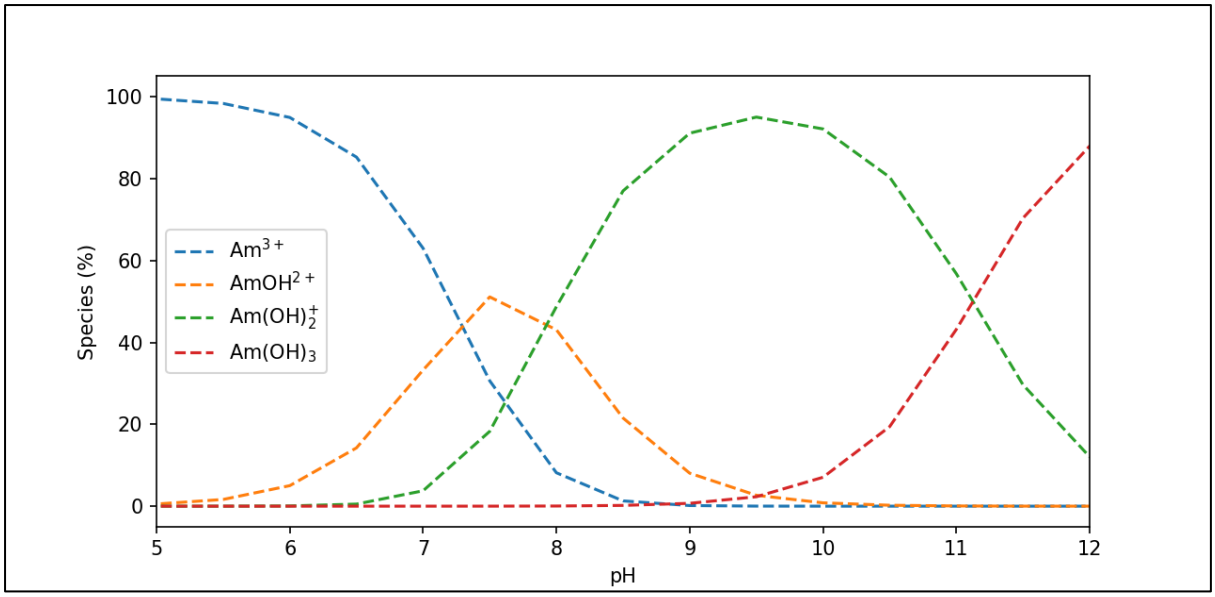

Figure 5-32: The aqueous speciation curve of Am as a function of pH

To successfully model Am sorption onto biotite at all three $NaClO_4$ concentrations (0.001 M, 0.01 M, and 0.1 M), three surface complexation species were considered $\equiv SOAm^{2+}$,$\equiv SOAm(OH)^{+}$, and $\equiv SOAm(OH)_2$. Additionally, one ion-exchange species, AmX_3, was included. Other potential species, such as $\equiv SOAm(OH)_3^-$ and $\equiv SOHAm^{3+}$ were excluded from the model after their contribution to model Am sorption was found to be negligible.

The modeling results, illustrated in Fig. 5-33, indicate that ion exchange (AmX_3) is the primary mechanism driving Am sorption in the pH range of approximately 6 to 7 across all ionic strengths (0.001 M, 0.01 M, and 0.1 M). Around pH 7, the $\equiv SOAm^{2+}$ species plays a modest role in sorption. However, at higher pH levels (above 8), Am sorption is predominantly governed by the hydroxylated species $\equiv SOAm(OH)_2$ and $\equiv SOAm(OH)^{+}$. Complete modeling results for Am sorption are provided in Appendix B (Fig. 14), while Table 5-7 lists all relevant reactions along with their corresponding cation exchange and surface complexation constants.

Table 5-7: Surface complexation and cation exchange reactions, along with their corresponding constants at zero ionic strength (log_k°) for Am. The selectivity coefficients apply to the specified ionic strength.

Reactions	**log k (25 °C)**
$\equiv SO^- + Am^{3+} \rightleftharpoons \equiv SOAm^{2+}$	6.1 ± 0.2
$\equiv SO^- + Am(OH)^{2+} \rightleftharpoons \equiv SOAm(OH)^{+}$	6.4 ± 0.7
$\equiv SO^- + Am(OH)_2^{+} \rightleftharpoons \equiv SOAm(OH)_2$	6.2 ± 0.4
$\equiv SOH + Am^{3+} \rightleftharpoons \equiv SOHAm^{3+}$	Not significant

Reaction/Ionic Strength at 25 °C	**0.001 M**	**0.01 M**	**0.1 M**
$Am^{3+} + 3NaX \rightleftharpoons AmX_3 + 3Na^{+}$	log_k_{ex} = -2.2	log_k_{ex} = 1.1	log_k_{ex} = 4.0

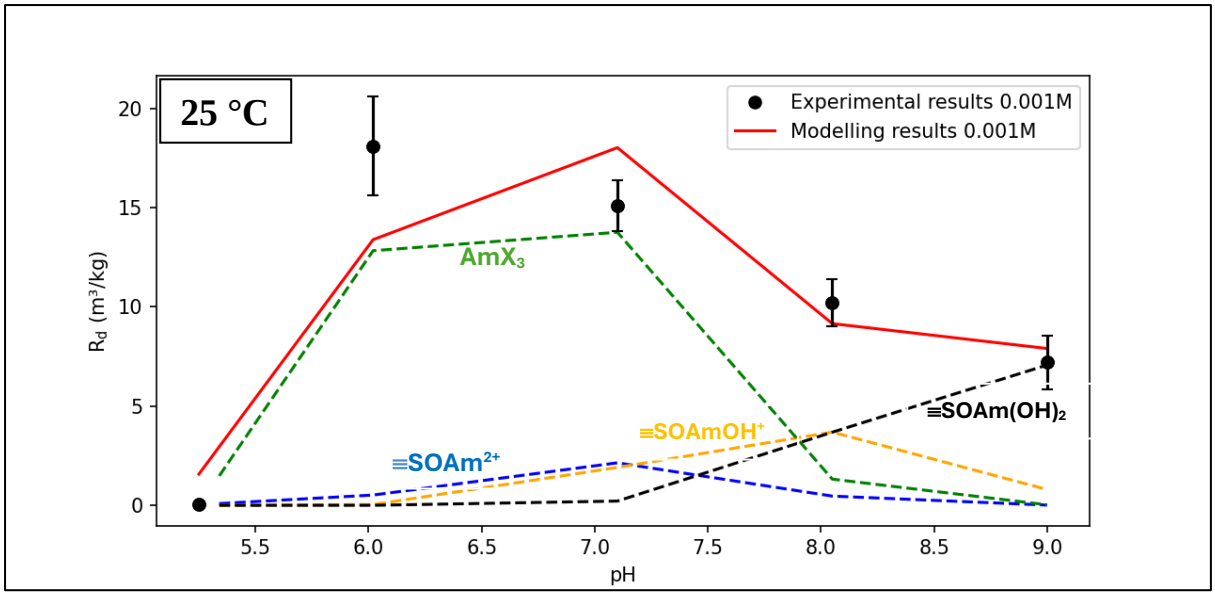

Figure 5-33. An example of Am sorption experimental (symbol) and modelling (continuous line) results on biotite in 0.001 M $NaClO_4$ solution at 25 °C . The contribution of different Am(III) species in its sorption is represented by different curves: (A: blue line) $\equiv SOAm,^{2+}$; (B: yellow line) $\equiv SOAm(OH)^{+}$; (C: green line) AmX_3; (D: black line). $\equiv SOAm(OH)_2$

5.4 Thermodynamic parameters

The equilibrium constants (log k) for the Cs, Ba, Co, and Eu radiotracers were determined at three different temperatures 25, 40 and 60°C. A linear relationship was observed when plotting log K against 1/T, with the slope corresponding to $-\Delta H^o/R$ and the intercept corresponding to $\Delta S^o/R$ as depicted in Fig. 5-34. The enthalpy and entropy values remain constant across the temperature range studied (25, 40, and 60 °C) with good linearity of the van´t Hoff equation (Eq. 23), see Fig 5-34.

Table 5-8 provides the values of ΔH^o and ΔS^o for the sorption reactions of all radiotracers, derived from the previously mentioned surface complexation constants and ion-exchange coefficients. Although variations of the latter were seen with the change of ionic strength for all elements except Cs, average values were used for the evaluation of the enthalpy and entropy parameters.

Table 5-8: Thermodynamic parameters for the sorption of cesium, barium, cobalt, and europium onto biotite

Surface complex/ion-exchange species for elements	ΔH^0 (**kJ mol^{-1}**)	ΔS^0(**JK^{-1}mol^{-1}**)
Cesium		
≡SOCs	38.1±0.9	165.1±0.9
CsX	–18.6±0.9	– 47.9±0.9
Barium		
≡ SOBa$^+$	20.9±0.9	111.6±0.9
≡ SOBaOH	12.4±0.9	117.6±0.9
BaX_2	–6.3±0.9	–16.71±0.9
XBaOH	–46.1±0.9	–95.4±0.9
Cobalt		
≡ SOCo$^+$	22.6±0.9	119.9 ±0.9
≡ SOCoOH	23.5±0.9	140.4 ±0.9
≡ $SOCo(OH)_2^-$	45.3±1.0	191.8±1.0
Europium		
≡ SOEu^{2+}	8.3±0.9	76.4±0.9
≡ SOEuOH$^+$	43.0 ±0.8	195.6±0.8
≡ $SOEu(OH)_2$	32.2±0.9	150.9±0.9
EuX_3	–9.6±0.9	–28.7 ±0.9

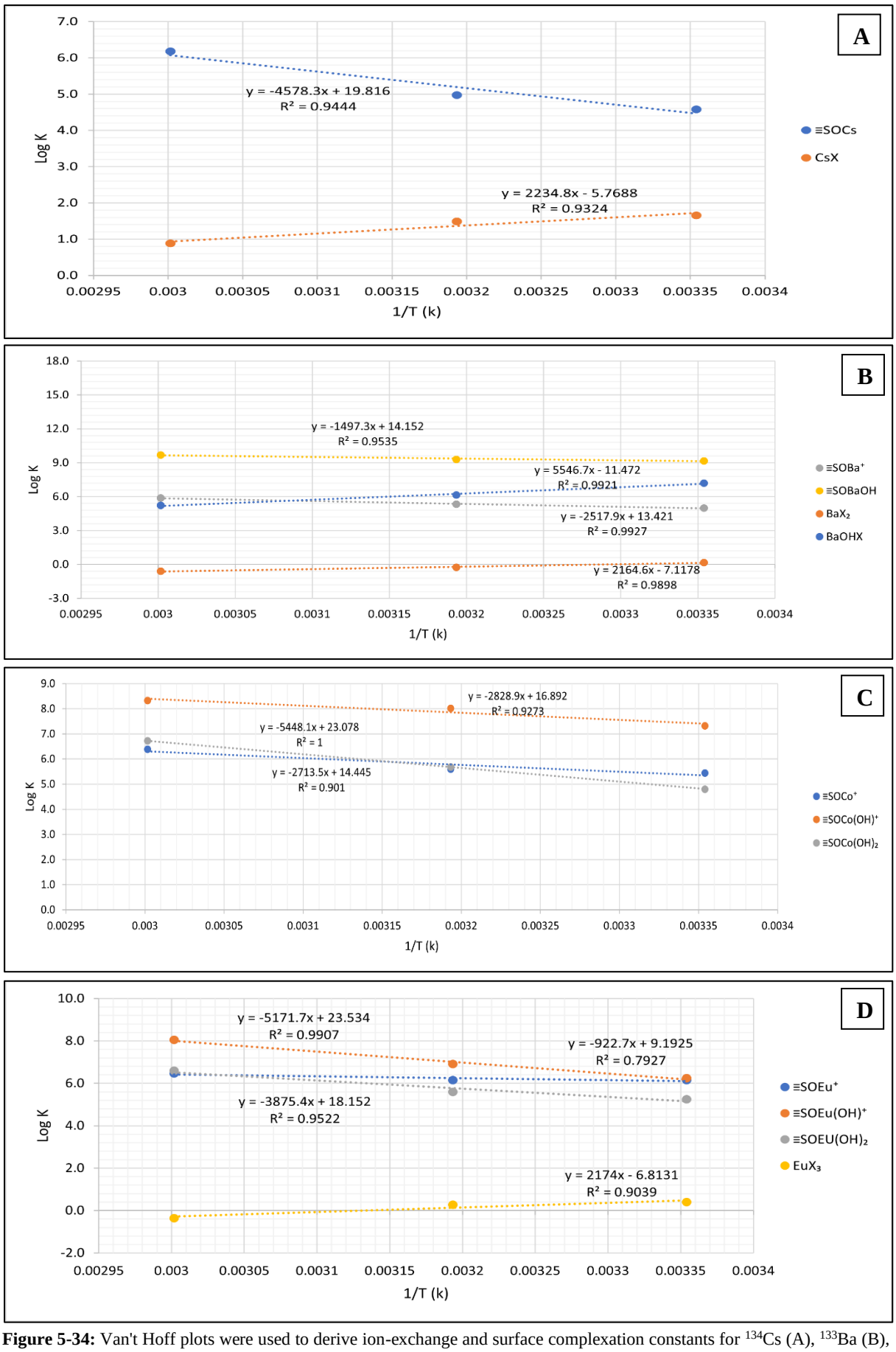

Figure 5-34: Van't Hoff plots were used to derive ion-exchange and surface complexation constants for ^{134}Cs (A), ^{133}Ba (B), ^{60}Co (C) and ^{152}Eu (D). The enthalpy of the sorption reactions was determined using the slopes of the correlation

The enthalpy of sorption for ≡SOCs was 38.1±0.9 kJ/mol. For Ba, the sorption enthalpy values were 20.9±0.9 for ≡ $SOBa^+$ and 12.4±0.9 kJ/mol for ≡ SOBaOH. The enthalpy values for the Co complexes ≡$SOCo^+$, ≡SOCoOH, and ≡$SOCo(OH)_2^-$ were 22.4±0.9, 23.5±0.9, and 45.3±1.0 kJ/mol, respectively. Eu exhibited enthalpies of 8.3±0.9, 43.0 ±0.8, and 32.2±0.9 kJ/mol for the ≡$SOEu^{2+}$, ≡$SOEuOH^+$, and ≡$SOEu(OH)_2$ complexes, respectively.

The analysis of thermodynamic parameters reveals that the surface complexes of Cs, Ba, Co, and Eu exhibit positive enthalpy and entropy. However, since the entropy term dominates over unfavorable enthalpy term, the resulting Gibbs free energy is negative (ln K > 1) and favorable, indicating that the formation of these surface complexes are driven by entropy, probably by releasing hydration shell around the cations when binding to surface. This in turn means that the surface complexes of the Cs, Ba, Co, and Eu is mainly sorbed by forming the inner-sphere complexes, where the hydration shell of the adsorbing species is at least partially released.

In aqueous solutions, cations are typically well-solvated by water molecules. For these ions to adsorb onto mineral surfaces by a chemical bond, dehydration of the associated water molecules is necessary. The temperature-dependent equilibrium constants for sorption reactions indicate endothermic enthalpy values, as shown in Table 5-8, reflects the heat-absorbing nature of these reactions. This suggests that significant energy is required to partially remove water molecules from the cation's hydration shell to facilitate the formation of inner-sphere complexes. Consequently, positive entropy is observed as water molecules are released from the hydration sphere during this process.

In contrast, the exchange surface species of Cs, Ba, Co, and Eu cations such as CsX, BaX_2, XBaOH, and EuX_3, exhibited enthalpy values of –18.6±0.9, –6.3±0.9, –46.1±0.9, and –9.6±0.9 $JK^{-1}mol^{-1}$, respectively, indicating that these reactions are exothermic (heat-releasing) and favorable from this lowering in enthalpy. The entropy term on the other is unfavorable, but do not dominate the overall energy for the reaction. The negative enthalpy values for these cation exchange species suggest that CsX, BaX_2, XBaOH, and EuX_3 are likely adsorbed via an ion-exchange mechanism where the hydration shell largely remains intact. This is in contrast to the positive enthalpy and entropy values observed for the surface complexes. Such reactions involve minor cation dehydration before adsorption onto the cation-exchange site (NaX or HX) of biotite, resulting in a negligible impact on entropy.

6. Conclusions

Radionuclide sorption experiments on mineral biotite have been conducted for a wide set of conditions, which is recommended for thermodynamic sorption modelling purposes.

The sorption experiments were conducted in two separate campaigns. In the first campaign, a mixture containing ^{134}Cs, ^{133}Ba, ^{60}Co, and ^{152}Eu at tracer concentrations (~10^{-8} M) was added with Na-converted biotite at a solid-to-liquid ratio of 1:50. The experiment was performed in triplicate across a pH range of 5–9, using background electrolyte solutions with $NaClO_4$ concentrations of 0.001, 0.01, and 0.1 M, and at temperatures of 25, 40, and 60°C.

The second campaign followed a similar procedure but was carried out only at 25°C and used a mixture of ^{226}Ra and ^{241}Am at tracer concentrations, with a solid-to-liquid ratio of approximately 1:500. The S:L was reduced since a strong sorption of Am was expected.

For all tracers, ionic strength predominantly influenced the sorption of the alkali and alkaline earth metals Cs, Ba and Ra, while pH had a significant effect on all studied elements. The sorption behavior of the pairs Ba and Ra, and Am and Eu appeared similar; however, Ra and Am exhibited higher sorption than Ba and Eu. This suggests that using Ba and Eu as analogue elements for Ra and Am, respectively, may underestimate their sorption potential.

Batch sorption and titration data were modeled using an optimization procedure implemented in PYTHON and PHREEQC geochemical modeling software. The analysis yielded distinct sets of cation selectivity coefficients and surface complexation constants for each metal.

The sorption data for all six elements were effectively reproduced using a model that incorporated a 2-pK_a surface complexation site, likely located on biotite edges, and a cation exchange site, likely situated on free basal planes. Interlayer exchange sites were not expected to participate in the sorption in non-degraded biotite and mineral dissolution was found to be limited during the course of the experiments

The modeling results showed that the sorption of Cs, Ba, and Ra were primarily governed by a cation exchange mechanism, though surface complexation also contributed in their sorption to some extent. At pH values above 8, ion-exchange of mono-hydroxide species of Ba and Ra appeared to play a role in their sorption. In contrast, Co sorption was solely governed by a surface complexation mechanism and its sorption remained unaffected by ionic strength. The sorption behavior of Am and Eu was more complex and required a modeling approach that incorporated both cation exchange and surface complexation, including interactions with hydrolyzed species.

Temperature-dependence analysis showed that temperature influenced the sorption of Cs, Co, and Eu but had minimal impact on Ba and this distinct pattern can be related to their sorption mechanism: surface complexation is temperature sensitive, while ion exchange is not. This

temperature dependency may be related to a shedding of the cation hydration shell, which will give a favorable entropy term for the surface complexation.

7. Future work

The next step in this work will involve Am and Ra for 40 and 60 ºC for which data exist but have not been evaluated.

In the future study this work may continue with other granitic minerals such as chlorite, K-feldspar, and labradorite, under conditions similar to those used for biotite.

Also in future study the resulting sorption data for each mineral may be combined into a sorption model for granitic rock using the component additive (CA) approach.

8. Acknowledgements

I would like to express my deep gratitude to the Swedish Radiation Safety Authority (SSM) for their generous sponsorship of this project.

My heartfelt thanks go to my exceptional supervisors, Prof. Christian Ekberg and Dr. Stellan Holgersson, for providing me with the opportunity to pursue my Ph.D. under their expert guidance. Your unwavering support and encouragement over these past five years have been invaluable, and I greatly appreciate the time you took from your busy schedules to address my questions.

I am also thankful to my tutor Dr. Anna-Maria Jakobsson for the extensive discussions on titration and for your insightful feedback on my manuscript. Your input has been incredibly valuable.

I would like to extend my appreciation to my examiner, Prof. Teodora Retegan Vollmer, for your valuable comments on my manuscripts and for offering the support that every student needs.

Thanks to my friends, lab partners, colleagues, and the research team for your kindness, inspiration, and support. I am grateful for the memorable moments we've shared and for always being there when I needed help.

Lastly, I would like to express my deepest gratitude to my family for their unwavering support. I would not have reached this milestone without your unconditional love, encouragement, and motivation.

References

[1] P. C. Jain, "Greenhouse effect and climate change: scientific basis and overview," *Renew Energy,* vol. 3, p. 403–420, 1993.

[2] Ember, “Electricity demand – Ember and Energy Institute” [dataset]. Ember, “Yearly Electricity Data” [original data]. Retrieved November 26, 2024. [Online]. Available: https://ourworldindata.org/grapher/electricity-demand?tab=chart.

[3] Available: https://www.uniper.energy/sweden/about-uniper-sweden/nuclear-power-sweden.

[4] WorldNuclearAssociation, 2024. [Online]. Available: https://world-nuclear.org/information-library/country-profiles/countries-o-s/sweden.

[5] Strålsäkerhetsmyndigheten, 2024. [Online]. Available: https://www.stralsakerhetsmyndigheten.se/en/areas/nuclear-power.

[6] UNSCEAR, "United Nations Scientific Committee on the Effects of Atomic Radiation," UNSCEAR, Vienna, AUSTRIA, 2000.

[7] SKB, "Long-term safety for the final repository for spent nuclear fuel at Forsmark Main report of the SR-Site project Volume I. SKB TR-11-01," Svensk Kärnbränslehantering AB, Stockholm, 2011.

[8] P. Sellin and X. Leupin, "The use of clay as an engineered barrier in radioactive-waste management - A review," *Clays Clay Miner.,* vol. 61, pp. 477-498, 2014.

[9] SKB, "Nuclear Waste Containment Materials (TR-01-25)," Svensk Kärnbränslehantering AB, Stockholm, 2001.

[10] L. Werme, "Design premises for canister for spent nuclear fuel Design premises for canister for spent nuclear fuel (TR-98-08)," Svensk Kärnbränslehantering AB, Stockholm, 1998.

[11] H. Drake, B. Sandström and E. Tullborg, "Mineralogy and geochemistry of rocks and fracture fillings from Forsmark and Oskarshamn: Compilation of data for SR-Can (R-06-109)," Svensk Kärnbränslehantering AB, Stockholm, 2006.

[12] E. Selnert, J. Byegård and H. Widestrand, "Forsmark site investigation Laboratory measurements within the site investigation programme for the transport properties of the rock (Report P- 07-139)," Svensk Kärnbränslehantering AB, Stockholm, 2008.

[13] J. Crawford, "Bedrock Kd data and uncertainty assessment for application in SR-Site geosphere transport calculations (R-10-48)," Svensk Kärnbränslehantering ABB, Stockholm, 2010.

[14] M. Hakanen, H. Ervanne and E. Puukko, "Safety case for the disposal of spent nuclear fuel at Olkiluoto - Radionuclide migration parameters for the geosphere (2012-41)," Posiva Oy, Olkiluoto, Finland, 2012.

[15] D. L. Parkhurst and C. A. J. Appelo, *PHREEQC version 3: Computer Program for Speciation, Batch-Reaction, One-Dimensional Transport, and Inverse Geochemical Calculations,* U.S. Geological Survey, 2021.

[16] J. A. Davis, J. A. Coston, D. B. Kent and C. C. Fuller, "Application of the surface complexation concept to complex mineral assemblages," *Env. Sci. Technol.,* vol. 32, pp. 2820-2828, 1998.

[17] J. A. Davis, D. E. Meece, M. Kohler and G. P. Curtis, "Approaches to surface complexation modeling of uranium(VI) adsorption on aquifier sediments," *Geochim. Cosmochim. Acta,* vol. 68, pp. 3261-3641, 2004.

[18] R. Cornell, "Adsorption of cesium on minerals: A review," *J. Radioanal. Nucl. Chem.,* vol. 171, pp. 483-500, 1993.

[19] S. Tsai, T. Wang, M. Li, Y. Wei and S. Teng, "Cesium adsorption and distribution onto crushed granite under different physicochemical conditions," *J. Hazard. Mater.,* vol. 161, pp. 854-861, 2009.

[20] K. Fukushi, Y. Hasegawa, K. Maeda, Y. Aoi, A. Tamura, S. Arai, Y. Yamamoto, D. Aosai and T. Mizuno, "Sorption of Eu(III) on granite: EPMA, LA-ICP-MS, batch and modeling studies," *Environ. Sci. Technol.,* vol. 47, pp. 12811-12818, 2013.

[21] E. Muuri, J. Ikonen, M. Matara-aho, A. Lindberg, S. Holgersson, M. Voutilainen, M. Siitari-Kauppi and A. Martin, "Bahavior of Cs in Grimsel granodiorite: sorption on main minerals and crushed rock," *Radiochim. Acta,* vol. 104, pp. 575-582, 2016.

[22] L. Sonnerfelt, P. Andersson, B. Brickstad, P. Ekström, G. G. Roldán, M. Kjellberg, F. Lanaro, J. Linder, G. Lindgren, J. Liu, M. Nordén, C. Pettersson, B. Strömberg, S. Xu, H. Ö. Fastställd and A. Gerhardsson, "Swedish Radiation Safety Authority (SE-171 16) Stockholm Beredning av tillståndsansökan: SKB (slutförvar för använt kärnbränsle)," SSM, Stockholm, 2018.

[23] T. E. Payne, V. Brendler, M. Ochs, B. Baeyens, P. L. Brown, J. A. Davis, C. Ekberg, D. A. Kulik, J. Luetzenkirchen, T. Missana, Y. Tachi, L. R. Van Loon and S. Altmann, "Guidelines for thermodynamic sorption modelling in the context of radioactive waste disposal," *Environ. Modell. Soft.,* vol. 42, pp. 143-156, 2013.

[24] S. Y. Yang and H. D. Yeh, "Modeling transient heat transfer in nuclear waste repositories," *J. Hazar. Materi.,* vol. 169, p. 108–112, 2009.

[25] SNSCW, "Nuclear Waste State of the Art Report – Society, technology and ethics," The Swedish National Council for Nuclear Waste, Stockholm, 2022.

[26] T. Hilding-Rydevik, "Why this hurry in relation to nuclear waste?," *Environ. Impact Asses. Rev.,* p. 98, 2023.

[27] SNSCW, "New insights into the repository's engineered barriers (Report 2014:1e)," Swedish National Council for Nuclear Waste, Stockholm, 2014.

[28] L. Aquilina, V. Vergnaud-Ayraud, A. A. Les Landes, H. Pauwels, P. Davy, E. Pételet-Giraud, T. Labasque, C. Roques, E. Chatton, O. Bour, S. Ben Maamar, A. Dufresne, M. Khaska, C. L. G. La Salle and F. Barbecot, "Impact of climate changes during the last 5 million years on groundwater in basement aquifers," *Sci. Repo.,* vol. 5, p. 14132, 2015.

[29] J. Byegård, E. Tullborg and J. Selroos, "Bedrock transport properties: preliminary site description Forsmark area-version 1.2," SKB, Stockholm, 2006.

[30] N. WD, Introduction to mineralogy, Oxford Univ: Press, 2012.

[31] M. Söderlund, H. Ervänne, E. Muuri and J. Lehto, "The sorption of alkaline earth metals on biotite," *Geochem. J.,* vol. 53, pp. 223-234, 2019.

[32] K. L. Nagy, "Dissolution and precipitation kinetics of sheet silicates," *Rev. Mineral.,* vol. 31, pp. 173-225, 1995.

[33] D. R. Ferreira, J. A. Thornhill, E. I. N. Roderick and Y. Li, "The Impact of pH and Ion Exchange on 133 Cs Adsorption on Vermiculite," *J. Environ. Qual.,* vol. 47, p. 1365–1370, 2018.

[34] S. Holgersson and P. Kumar, "A literature review on thermodynamic sorption models of radionuclides with some selected granitic minerals," *Front. Nucl. Eng.,* p. 1227170, 2023.

[35] X. Li, E. Puhakka, L. Liu, W. Zhang, J. Ikonen, A. Lindberg and M. Siitari-Kauppi, "Multi-site surface complexation modelling of Se(IV) sorption on biotite," *Chem. Geol.,* vol. 533, 2020.

[36] J. McKinley, J. Zachara, S. Heald, A. Dohnalkova, M. Newville and S. Sutton, "Microscale distribution of cesium sorbed to biotite and muscovite," *Environ. Sci. Tech.,* vol. 38, pp. 1017-1023, 2004.

[37] SKB, "Radionuclide transport report for the safety assessment SR-Site (TR-10-50)," Svensk Kärnbränslehantering AB, Stockholm, 2010 (a).

[38] SKB, "Spent nuclear fuel for disposal in the KBS-3 repository (TR-10-13)," Svensk Kärnbränslehantering AB, Stockholm, 2010(b).

[39] M. Jaremalm, S. Köhler and F. Lidman, "Precipitation of barite in the biosphere and its consequences for the mobility of Ra in Forsmark and Simpevarp (TR-13-28) (p. 203)," Svensk Kärnbränslehantering AB , Stockholm, 2013.

[40] SKB, "Long-term safety for KBS-3 repositories at Forsmark and Laxemar – a first evaluation. Main Report of the SR-Can project," Svensk Kärnbränslehantering AB, Stockholm, 2006.

[41] D. R. Brookshaw and J. R. Lloyd, "Effects of Microbial Fe(III) Reduction on the Sorption of Cs and Sr on Biotite and Chlorite," *Geomicrobiology J.,* vol. 33, pp. 206-215, 2016.

[42] J. Kyllönen, M. Hakanen, A. Lindberg, R. Harjula, M. Vehkamäki and . J. Lehto, "Modeling of cesium sorption on biotite using cation exchange selectivity coefficients," *Radiochim. Acta,* vol. 102, pp. 919-929, 2014.

[43] J. Lehto, E. Puukko, A. Lindberg and M. Voutilainen, "Batch sorption experiments of cesium and strontium on crushed rock and biotite for the estimation of distribution coefficients on intact crystalline rock," *Heliyon,* vol. 5, 2019.

[44] E. Muuri, M. Siitari-Kauppi, M. Matara-aho, J. Ikonen, A. Lindberg, L. Qian and L. Koskinen, "Cesium sorption and diffusion on crystalline rock: Olkiluoto case study," *J. Radioanal. Nucl. Chem.,* vol. 311, pp. 439-446, 2017.

[45] M. H. Bradbury and B. Baeyens, "A generalized sorption model for the concentration dependent uptake of caesium by argillaceous rocks," *J. Contami. Hydro.,* vol. 42, pp. 141-163, 2000.

[46] E. Muuri, M. Matara-aho, E. Puhakka, J. Ikonen, A. Martin, L. Koskinen and M. Siitari-Kauppi, "The sorption and diffusion of 133Ba in crushed and intact granitic rocks from the Olkiluoto and Grimsel in-situ test sites," *Appl. Geochem.,* vol. 89, pp. 138-149, 2018.

[47] E. Puukko, M. Olin, E. Puhakka, M. Hakanen, A. Lindberg and J. Lehikoinen, "Sorption of nickel and europium on biotite 3rd Ann. Workshop Proceedings ECFP-FUNMIG," Nuclear Decommisioning Authority, Moor Row, UK, 2007.

[48] N. Jordan, T. Thoenen, K. Spahiu, J. Kelling, S. Starke and V. Brendler, "A critical review of the solution chemistry, solubility, and thermodynamics of europium: Recent advances on the Eu(III) hydrolysis," *Coordin. Chem. Review,* vol. 510, p. 215702, 2024.

[49] J. A. Davis and D. Kent, "Surface complexation modeling in aqueous geochemistry," *Reviews in Min. & Geochem.,* vol. 23, pp. 177-260, 1990.

[50] K. F. Hayes, G. Redden, W. Ela and J. O. Leckie, "Surface complexation models: An evaluation of model parameter estimation using FITEQL and oxide mineral titration data," *J. Colloid and Inter. Sci.,* vol. 142, p. 448–469, 1991.

[51] L. K. Koopal, "Chapter 3.5 Ion adsorption on mineral oxide surfaces," *Studi. Surf. Sci. Catalys.,* vol. 99, p. 757–796, 1996.

[52] W. Stumm and J. Morgan, Aquatic chemistry: chemical equilibria and rates in natural waters, New York: John Wiley & Son, 2013.

[53] Y. Berube, G. Onoda Jr and P. De Bruyn, "Proton adsorption at the ferric oxide/aqueous solution interface: Ii. analysis of kinetic data," *Surf. Sci.,* vol. 7, pp. 448-461, 1967.

[54] C. Schollenberger and R. Simon, "Determination of exchange capacity and exchangeable bases in soil—ammonium acetate method," *Soil Sci.,* vol. 59, pp. 13-24, 1945.

[55] S. Brunauer, P. Emmett and E. Teller, "Adsorption of gases in multimolecular layers," *J. Ameri. Chem. Soci.,* vol. 60, pp. 309-319, 1938.

[56] T. Hiemstra, W. H. Van Riemsdijk and G. H. Bolt, "Multisite proton adsorption modeling at the solid/solution interface of (hydr)oxides: A new approach: I. Model description and evaluation of intrinsic reaction constants," *J. Colloid and Inter. Sci.,* vol. 133, pp. 91-104, 1989.

[57] J. Lutzenkirchen, "The Constant Capacitance Model and Variable Ionic Strength: An Evaluation of Possible Applications and Applicability," *J. Colloid and Inter. Sci.,* vol. 217, pp. 8-18, 1999.

[58] H. Helmholtz, "Ueber einige Gesetze der Vertheilung elektrischer Ströme in körperlichen Leitern mit Anwendung auf die thierisch-elektrischen Versuche," *Annalen der Physik,* vol. 165, pp. 211-233, 1853.

[59] M. Gouy, "Sur la constitution de la charge electrique a la surface dún electrolyte," *Journal de Physique,* vol. 9, pp. 457-468, 1910.

[60] D. L. Chapman, "A contribution to the theory of electrocapillarity," *Philosophical Magazine,* vol. 25, pp. 475-481, 1913.

[61] D. A. Dzombak and F. M. M. Morel, Surface Complexation Modeling: Hydrous Ferric Oxide, A Wiley-Interscience publication, 1990.

[62] O. Stern, "Zur Theorie der elektrolytischen Doppelschicht," *Zeitschrift fur Elektrochemie,* vol. 30, pp. 21-22, 1924.

[63] P. Leroy and A. Revil, "A triple-layer model of the surface electrochemical properties of clay minerals," *Journal of Colloid and Interface Science,* vol. 270, pp. 371-380, 2004.

[64] S. Holgersson, H. Drake, A. Karlsson and L. Krall, "Biotite dissolution kinetics at pH 4 and 6.5 under anaerobic conditions and the release of dissolved Fe(II)," *Chem. Geo.,* vol. 662, p. 122204, 2024.

[65] I. Dubois, *Specific surface area of some minerals commonly found in granite,* Stockholm: Kungliga Tekniska Högskolan, 2011.

[66] A. Jakobsson, Y. Albinsson and R. Rundberg, "Studies of surface complexation of H+ , NpO2+, Co2+, Th4+ onto TiO2 and H+, UO22+ onto alumina (TR-98-15)," Svensk Kärnbränslehantering AB, Stockholm, 1998.

[67] Å. Zazzi, A. Jakobsson and S. Wold, "Ni (II) sorption on natural chlorite," *Applied geochem.,* vol. 27, pp. 1189-1193, 2012.

[68] G. Gran, "Determination of the equivalence point in potentiometric titrations. Part II.," *Analyst,* vol. 77, pp. 661-671, 1952.

[69] Q. Yu, A. Kandegedara, Y. Xu and D. B. Rorabacher, “Avoiding interferences from Good´s buffers: a contiuous series of noncomplexing tertiary amine buffers covering the entire range of pH 3-11,” *Analyt. Biochem.,* vol. 253, pp. 50-56, 1997.

[70] M. Andersson, H. Ervanne, M. A. Glaus, S. Holgersson, P. Karttunen, H. Laine, B. Lothenbach, I. Puigdomenech, B. Schwyn, M. Snellman, H. Ueda, M. Vuorio, E. Wieland

and T. Yamamoto, "Development of methodology for evaluation of long-term safety aspects of organic cement paste components," POSIVA, Olkiluoto, 2008.

[71] D. L. Parkhurst and C. A. J. Appelo, *PHREEQC version 3: Computer Program for Speciation, Batch-Reaction, One-Dimensional Transport, and Inverse Geochemical Calculations,* U.S. Geological Survey, 2021.

[72] S. R. Charlton and D. L. Parkhurst, "Modules based on the geochemical model PHREEQC for use in scripting and programming languages," *Comput. Geosci.,* vol. 37, pp. 1653-1663, 2011.

[73] L. Wissmeier and D. A. Barry, "Simulation tool for variably saturated flow with comprehensive geochemical reaction in the two and three dimensional domains," *Env. Modell. Softw.,* vol. 26, pp. 210-218, 2011.

[74] Y. Iida, T. Yamaguchi, T. Tanaka and K. Hemmi, "Sorption behavior of thorium onto granite and its constituent minerals," *J. Nucl .Sci. Tech.,* vol. 53, pp. 1573-1584, 2016.

[75] J. Luetzenkirchen, "Ionic strength effects on cation sorption to oxides: Macroscopic observations and their significance in microscopic interpretation," *J. Colloid. and Inter. Sci.,* vol. 195, pp. 149-155, 1997.

[76] S. Rodriguez-Cruz and R. a. W. E. Jockusch, "Hydration energies and structures of alkaline earth metal ions, M2+ (H2O) n, n= 5− 7, M= Mg, Ca, Sr, and Ba," *J. Ameri. Chem. Soci.,* vol. 121, pp. 8898-8906, 1999.

[77] B. Allard, G. Beall and T. Krajewski, "The sorption of actinides in igneous rocks," *Nucl. Tech.,* pp. 474-480, 1980.

[78] M. Löfgren, Diffusive properties of granitic rock as measured by in-situ electrical methods (Doctoral dissertation, KTH), Sweden: Royal Institute of Technology, 2005.

[79] J. Lehto and X. Hou, Chemistry and analysis of radionuclides: laboratory techniques and methodology, John Wiley & Sons, 2011.

[80] C. Ekberg and P. L. Brown, Hydrolysis of metal ions. Vol. 1 and 2., Wiley-VCH, 2016.

Appendix

Appendix A: Sorption data

Sorption data for cesium, barium, cobalt, and europium for 0.001, 0.01, and 0.1M at 25, 40 and 60 °C

A1: Sorption Data for cesium for 0.001, 0.01, and 0.1M at 40 and 60 °C

0.001M at 25 °C

Days/pH	5.67 ± 0.04	6.08 ± 0.02	7.10 ± 0.04	8.05 ± 0.01	8.58 ± 0.07
2	0.12 ± 0.02	0.21 ± 0.08	0.18 ± 0.02	0.15 ± 0.01	0.21 ± 0.03
14	0.34 ± 0.07	0.64 ± 0.02	0.83 ± 0.12	0.72 ± 0.20	0.88 ± 0.08
28	0.45 ± 0.07	1.02 ± 0.09	1.46 ± 0.36	1.26 ± 0.09	1.50 ± 0.09
64	0.61 ± 0.08	1.31 ± 0.10	1.52 ± 0.10	1.24 ± 0.17	1.24 ± 0.12

0.01M at 25 °C

Days/pH	5.17 ± 0.01	6.08 ± 0.01	7.08 ± 0.01	8.11 ± 0.01	9.04 ± 0.02
2	0.06 ± 0.01	0.10 ± 0.01	0.12 ± 0.04	0.11 ± 0.01	0.08 ± 0.01
14	0.12 ± 0.00	0.32 ± 0.03	0.39 ± 0.05	0.33 ± 0.04	0.41 ± 0.03
28	0.15 ± 0.02	0.43 ± 0.03	0.51 ± 0.03	0.51 ± 0.01	0.61 ± 0.04
64	0.14 ± 0.00	0.42 ± 0.00	0.54 ± 0.03	0.48 ± 0.02	0.66 ± 0.04

0.1M at 25 °C

Days/pH	5.12 ± 0.01	6.06 ± 0.02	7.08 ± 0.00	8.11 ± 0.02	9.02 ± 0.00
2	0.04 ± 0.01	0.07 ± 0.02	0.07 ± 0.02	0.07 ± 0.01	0.04 ± 0.01
14	0.06 ± 0.01	0.14 ± 0.02	0.14 ± 0.02	0.13 ± 0.00	0.12 ± 0.02
28	0.05 ± 0.02	0.05 ± 0.06	0.14 ± 0.02	0.12 ± 0.01	0.13 ± 0.00
64	0.04 ± 0.01	0.15 ± 0.01	0.21 ± 0.03	0.17 ± 0.00	0.16 ± 0.01

0.001M at 40 °C

Days/pH	5.56 ± 0.04	6.02 ± 0.01	7.02 ± 0.05	8.01 ± 0.08	8.65 ± 0.09
2	0.10 ± 0.00	0.17 ± 0.01	0.23 ± 0.02	0.24 ± 0.02	0.24 ± 0.05
14	0.34 ± 0.03	0.70 ± 0.07	0.87 ± 0.10	0.72 ± 0.15	0.79 ± 0.15
28	0.55 ± 0.05	1.48 ± 0.14	1.68 ± 0.17	1.47 ± 0.18	1.38 ± 0.03
64	0.64 ± 0.06	1.82 ± 0.22	2.34 ± 0.34	1.65 ± 0.44	1.38 ± 0.22

0.01M at 40 °C

Days/pH	5.17 ± 0.01	6.08 ± 0.01	7.08 ± 0.01	8.11 ± 0.01	9.04 ± 0.02
2	0.07 ± 0.01	0.11 ± 0.01	0.13 ± 0.02	0.13 ± 0.01	0.15 ± 0.02
14	0.13 ± 0.01	0.38 ± 0.06	0.45 ± 0.07	0.35 ± 0.02	0.44 ± 0.05
28	0.19 ± 0.04	0.53 ± 0.04	0.62 ± 0.05	0.49 ± 0.05	0.60 ± 0.08
64	0.19 ± 0.01	0.69 ± 0.06	0.77 ± 0.09	0.59 ± 0.01	0.61 ± 0.06

0.1M at 40 °C

Days/pH	5.12 ± 0.01	6.06 ± 0.02	7.08 ± 0.00	8.11 ± 0.02	9.02 ± 0.00
2	0.02 ± 0.00	0.03 ± 0.01	0.05 ± 0.01	0.04 ± 0.01	0.05 ± 0.00
14	0.05 ± 0.01	0.15 ± 0.01	0.14 ± 0.02	0.14 ± 0.01	0.17 ± 0.00
28	0.03 ± 0.00	0.05 ± 0.07	0.15 ± 0.01	0.11 ± 0.01	0.13 ± 0.01
64	0.05 ± 0.00	0.20 ± 0.01	0.18 ± 0.01	0.17 ± 0.01	0.20 ± 0.01

0.001M at 60 °C

Days/pH	5.50 ± 0.02	6.05 ± 0.01	6.95 ± 0.02	8.23 ± 0.10	8.90 ± 0.09
2	0.15 ± 0.02	0.25 ± 0.02	0.27 ± 0.02	0.31 ± 0.04	0.34 ± 0.03
14	0.44 ± 0.00	1.13 ± 0.18	1.26 ± 0.06	1.18 ± 0.35	1.04 ± 0.19
28	0.71 ± 0.12	3.10 ± 0.93	8.50 ± 3.57	10.62 ± 5.44	3.11 ± 0.69
64	0.72 ± 0.02	3.78 ± 2.55	7.80 ± 1.27	4.42 ± 0.78	3.42 ± 0.74

0.01M at 60 °C

Days/pH	5.17 ± 0.01	6.08 ± 0.01	7.08 ± 0.01	8.11 ± 0.01	9.04 ± 0.02
2	0.07 ± 0.01	0.15 ± 0.03	0.17 ± 0.03	0.16 ± 0.02	0.19 ± 0.03
14	0.12 ± 0.01	0.86 ± 0.12	0.85 ± 0.08	0.64 ± 0.04	0.67 ± 0.12
28	0.14 ± 0.01	1.02 ± 0.04	0.98 ± 0.28	0.94 ± 0.05	1.00 ± 0.11
64	0.16 ± 0.01	1.38 ± 0.11	1.84 ± 0.16	2.36 ± 0.63	3.17 ± 0.43

0.1M at 60 °C

Days/pH	5.12 ± 0.01	6.06 ± 0.02	7.08 ± 0.00	8.11 ± 0.02	9.02 ± 0.00
2	0.30 ± 0.48	0.08 ± 0.01	0.07 ± 0.01	0.07 ± 0.01	0.08 ± 0.01
14	0.06 ± 0.00	0.23 ± 0.04	0.23 ± 0.01	0.21 ± 0.03	0.20 ± 0.03
28	0.01 ± 0.05	0.09 ± 0.14	0.21 ± 0.01	0.19 ± 0.02	0.19 ± 0.00
64	0.06 ± 0.00	0.38 ± 0.03	0.40 ± 0.00	0.33 ± 0.05	0.55 ± 0.31

A2: Sorption Data for barium for 0.001, 0.01, and 0.1M at 25, 40, and 60 °C

0.001M at 25 °C

Days/pH	5.67 ± 0.04	6.08 ± 0.02	7.10 ± 0.04	8.05 ± 0.01	8.58 ± 0.07
2	0.07 ± 0.02	0.51 ± 0.19	0.83 ± 0.01	0.83 ± 0.07	1.25 ± 0.30
14	0.13 ± 0.04	1.05 ± 0.09	2.86 ± 0.23	4.13 ± 0.17	4.08 ± 0.36
28	0.16 ± 0.03	1.20 ± 0.08	3.77 ± 0.37	6.45 ± 1.10	9.30 ± 3.24
64	0.20 ± 0.05	1.20 ± 0.07	3.29 ± 0.13	4.27 ± 0.94	4.47 ± 0.69

0.01M at 25°C

Days/pH	5.17 ± 0.01	6.08 ± 0.01	7.08 ± 0.01	8.11 ± 0.01	9.04 ± 0.02
2	0.02 ± 0.01	0.26 ± 0.03	0.43 ± 0.13	0.54 ± 0.08	0.88 ± 0.11
14	0.03 ± 0.00	0.66 ± 0.05	1.30 ± 0.05	1.60 ± 0.32	3.68 ± 0.09
28	0.03 ± 0.01	0.72 ± 0.05	1.42 ± 0.07	2.08 ± 0.14	4.77 ± 0.65
64	0.02 ± 0.00	0.56 ± 0.02	1.36 ± 0.09	1.87 ± 0.08	5.92 ± 0.17

0.1M at 25 °C

Days/pH	5.12 ± 0.01	6.06 ± 0.02	7.08 ± 0.00	8.11 ± 0.02	9.02 ± 0.00
2	0.03 ± 0.01	0.05 ± 0.01	0.07 ± 0.02	0.11 ± 0.02	0.13 ± 0.03
14	0.03 ± 0.01	0.06 ± 0.00	0.09 ± 0.01	0.20 ± 0.00	0.37 ± 0.06
28	0.02 ± 0.01	0.04 ± 0.00	0.06 ± 0.00	0.15 ± 0.00	0.37 ± 0.01
64	0.02 ± 0.00	0.03 ± 0.01	0.06 ± 0.00	0.16 ± 0.01	0.38 ± 0.01

0.001M at 40 °C

Days/pH	5.56 ± 0.04	6.02 ± 0.01	7.02 ± 0.05	8.01 ± 0.08	8.65 ± 0.09
2	0.05 ± 0.01	0.53 ± 0.04	1.12 ± 0.20	1.86 ± 0.30	2.61 ± 0.54
14	0.13 ± 0.01	1.35 ± 0.17	3.52 ± 0.15	4.61 ± 0.78	8.73 ± 2.15
28	0.19 ± 0.03	2.10 ± 0.06	5.02 ± 0.10	7.10 ± 1.51	12.00 ± 0.60
64	0.22 ± 0.01	1.44 ± 0.10	3.73 ± 0.53	3.45 ± 1.14	3.82 ± 0.44

0.01M at 40 °C

Days/pH	5.17 ± 0.01	6.08 ± 0.01	7.08 ± 0.01	8.11 ± 0.01	9.04 ± 0.02
2	0.02 ± 0.00	0.40 ± 0.04	0.65 ± 0.07	0.89 ± 0.15	1.84 ± 0.13
14	0.02 ± 0.01	0.74 ± 0.06	1.47 ± 0.17	1.91 ± 0.22	5.18 ± 0.89
28	0.04 ± 0.01	0.72 ± 0.11	1.79 ± 0.10	2.31 ± 0.36	6.17 ± 0.48
64	0.03 ± 0.00	0.62 ± 0.09	1.70 ± 0.06	2.19 ± 0.04	5.08 ± 0.51

0.1M at 40 °C

Days/pH	5.12 ± 0.01	6.06 ± 0.02	7.08 ± 0.00	8.11 ± 0.02	9.02 ± 0.00
2	0.01 ± 0.00	0.02 ± 0.01	0.05 ± 0.01	0.09 ± 0.01	0.15 ± 0.03
14	0.03 ± 0.00	0.05 ± 0.01	0.10 ± 0.02	0.23 ± 0.01	0.46 ± 0.12

28	0.01 ± 0.00	-0.01 ± 0.03	0.07 ± 0.00	0.14 ± 0.01	0.34 ± 0.09
64	0.02 ± 0.00	0.03 ± 0.00	0.07 ± 0.01	0.19 ± 0.01	0.43 ± 0.12

0.001M at 60 °C

Days/pH	5.50 ± 0.02	6.05 ± 0.01	6.95 ± 0.02	8.23 ± 0.10	8.90 ± 0.09
2	0.08 ± 0.01	0.78 ± 0.18	1.53 ± 0.21	2.46 ± 0.37	3.43 ± 0.39
14	0.17 ± 0.02	1.73 ± 0.10	4.11 ± 0.29	6.33 ± 1.83	6.34 ± 0.28
28	0.28 ± 0.04	2.26 ± 0.07	5.41 ± 0.21	13.36 ± 1.39	13.45 ± 2.54
64	0.30 ± 0.01	1.57 ± 0.17	3.45 ± 0.10	4.25 ± 0.58	4.40 ± 0.81

0.01M at 60 °C

Days/pH	5.17 ± 0.01	6.08 ± 0.01	7.08 ± 0.01	8.11 ± 0.01	9.04 ± 0.02
2	0.03 ± 0.00	0.50 ± 0.08	0.91 ± 0.23	0.88 ± 0.24	2.07 ± 0.34
14	0.00 ± 0.00	0.83 ± 0.04	1.95 ± 0.28	2.86 ± 0.31	6.38 ± 1.01
28	0.00 ± 0.00	0.74 ± 0.10	1.50 ± 0.50	2.59 ± 0.50	7.45 ± 0.51
64	0.02 ± 0.00	0.61 ± 0.07	1.38 ± 0.39	3.00 ± 0.21	8.11 ± 1.49

0.1M at 60 °C

Days/pH	5.12 ± 0.01	6.06 ± 0.02	7.08 ± 0.00	8.11 ± 0.02	9.02 ± 0.00
2	0.01 ± 0.01	0.03 ± 0.01	0.05 ± 0.01	0.12 ± 0.02	0.25 ± 0.02
14	0.03 ± 0.00	0.05 ± 0.01	0.11 ± 0.01	0.38 ± 0.06	0.77 ± 0.08
28	-0.02 ± 0.04	0.00 ± 0.04	0.08 ± 0.00	0.29 ± 0.00	0.62 ± 0.01
64	0.05 ± 0.00	0.04 ± 0.00	0.10 ± 0.01	0.35 ± 0.02	0.79 ± 0.00

A3: Sorption data for cobalt for 0.001, 0.01, and 0.1M at 25, 40, and 60 °C

0.001M at 25 °C

Days/pH	5.67 ± 0.04	6.08 ± 0.02	7.10 ± 0.04	8.05 ± 0.01	8.58 ± 0.07
2	0.02 ± 0.01	0.13 ± 0.05	0.21 ± 0.03	0.42 ± 0.07	0.71 ± 0.20
14	0.02 ± 0.01	0.17 ± 0.03	1.02 ± 0.25	5.29 ± 1.41	1.58 ± 0.19
28	0.02 ± 0.01	0.16 ± 0.01	1.74 ± 0.36	6.96 ± 1.06	2.49 ± 0.31
64	0.01 ± 0.01	0.16 ± 0.01	2.25 ± 0.47	5.03 ± 1.85	2.03 ± 0.15

0.01M at 25 °C

Days/pH	5.17 ± 0.01	6.08 ± 0.01	7.08 ± 0.01	8.11 ± 0.01	9.04 ± 0.02
2	0.01 ± 0.01	0.06 ± 0.01	0.30 ± 0.11	0.73 ± 0.11	0.42 ± 0.08
14	0.01 ± 0.00	0.10 ± 0.01	1.83 ± 0.25	3.96 ± 0.52	1.86 ± 0.29
28	0.01 ± 0.00	0.10 ± 0.00	2.11 ± 0.60	6.52 ± 2.44	2.23 ± 0.46
64	0.00 ± 0.00	0.07 ± 0.00	1.65 ± 0.19	7.46 ± 1.33	3.51 ± 0.28

0.1M at 25 °C

Days/pH	5.12 ± 0.01	6.06 ± 0.02	7.08 ± 0.00	8.11 ± 0.02	9.02 ± 0.00
2	0.02 ± 0.01	0.02 ± 0.01	0.07 ± 0.02	0.27 ± 0.07	0.18 ± 0.03
14	0.02 ± 0.01	0.04 ± 0.00	0.31 ± 0.03	2.77 ± 0.74	0.52 ± 0.10
28	0.01 ± 0.01	0.02 ± 0.00	0.44 ± 0.05	4.43 ± 1.80	0.89 ± 0.04
64	0.00 ± 0.00	0.02 ± 0.00	0.52 ± 0.02	4.74 ± 0.42	1.83 ± 0.14

0.001M at 40 °C

Days/pH	5.56 ± 0.04	6.02 ± 0.01	7.02 ± 0.05	8.01 ± 0.08	8.65 ± 0.09
2	0.01 ± 0.00	0.11 ± 0.00	0.47 ± 0.08	1.86 ± 0.70	1.06 ± 0.24
14	0.03 ± 0.00	0.20 ± 0.03	3.77 ± 1.40	5.99	3.29 ± 0.57
28	0.03 ± 0.01	0.30 ± 0.03	4.57 ± 0.97	19.36	5.44 ± 1.77
64	0.02 ± 0.00	0.23 ± 0.01	4.01 ± 0.59	3.55 ± 2.04	2.30 ± 0.33

0.01M at 40 °C

Days/pH	5.17 ± 0.01	6.08 ± 0.01	7.08 ± 0.01	8.11 ± 0.01	9.04 ± 0.02
2	0.01 ± 0.00	0.08 ± 0.01	1.16 ± 0.22	1.99 ± 0.29	1.06 ± 0.02
14	0.01 ± 0.00	0.12 ± 0.02	2.43 ± 0.58	6.96	3.39 ± 0.37
28	0.01 ± 0.01	0.13 ± 0.01	2.54 ± 0.43	9.25 ± 3.00	4.20 ± 0.61
64	0.01 ± 0.00	0.12 ± 0.01	2.48 ± 0.20	10.86 ± 6.23	4.13 ± 1.36

0.1M at 40 °C

Days/pH	5.12 ± 0.01	6.06 ± 0.02	7.08 ± 0.00	8.11 ± 0.02	9.02 ± 0.00
2	0.00 ± 0.00	0.00 ± 0.01	0.11 ± 0.01	0.67 ± 0.08	0.28 ± 0.01
14	0.01 ± 0.00	0.04 ± 0.01	0.93 ± 0.16	8.56 ± 3.81	3.35 ± 0.21
28	0.01 ± 0.00	0.02 ± 0.00	0.82 ± 0.17	5.15	2.90 ± 0.95
64	0.00 ± 0.00	0.02 ± 0.00	0.77 ± 0.06	8.61 ± 0.05	3.84 ± 0.75

0.001M at 60 °C

Days/pH	5.50 ± 0.02	6.05 ± 0.01	6.95 ± 0.02	8.23 ± 0.10	8.90 ± 0.09
2	0.01 ± 0.00	0.17 ± 0.01	1.27 ± 0.63	4.28 ± 0.83	1.94 ± 0.46
14	0.03 ± 0.00	0.45 ± 0.04	7.72 ± 2.04	3.51	2.71 ± 0.37
28	0.04 ± 0.01	0.66 ± 0.07	14.25	5.00	3.77
64	0.03 ± 0.00	0.65 ± 0.10	5.77 ± 0.69	3.50 ± 0.55	2.38 ± 0.25

0.01M at 60 °C

Days/pH	5.17 ± 0.01	6.08 ± 0.01	7.08 ± 0.01	8.11 ± 0.01	9.04 ± 0.02
2	0.03 ± 0.00	0.16 ± 0.03	1.77 ± 0.36	3.09 ± 0.95	2.25 ± 0.79
14	0.02 ± 0.00	0.39 ± 0.05	8.02 ± 1.91	3.12	6.43 ± 0.41
28	0.02 ± 0.00	0.42 ± 0.03	2.23	2.31 ± 1.11	7.17 ± 2.20

64	0.00 ± 0.00	0.49 ± 0.02	14.73 ± 3.52	19.28 ± 8.26	11.21 ± 3.40

0.1M at 60 °C

Days/pH	5.12 ± 0.01	6.06 ± 0.02	7.08 ± 0.00	8.11 ± 0.02	9.02 ± 0.00
2	0.00 ± 0.00	0.03 ± 0.00	0.53 ± 0.08	2.14 ± 0.41	1.72 ± 0.30
14	0.01 ± 0.00	0.08 ± 0.02	2.20 ± 0.46	8.87	5.68 ± 1.74
28	0.03 ± 0.03	0.04 ± 0.01	2.72 ± 0.35	14.12	8.06
64	0.01 ± 0.00	0.10 ± 0.01	3.58 ± 0.38	18.02 ± 1.16	9.29 ± 2.16

A4: Sorption data for europium for 0.001, 0.01, and 0.1M at 25, 40, and 60 °C

0.001M at 25 °C

Days/pH	5.67 ± 0.04	6.08 ± 0.02	7.10 ± 0.04	8.05 ± 0.01	8.58 ± 0.07
2	0.51 ± 0.18	1.95 ± 0.74	1.39 ± 0.08	0.73 ± 0.03	0.78 ± 0.25
14	3.36 ± 0.91	7.00	4.10 ± 1.92	2.41 ± 0.66	1.77 ± 0.25
28	3.41 ± 1.60	7.90	5.05	4.70 ± 1.26	3.05 ± 0.63
64	3.72 ± 1.29	17.77 ± 1.64	5.18 ± 0.66	2.23 ± 0.56	1.57 ± 0.02

0.01M at 25 °C

Days/pH	5.17 ± 0.01	6.08 ± 0.01	7.08 ± 0.01	8.11 ± 0.01	9.04 ± 0.02
2	0.08 ± 0.02	7.30 ± 2.68	10.00	2.54 ± 0.80	0.42 ± 0.10
14	0.20 ± 0.01	10.00	15.00	7.77	1.81 ± 0.43
28	0.14 ± 0.01	20.49	20.00	9.03	1.62 ± 0.14
64	0.11 ± 0.02	12.50	16.20	12.50	2.76 ± 0.57

0.1M at 25 °C

Days/pH	5.12 ± 0.01	6.06 ± 0.02	7.08	8.11 ± 0.02	9.02
2	0.55 ± 0.19	1.32 ± 0.35	2.22 ± 0.67	1.83	2.11 ± 0.74
14	2.38 ± 2.15	5.42 ± 2.33	10.70	15.00	2.72
28	1.13 ± 0.96	10.00	20.00	25.00	1.00
64	2.13 ± 0.66	4.78 ± 0.56	6.66 ± 0.89	2.75 ± 0.39	1.01 ± 0.30

0.001M at 40 °C

Days/pH	5.56 ± 0.04	6.02 ± 0.01	7.02 ± 0.05	8.01 ± 0.08	8.65 ± 0.09
2	0.53 ± 0.14	12.14 ± 11.41	2.04 ± 0.57	1.63 ± 0.53	1.46 ± 0.17
14	1.97 ± 0.19	11.41	12.99	3.54 ± 1.11	3.55 ± 0.32
28	2.88 ± 0.39	11.41 ± 0.00	9.62 ± 2.37	5.49 ± 0.18	2.98 ± 1.44
64	2.36 ± 0.09	11.29 ± 5.11	7.00 ± 4.01	2.07 ± 0.84	1.43 ± 0.32

0.01M at 40 °C

Days/pH	5.17 ± 0.01	6.08 ± 0.01	7.08 ± 0.01	8.11 ± 0.01	9.04 ± 0.02
2	0.10 ± 0.01	15.37 ± 1.17	5.79	3.41	0.87 ± 0.10
14	0.18 ± 0.02	15.12	17.50	5.71	1.76 ± 0.03
28	0.22 ± 0.05	14.31	22.50	5.99	2.00 ± 0.22
64	0.24 ± 0.04	12.61±1.00	26.92 ± 6.48	21.99 ± 17.05	1.83 ± 0.31

0.1M at 40 °C

Days/pH	5.12 ± 0.01	6.06 ± 0.02	7.08 ± 0.00	8.11 ± 0.02	9.02 ± 0.00
2	0.54 ± 0.06	1.03 ± 0.34	4.83	3.12	2.01
14	1.31 ± 0.20	2.30	5.30	4.01	2.89
28	3.15 ± 1.50	4.51	8.56	7.45	5.63
64	2.69 ± 0.47	6.79 ± 0.54	13.63 ± 0.34	10.69 ± 6.94	7.88 ± 6.59

0.001M at 60 °C

Days/pH	5.50 ± 0.02	6.05 ± 0.01	6.95 ± 0.02	8.23 ± 0.10	8.90 ± 0.09
2	0.73 ± 0.15	8.63 ± 0.35	3.21 ± 0.91	2.85 ± 0.11	1.94 ± 0.54
14	2.60 ± 0.57	9.00	4.00	3.10 ± 0.53	2.34 ± 0.59
28	3.58 ± 0.38	9.00	5.87	16.13 ± 13.88	4.30 ± 0.62
64	3.09 ± 0.41	18.3 ± 8.91	4.76 ± 0.69	1.90 ± 0.60	1.21 ± 0.40

0.01M at 60 °C

Days/pH	5.17 ± 0.01	6.08 ± 0.01	7.08 ± 0.01	8.11 ± 0.01	9.04 ± 0.02
2	0.10 ± 0.02	14.83 ± 5.06	3.44	1.43	1.21 ± 0.41
14	0.19 ± 0.01	17.43	7.83	4.14	3.34 ± 0.30
28	0.19 ± 0.03	25.65	10.32	1.99	2.49 ± 0.71
64	0.18 ± 0.04	35.11±3.93	19.12±3.8	8.50	4.48 ± 1.95

0.1M at 60 °C

Days/pH	5.12 ± 0.01	6.06 ± 0.02	7.08 ± 0.00	8.11 ± 0.02	9.02 ± 0.00
2	0.66 ± 0.08	1.34 ± 0.11	5.32	3.80	1.23
14	1.79	6.44	11.23	7.54	3.21
28	2.34	10.90	18.96	13.45	5.21
64	3.75 ± 1.38	7.20 ± 2.24	27.50	23.10	7.75 ± 1.3

A5: Sorption Data for radium for 0.001, 0.01, and 0.1M at 25°C

0.001M at 25 °C

Days/pH	5.11 ± 0.04	6.08 ± 0.02	7.10 ± 0.04	8.05 ± 0.01	8.97 ± 0.07
2	0.08 ± 0.00	0.62 ± 0.29	1.45 ± 0.24	2.09 ± 0.47	2.00 ± 0.00
14	0.12 ± 0.05	1.45 ± 0.36	2.59 ± 0.67	3.50 ± 2.72	4.50 ± 0.00
28	0.13 ± 0.06	1.81 ± 0.28	4.06 ± 0.00	5.50 ± 1.35	7.50 ± 0.50
64	0.21 ± 0.01	3.22 ± 0.72	7.88 ± 2.76	9.54 ± 1.48	9.79 ± 3.56

0.01M at 25°C

Days/pH	5.17 ± 0.01	6.08 ± 0.01	7.08 ± 0.01	8.11 ± 0.01	9.04 ± 0.02
2	0.06 ± 0.07	0.63 ± 0.21	1.32 ± 0.41	1.30 ± 0.45	1.51 ± 0.22
14	0.06 ± 0.05	0.68 ± 0.19	1.50 ± 0.30	1.65 ± 0.28	3.15 ± 0.10
28	0.09 ± 0.03	0.88 ± 0.30	2.10 ± 0.00	1.86 ± 0.14	3.41 ± 0.83
64	0.08 ± 0.02	1.11 ± 0.44	2.20 ± 0.00	2.50 ± 0.00	3.79 ± 0.40

0.1M at 25 °C

Days/pH	5.12 ± 0.01	6.06 ± 0.02	7.08 ± 0.00	8.11 ± 0.02	9.02 ± 0.00
2	0.05 ± 0.00	0.17 ± 0.00	0.33 ± 0.00	0.57 ± 0.15	0.55 ± 0.03
14	0.12 ± 0.02	0.22 ± 0.02	0.38 ± 0.05	0.78 ± 0.08	0.89 ± 0.19
28	0.19 ± 0.04	0.22 ± 0.07	0.32 ± 0.09	0.83 ± 0.33	0.87 ± 0.06
64	0.15 ± 0.00	0.28 ± 0.03	0.46 ± 0.06	1.26 ± 0.17	1.80 ± 0.23

A6: Sorption Data for americium for 0.001, 0.01, and 0.1M at 25°C

0.001M at 25 °C

Days/pH	5.11 ± 0.04	6.08 ± 0.02	7.10 ± 0.04	8.05 ± 0.01	8.97 ± 0.07
2	0.05 ± 0.03	2.14 ± 0.19	2.86 ± 0.74	2.15 ± 0.34	1.71 ± 0.21
14	0.04 ± 0.02	8.32 ± 0.67	8.06 ± 0.54	5.96 ± 0.00	3.08 ± 1.10
28	0.06 ± 0.02	13.83 ± 0.35	11.98 ± 0.26	7.77 ± 0.70	4.99 ± 1.08
64	0.04 ± 0.00	18.15 ± 2.49	15.13 ± 1.28	10.18 ± 1.19	7.23 ± 1.36

0.01M at 25 °C

Days/pH	5.17 ± 0.01	6.08 ± 0.01	7.08 ± 0.01	8.11 ± 0.01	9.04 ± 0.02
2	0.13 ± 0.04	8.77 ± 1.39	9.63 ± 0.46	6.18 ± 1.28	4.66 ± 0.21
14	0.16 ± 0.02	22.60 ± 4.79	17.97 ± 2.64	11.16 ± 0.92	7.31 ± 2.85
28	0.22 ± 0.02	28.57 ± 3.17	23.50 ± 4.41	15.02 ± 2.79	10.76 ± 0.00
64	0.30 ± 0.05	52.43 ± 2.18	38.25 ± 6.18	21.48 ± 2.60	17.75 ± 10.57

0.1M at 25 °C

Days/pH	5.12 ± 0.01	6.06 ± 0.02	7.08 ± 0.00	8.11 ± 0.02	9.02 ± 0.00
2	0.15 ± 0.06	2.68 ± 0.15	5.45 ± 0.00	7.63 ± 0.00	7.29 ± 0.00
14	0.16 ± 0.03	5.65 ± 0.74	7.20 ± 0.00	12.00 ± 0.00	9.00 ± 0.00
28	0.23 ± 0.04	9.89 ± 0.02	11.00 ± 0.00	17.81 ± 0.00	15.00 ± 0.00
64	0.20 ± 0.01	16.64 ± 2.18	19.96 ± 2.02	25.66 ± 4.58	21.29 ± 9.81

Appendix B: Modelling Results

Batch sorption experimental and modelling results for Cs, Ba, Co, and Eu for 0.001M, 0.01M and 0.1M, five pH values (5 to 9) and at 25°C

1.1 Cesium

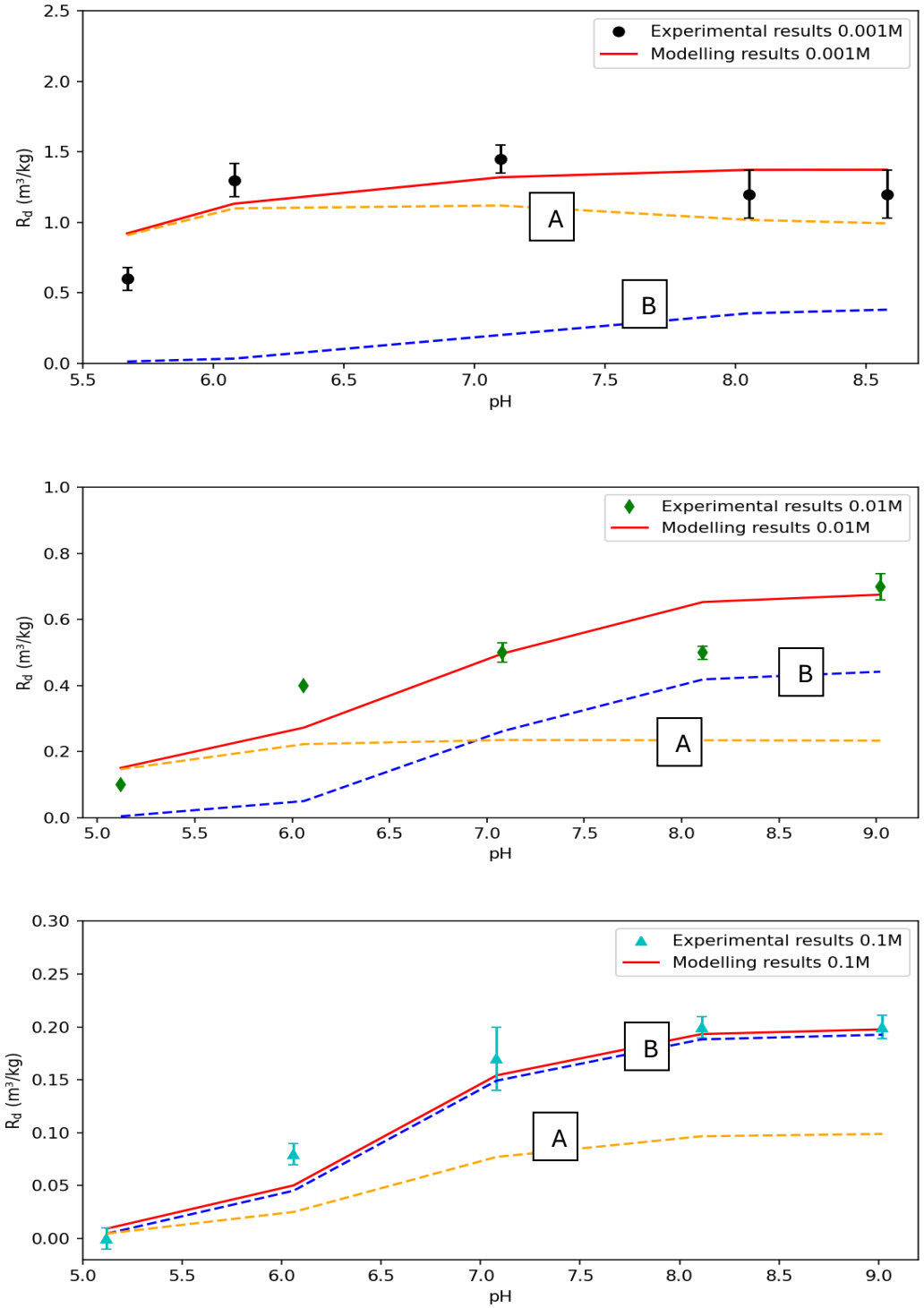

Figure 1: Cs sorption measurement (symbol) and modelling (continuous line) on biotite mineral in 0.001M,0.01M, and 0.1M $NaClO_4$ solution at 25 ºC. The contribution of different Cs(I) species in its sorption is represented by different curves: (A: yellow line) CsX; (B: Blue line) ≡SOCs

1.2 Barium

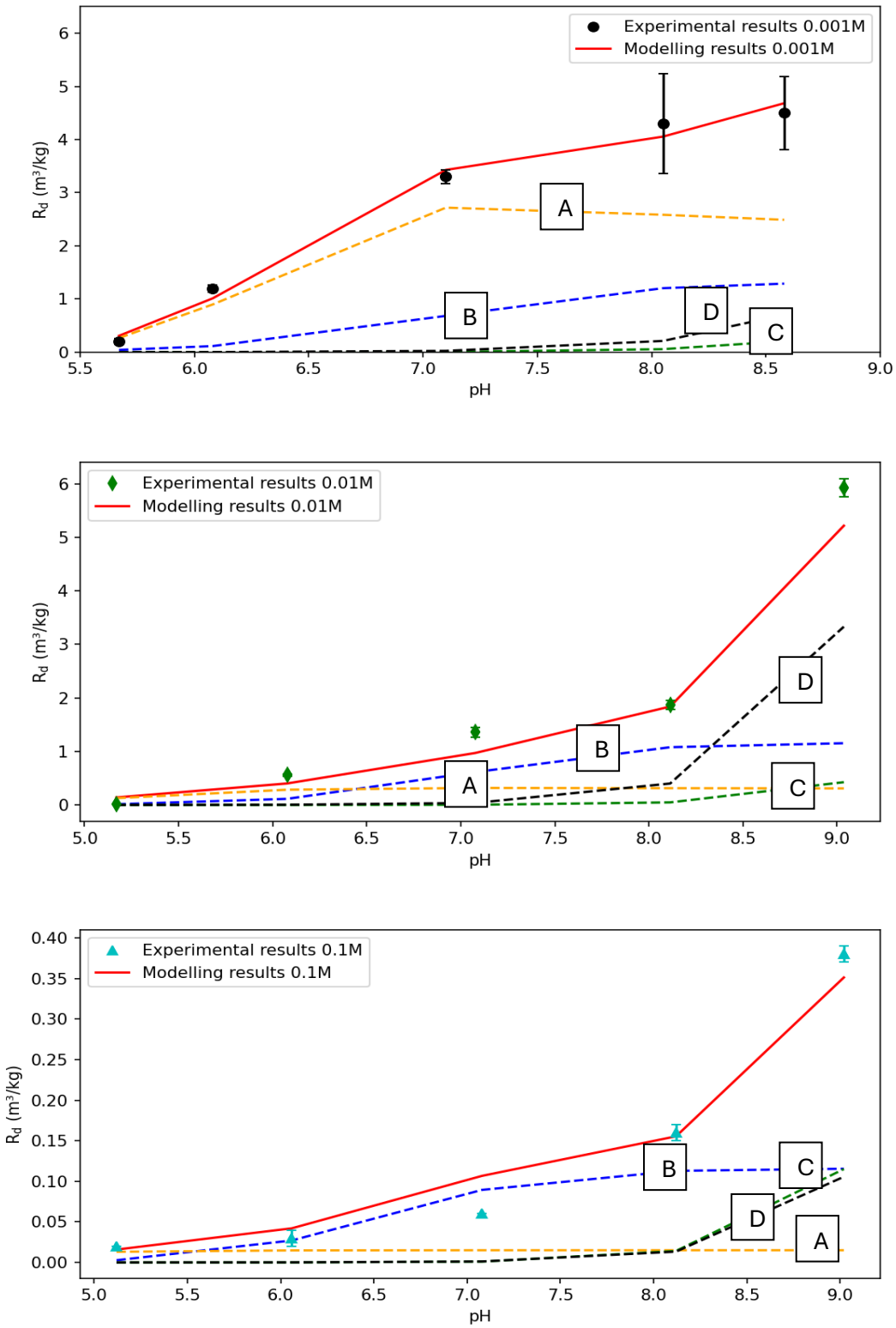

Figure 2: Ba sorption measurement (symbol) and modelling (continuous line) on biotite mineral in 0.001M, 0.01M and 0.1M $NaClO_4$ solution at 25 °C. The contribution of different Ba(II) species in its sorption is represented by different curves:(A: Yellow line) BaX_2; (B: Blue line) $\equiv SOBa^+$; (C: Green line)) ≡SOBaOH; (D: Black line) XBaOH.

1.3 Cobalt

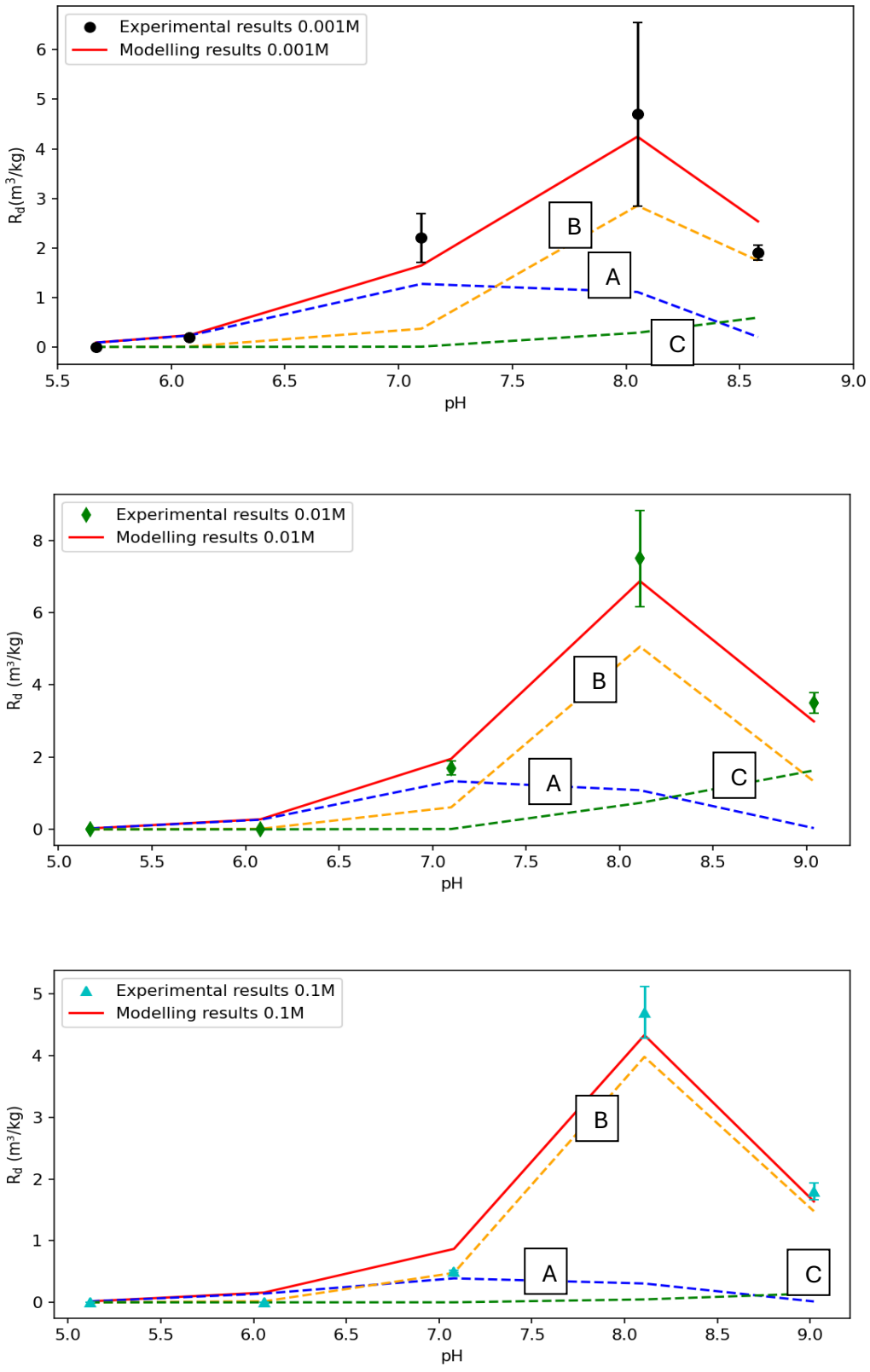

Figure 3: Co sorption measurement (symbol) and modelling (continuous line) on biotite mineral in 0.001M, 0.01M and 0.1M $NaClO_4$ solution at 25 °C. The contribution of different Co(II) species in its sorption is represented by different curves: (A: Blue line)≡$SOCo^+$; (B: Yellow line)≡SOCoOH; (C: Green line) ≡ $SOCo(OH)_2^-$.

1.4 Europium

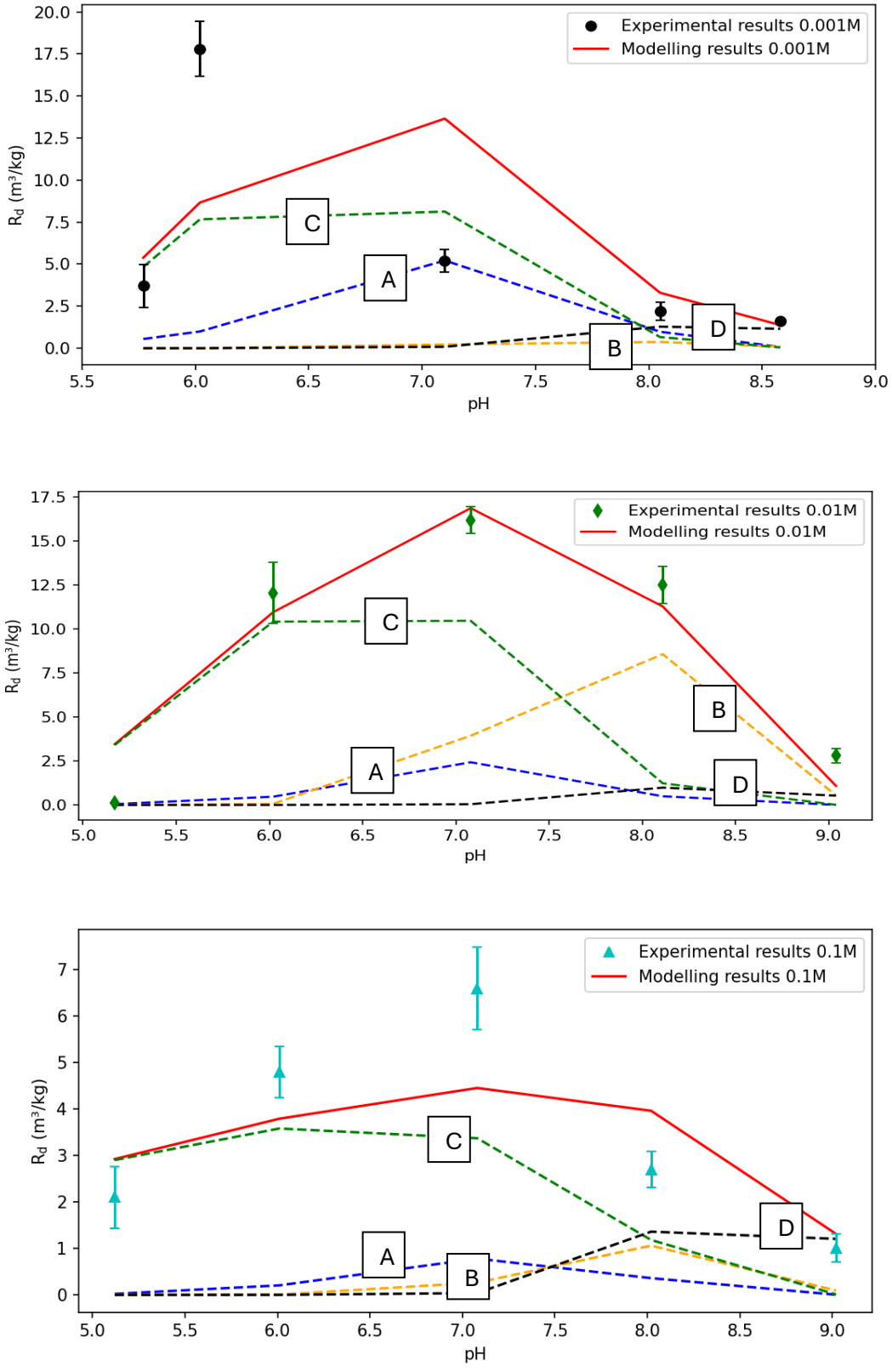

Figure 4: Eu sorption measurement (symbol) and modelling (continuous line) on biotite mineral in 0.001M,0.01M, and 0.1M NaClO4 solution at 25 ºC. The contribution of different Eu(III) species in its sorption is represented by different curves: (A: blue line)≡ $SOEu^{2+}$; (B: yellow line) ≡ $SOEu(OH)^{+}$; (C: green line) EuX_3; (D: black line) ≡ $SOEu(OH)_2$

2. Batch sorption experimental and modelling results for Cs, Ba, Co, and Eu for 0.001M, 0.01M and 0.1M, five pH values (5 to 9) and at 40°C

2.1 Cesium

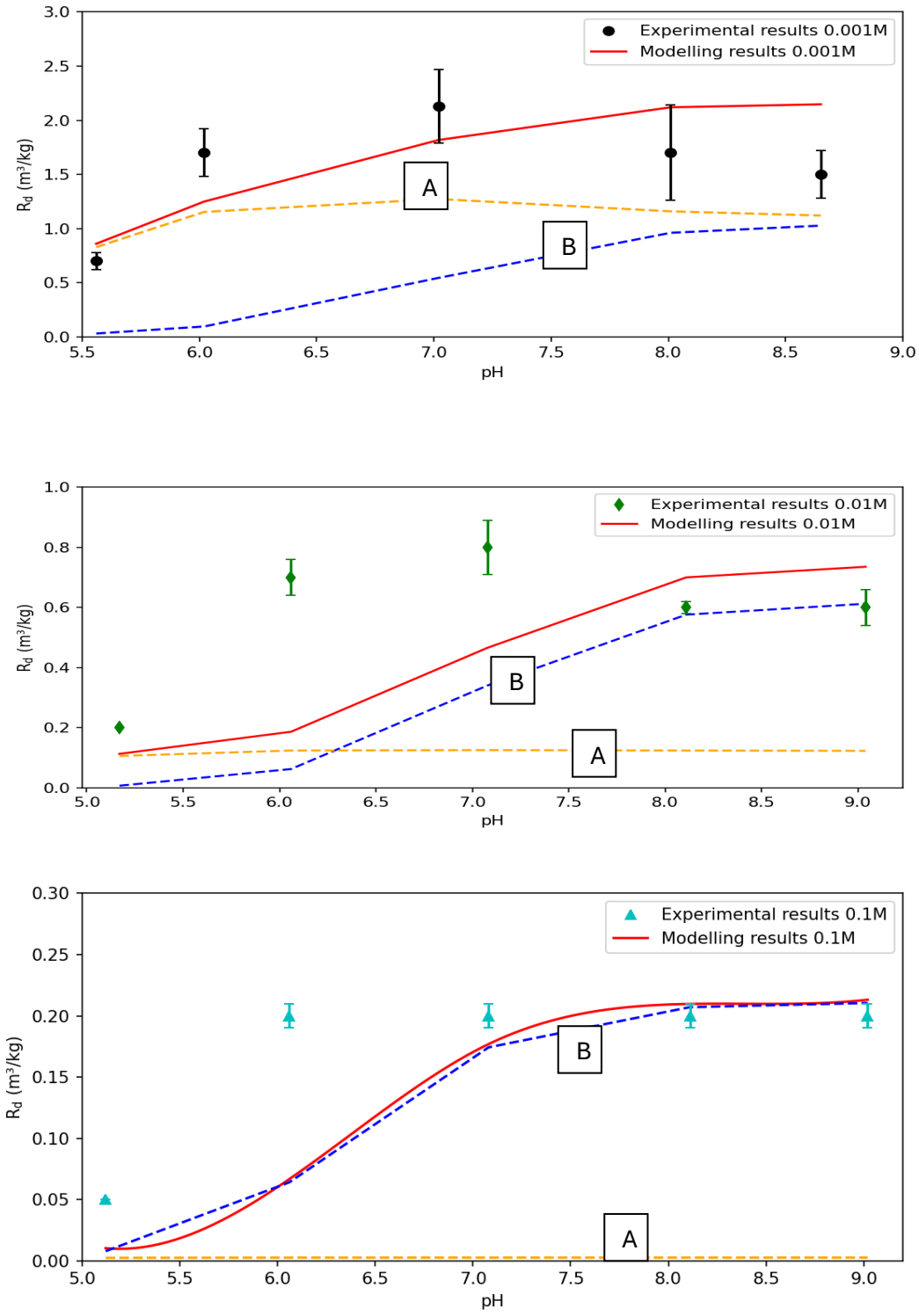

Figure 5: Cs sorption measurement (symbol) and modelling (continuous line) on biotite mineral in 0.001M,0.01M, and 0.1M $NaClO_4$ solution at 40 ºC. The contribution of different Cs(I) species in its sorption is represented by different curves: (A) CsX; (B) ≡SOCs

2.2 Barium

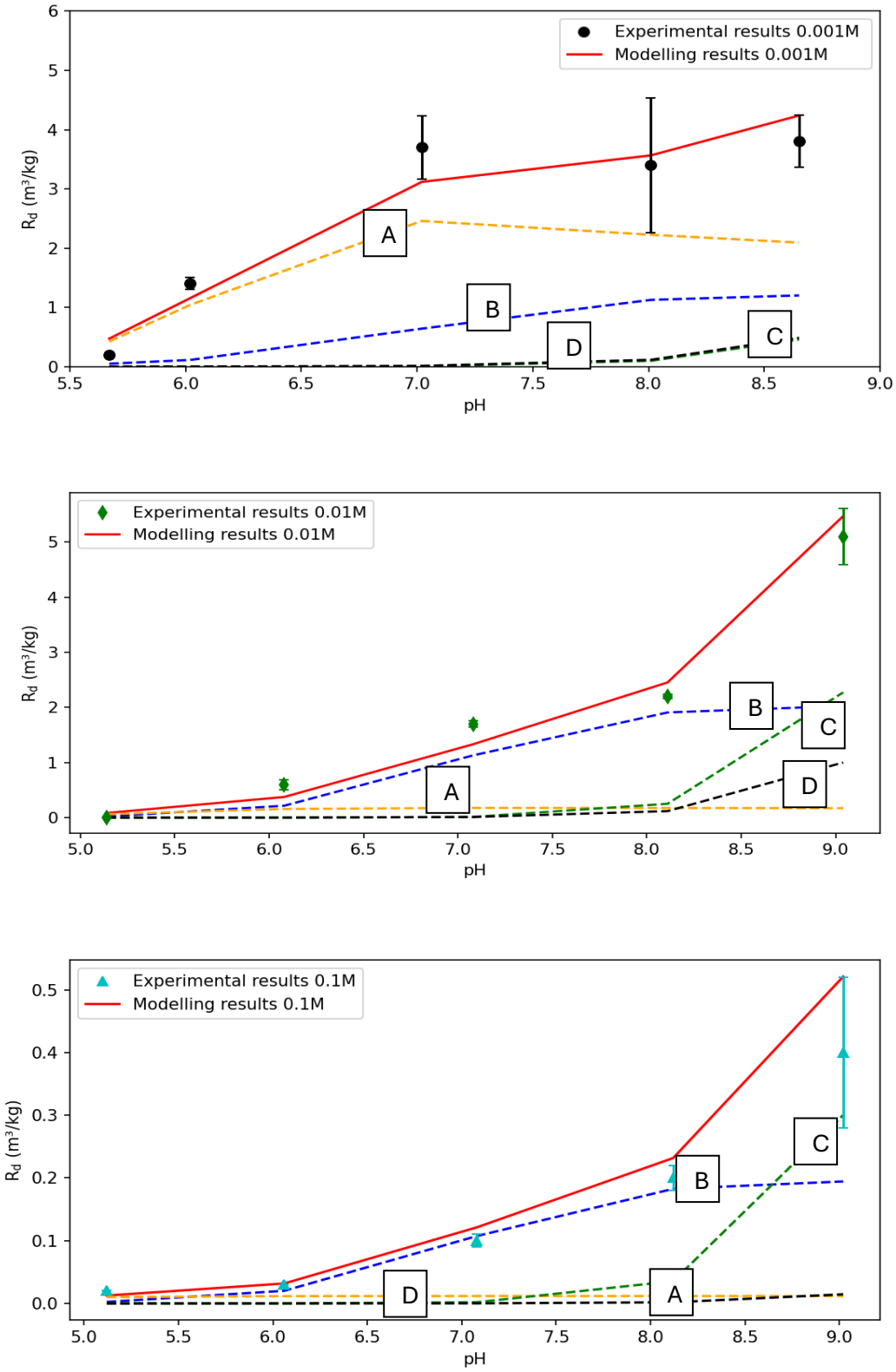

Figure 6: Ba sorption measurement (symbol) and modelling (continuous line) on biotite mineral in 0.001M, 0.01M and 0.1M $NaClO_4$ solution at 40 °C. The contribution of different Ba(II) species in its sorption is represented by different curves:(A: Yellow line) BaX_2; (B: Blue line) $\equiv SOBa^+$; (C: Green line)) ≡SOBaOH; (D: Black line) XBaOH.

2.3 Cobalt

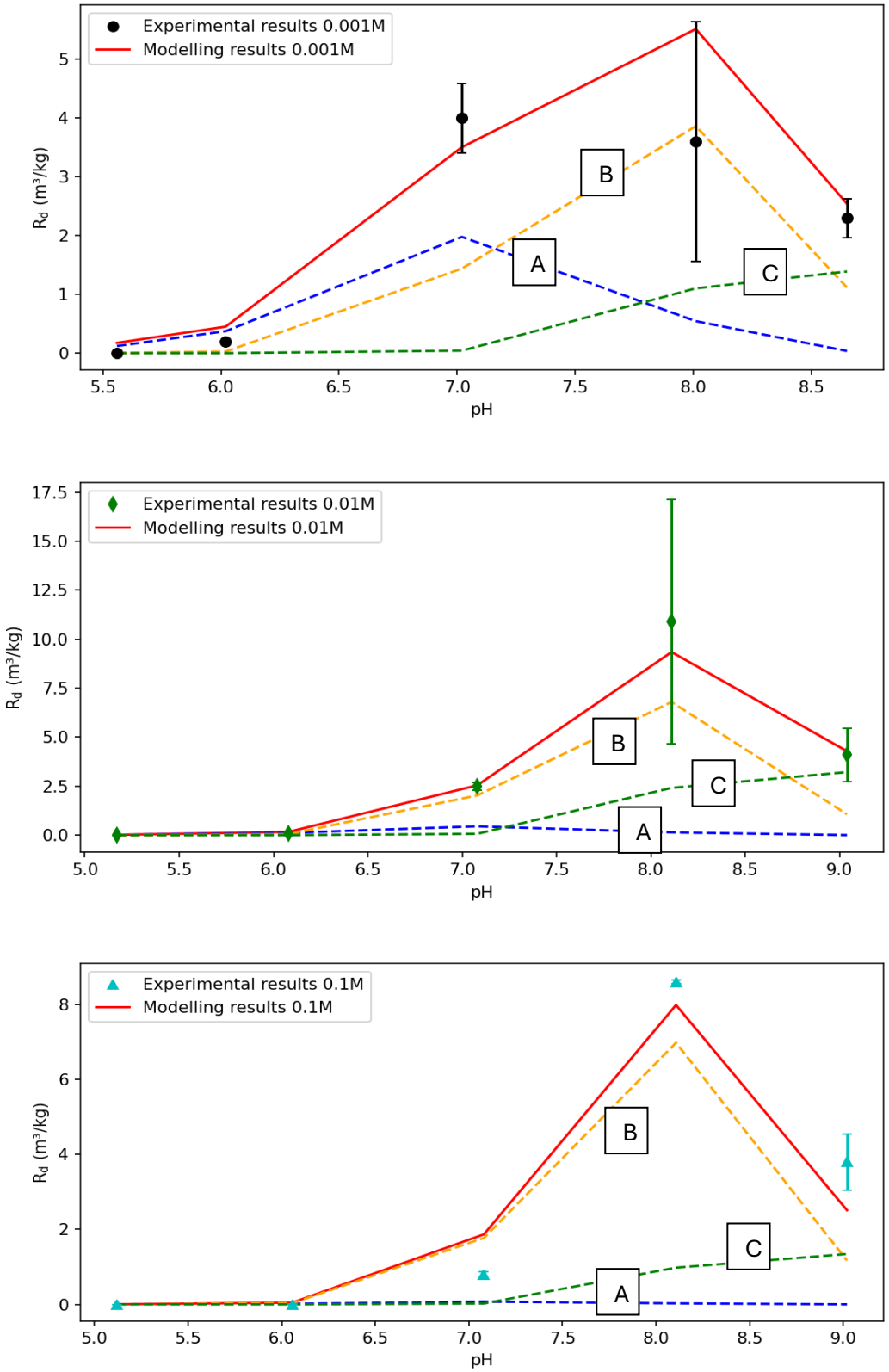

Figure 7: Co sorption measurement (symbol) and modelling (continuous line) on biotite mineral in 0.001M, 0.01M and 0.1M $NaClO_4$ solution at 40 °C. The contribution of different Co(II) species in its sorption is represented by different curves: (A: Blue line)≡$SOCo^+$; (B: Yellow line)≡SOCoOH; (C: Green line) ≡ $SOCo(OH)_2^-$.

2.4 Europium

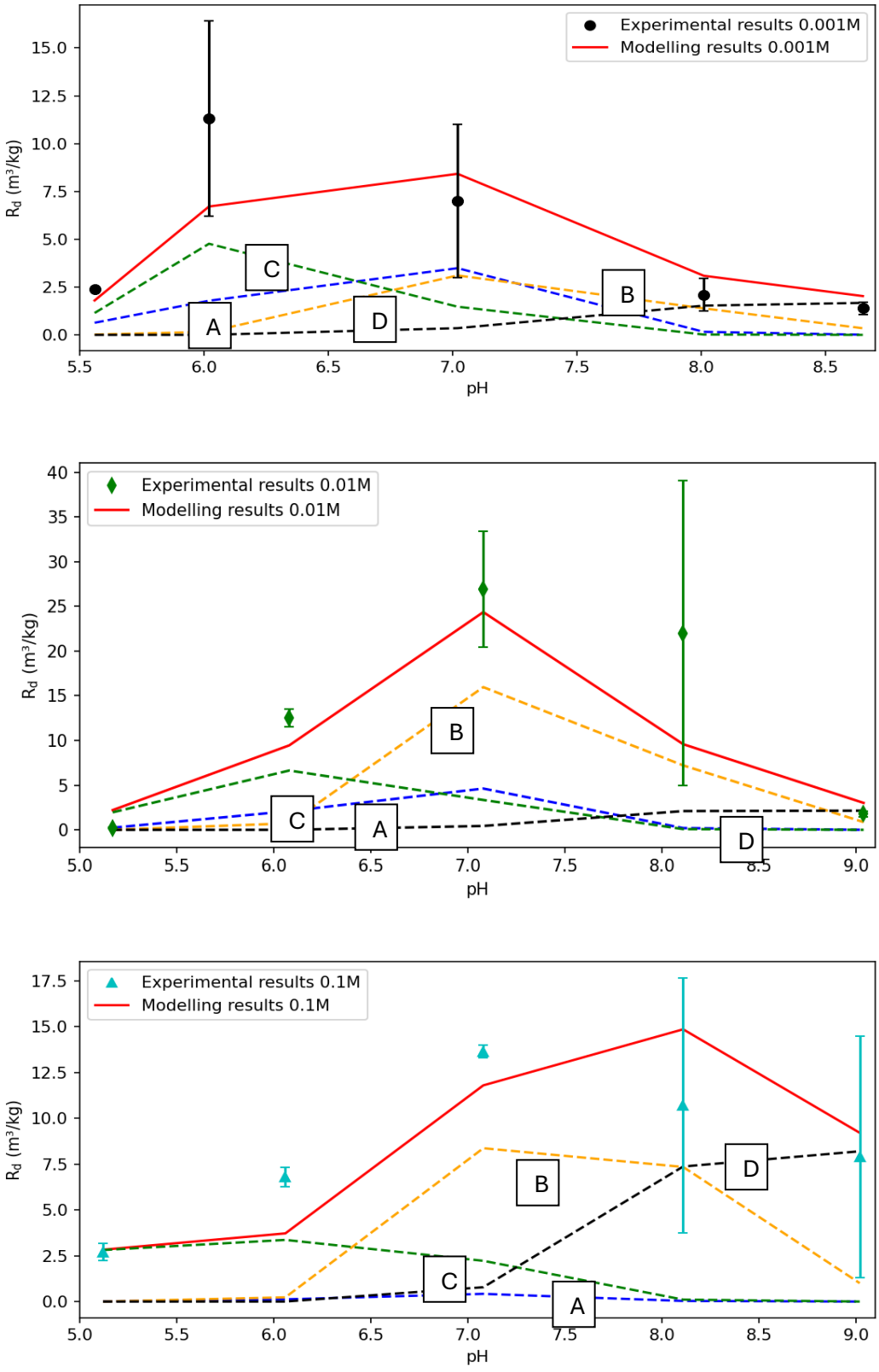

Figure 8: Eu sorption measurement (symbol) and modelling (continuous line) on biotite mineral in 0.001M,0.01M, and 0.1M NaClO4 solution at 40 ºC. The contribution of different Eu(III) species in its sorption is represented by different curves: (A: blue line)≡ $SOEu^{2+}$; (B: yellow line) ≡ $SOEu(OH)^{+}$; (C: green line) EuX_3; (D: black line) ≡ $SOEu(OH)_2$

3. Batch sorption experimental and modelling results for Cs, Ba, Co, and Eu for 0.001M, 0.01M and 0.1M, five pH values (5 to 9) and at 60°C

3.1 Cesium

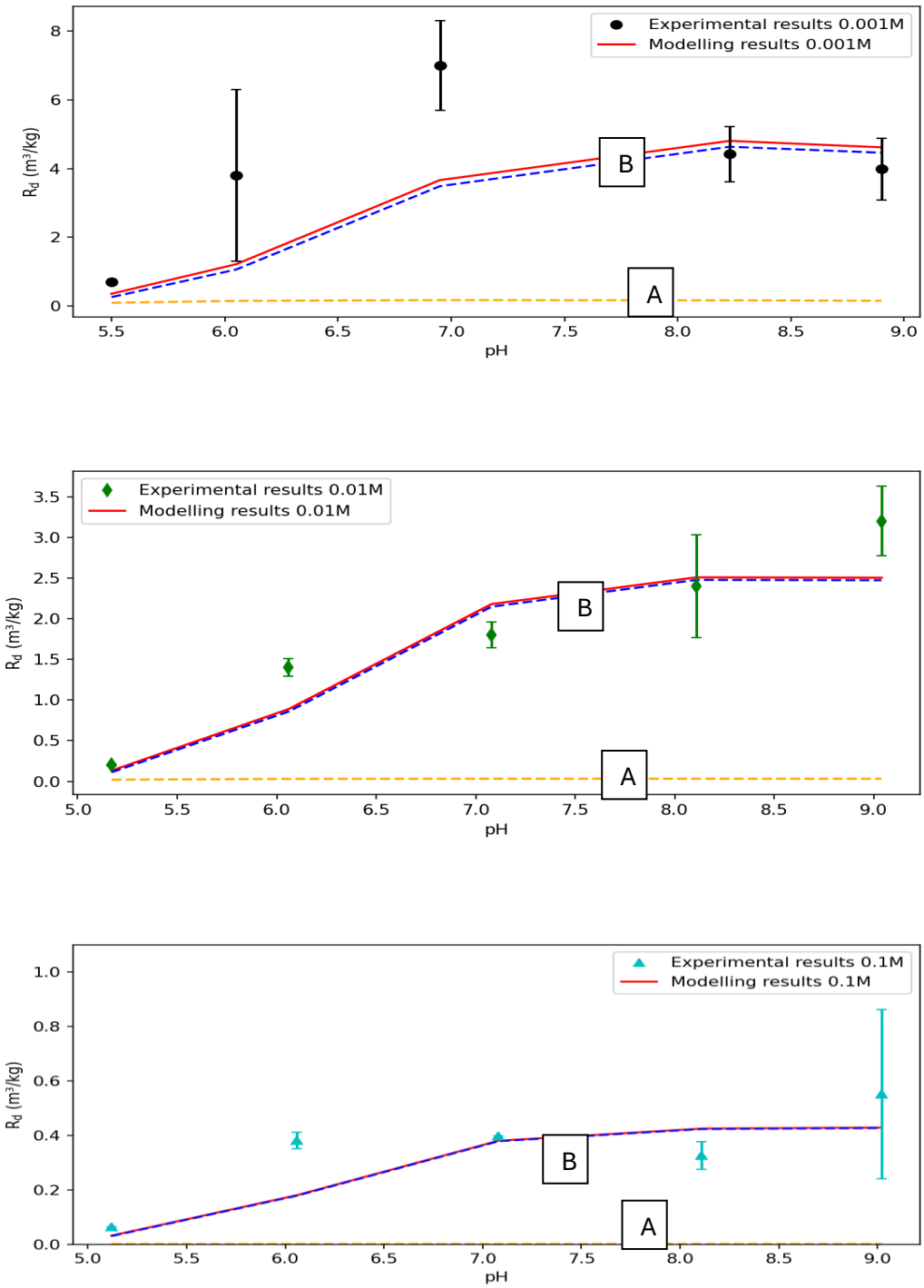

Figure 9: Cs sorption measurement (symbol) and modelling (continuous line) on biotite mineral in 0.001M,0.01M and 0.1M $NaClO_4$ solution at 60 ºC. The contribution of different Cs(I) species in its sorption is represented by different curves: (A) CsX; (B) ≡SOCs

3.2 Barium

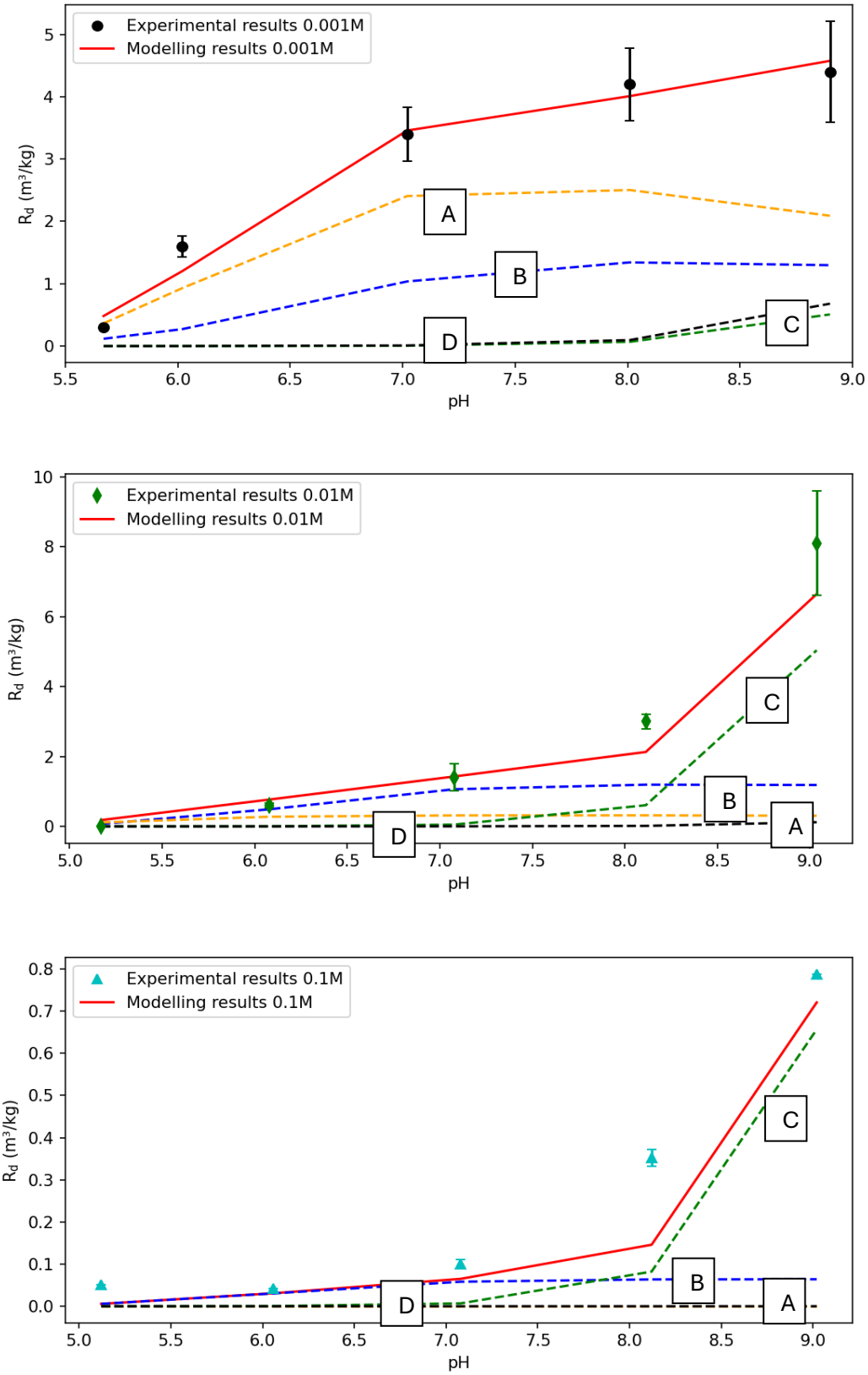

Figure 10: Ba sorption measurement (symbol) and modelling (continuous line) on biotite mineral in 0.001M, 0.01M and 0.1M $NaClO_4$ solution at 60 °C. The contribution of different Ba(II) species in its sorption is represented by different curves:(A: Yellow line) BaX_2; (B: Blue line) $\equiv SOBa^+$; (C: Green line)) ≡SOBaOH; (D: Black line) XBaOH.

3.3 Cobalt

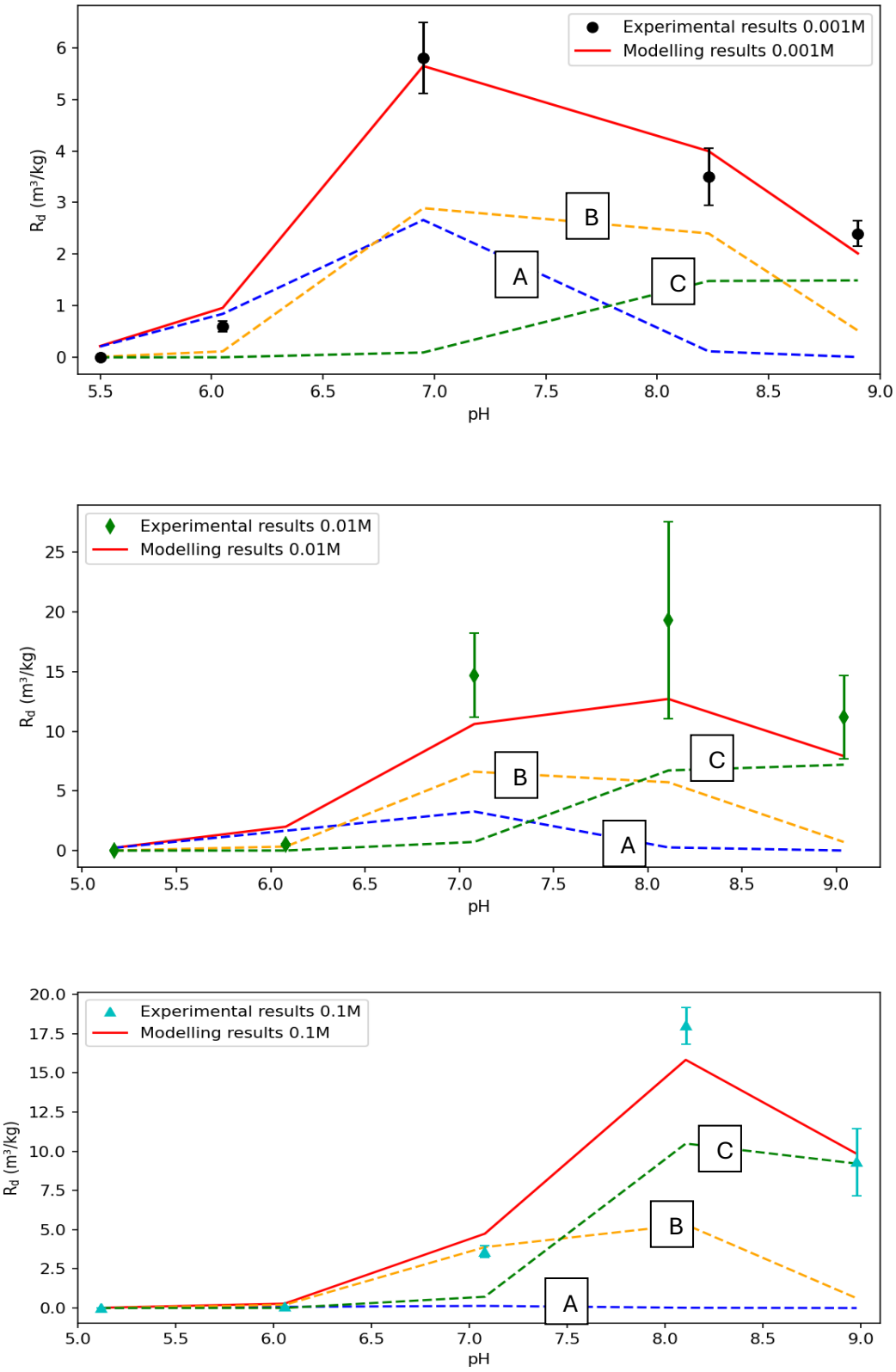

Figure 11: Co sorption measurement (symbol) and modelling (continuous line) on biotite mineral in 0.001M, 0.01M and 0.1M $NaClO_4$ solution at 60 °C. The contribution of different Co(II) species in its sorption is represented by different curves: (A: Blue line)≡$SOCo^+$; (B: Yellow line)≡SOCoOH; (C: Green line) ≡ $SOCo(OH)_2^-$.

3.4 Europium

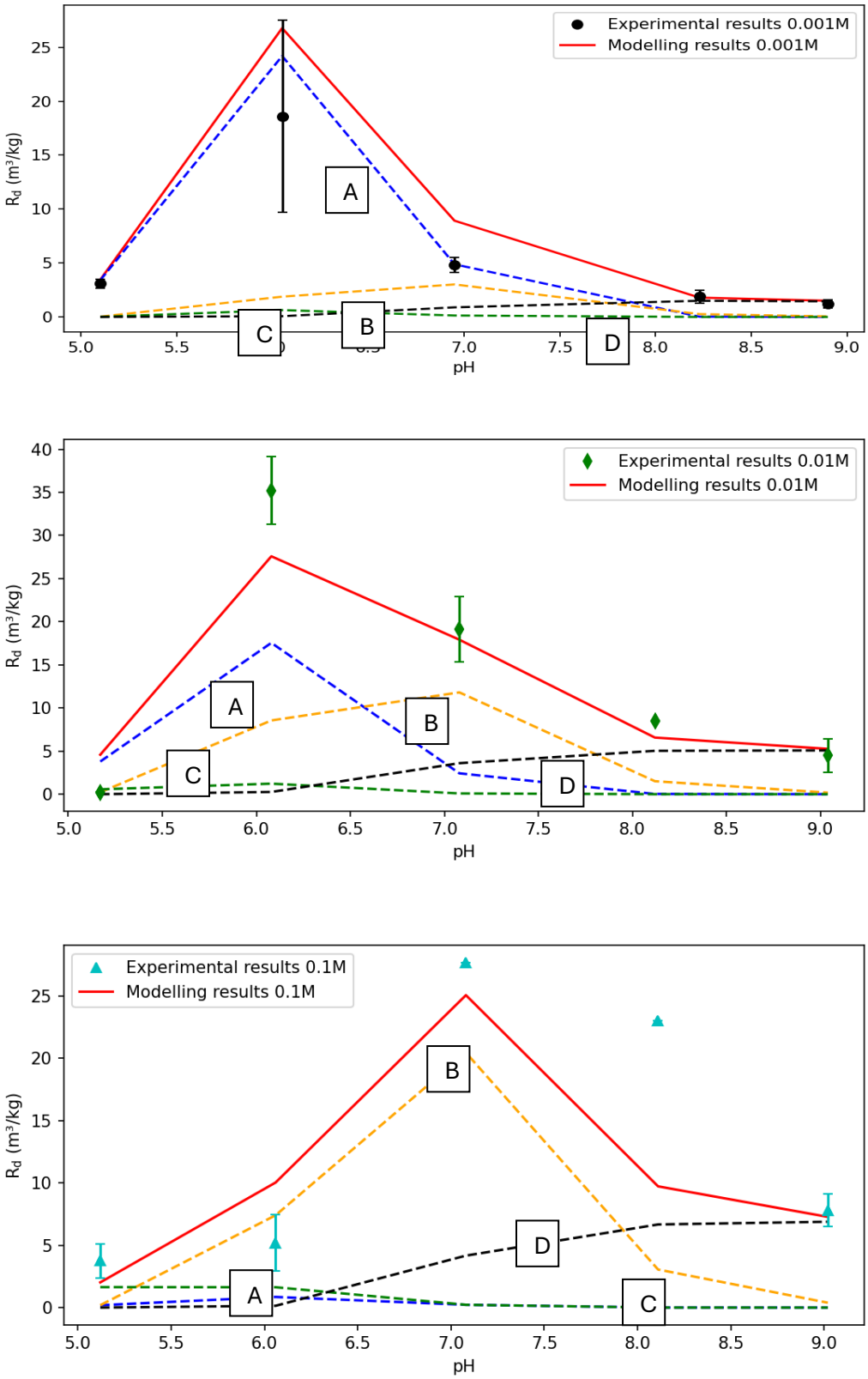

Figure 12: Eu sorption measurement (symbol) and modelling (continuous line) on biotite mineral in 0.001M,0.01M, and 0.1M NaClO4 solution at 60 ºC. The contribution of different Eu(III) species in its sorption is represented by different curves: (A: blue line)≡ $SOEu^{2+}$; (B: yellow line) ≡ $SOEu(OH)^{+}$; (C: green line) EuX_3; (D: black line) ≡ $SOEu(OH)_2$

3.5 Radium

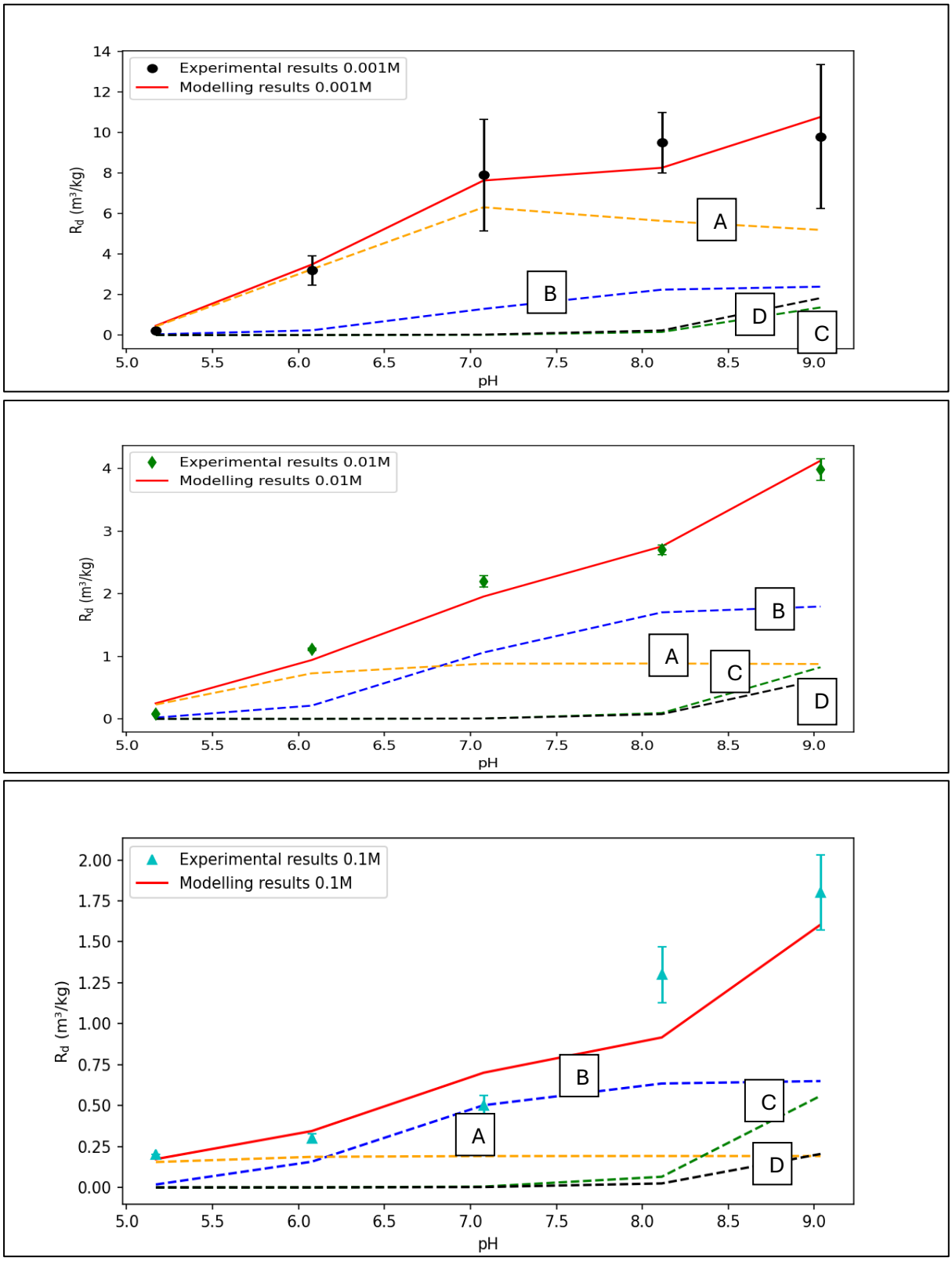

Figure 13. Experimental (symbol) and modelling (continuous line) results for Ra sorption onto biotite in 0.001 M, 0.01 M and 0.1 M $NaClO_4$ solution at 25 °C. The contribution of different Ra(II) species in its sorption is represented by different curves:(A: Yellow line) RaX_2; (B: Blue line) $\equiv SORa^+$; (C: Green line)) ≡SORaOH; (D: Black line) XRaOH

3.6 Americium

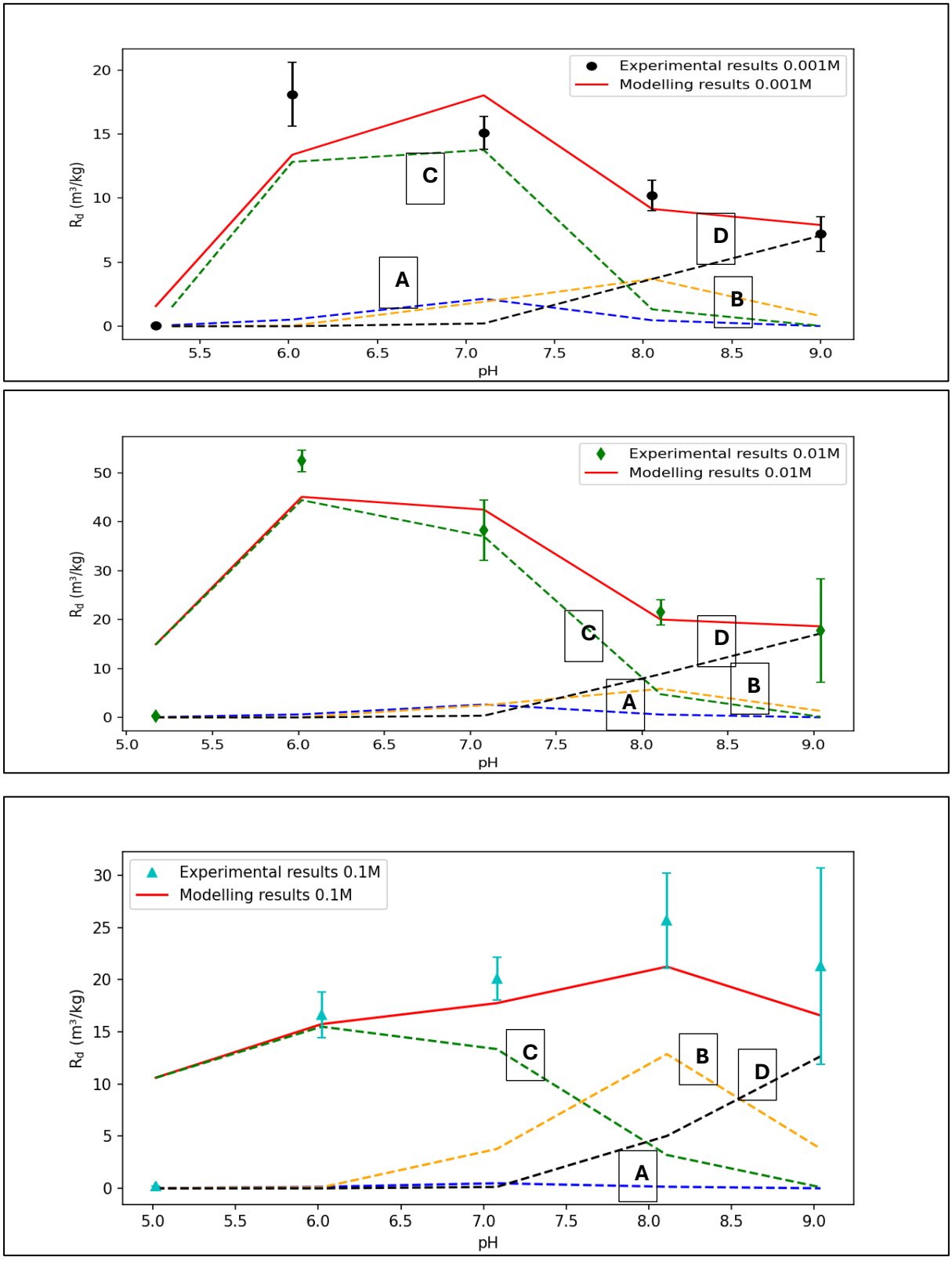

Figure 14. Am sorption experimental (symbol) and modelling (continuous line) results on biotite in 0.001 M, 0.01 M and 0.1 M $NaClO_4$ NaClO solution at 25 °C . The contribution of different Am(III) species in its sorption is represented by different curves: (A: blue line)≡ $SOAm,^{2+}$; *(B: yellow line)* ≡ $SOAm(OH)^{+}$; *(C: green line)* AmX_3;

4. Temperature dependent experimental and modelling results for all three ionic strengths (0.001M,0.01M, and 0.1M), five pH values (5 to 9) and at 25, 40, and 60 ºC

4.1 Cesium

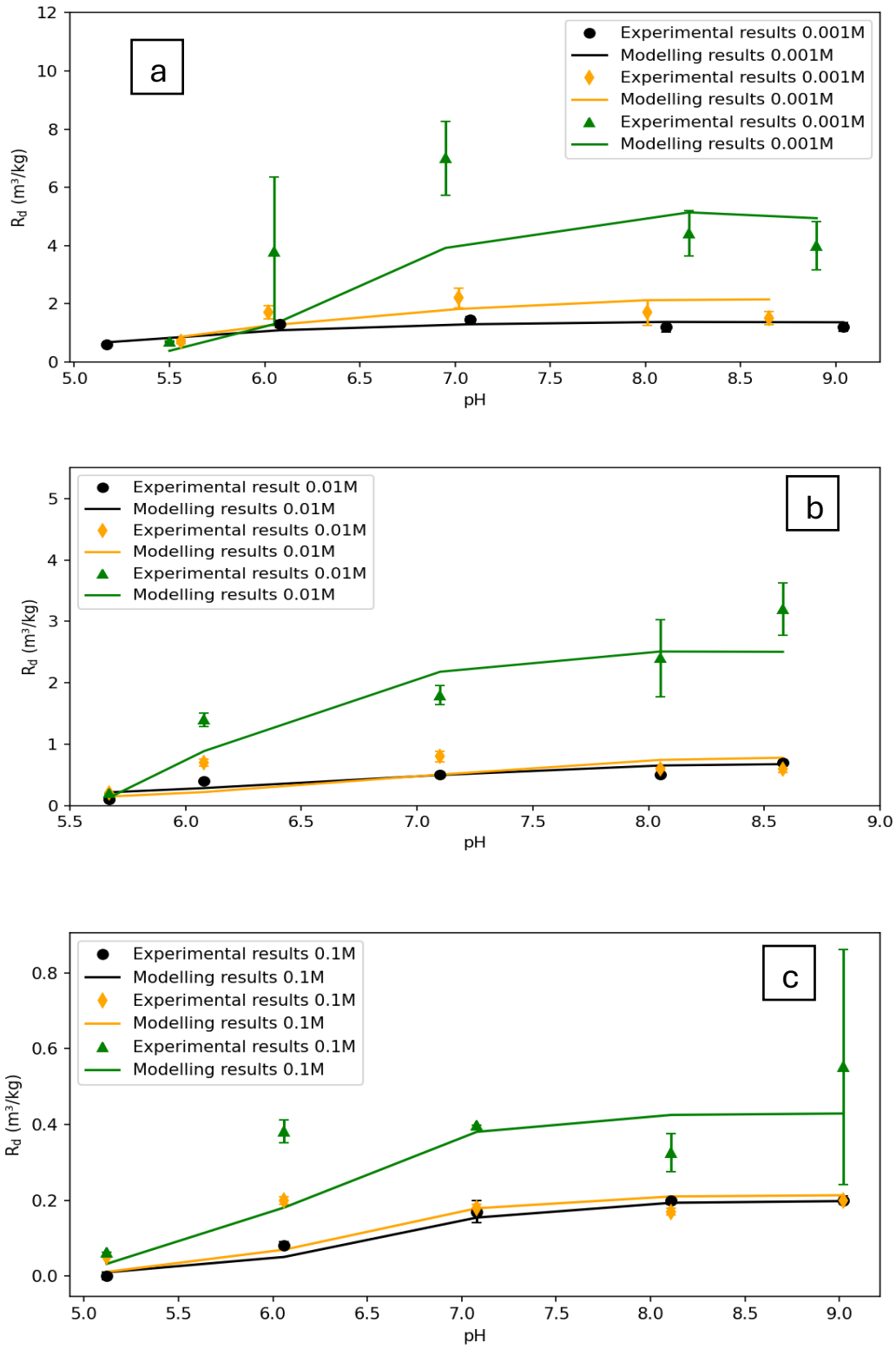

Figure 13: Cs sorption measurement (symbol) and modelling (continuous line) on biotite at 25 (Blank line), 40 (Yellow line), and 60 °C (Green line) in a) 0.001M, b) 0.01M and c) 0.1M $NaClO_4$ solution as a function of pH.

4.2 Barium

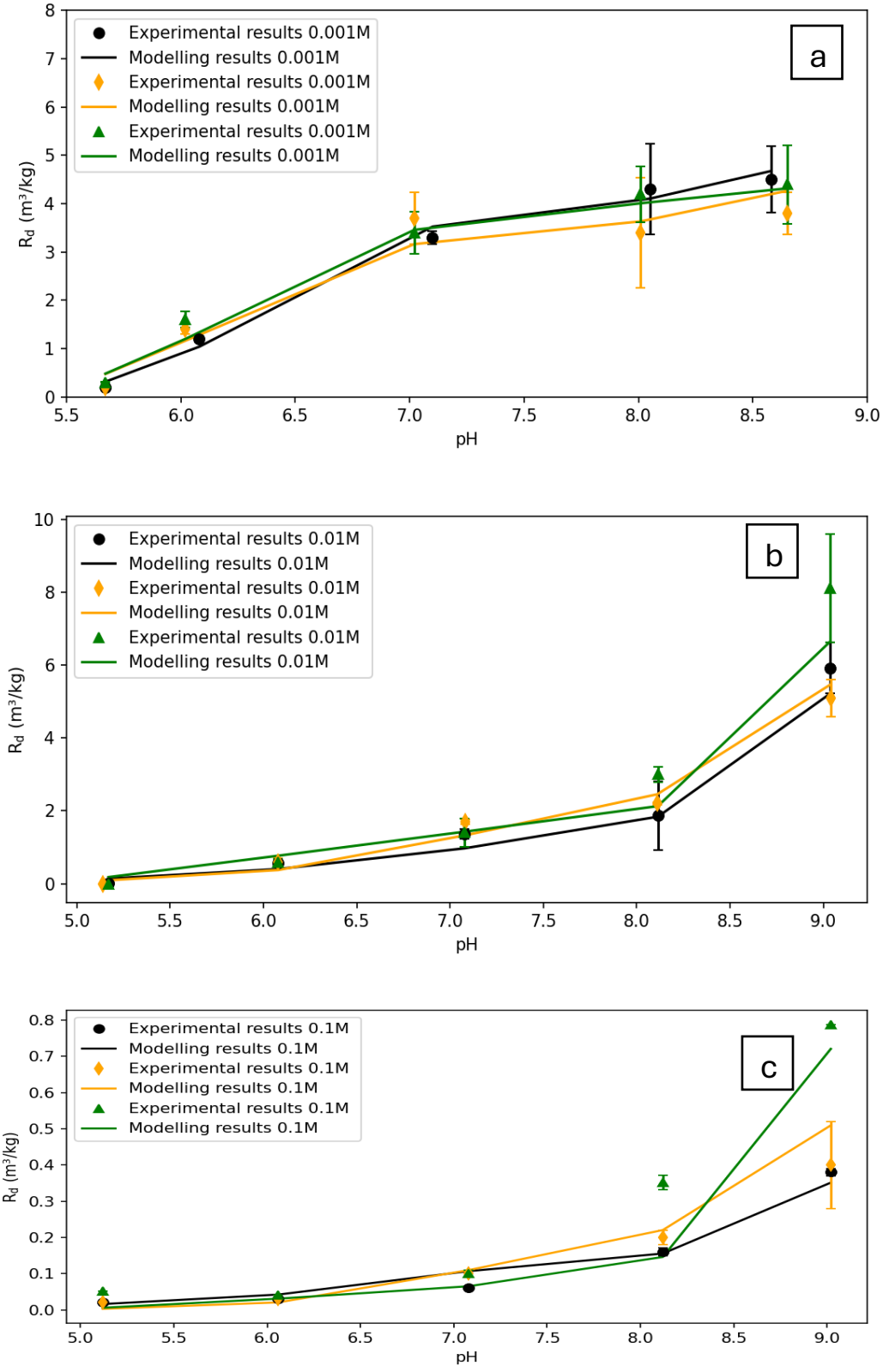

Figure 14: Ba sorption measurement (symbol) and modelling (continuous line) on biotite at 25 (Blank line), 40 (Yellow line), and 60 °C (Green line) in a) 0.001M, b) 0.01M and c) 0.1M $NaClO_4$ solution as a function of pH.

4.3 Cobalt

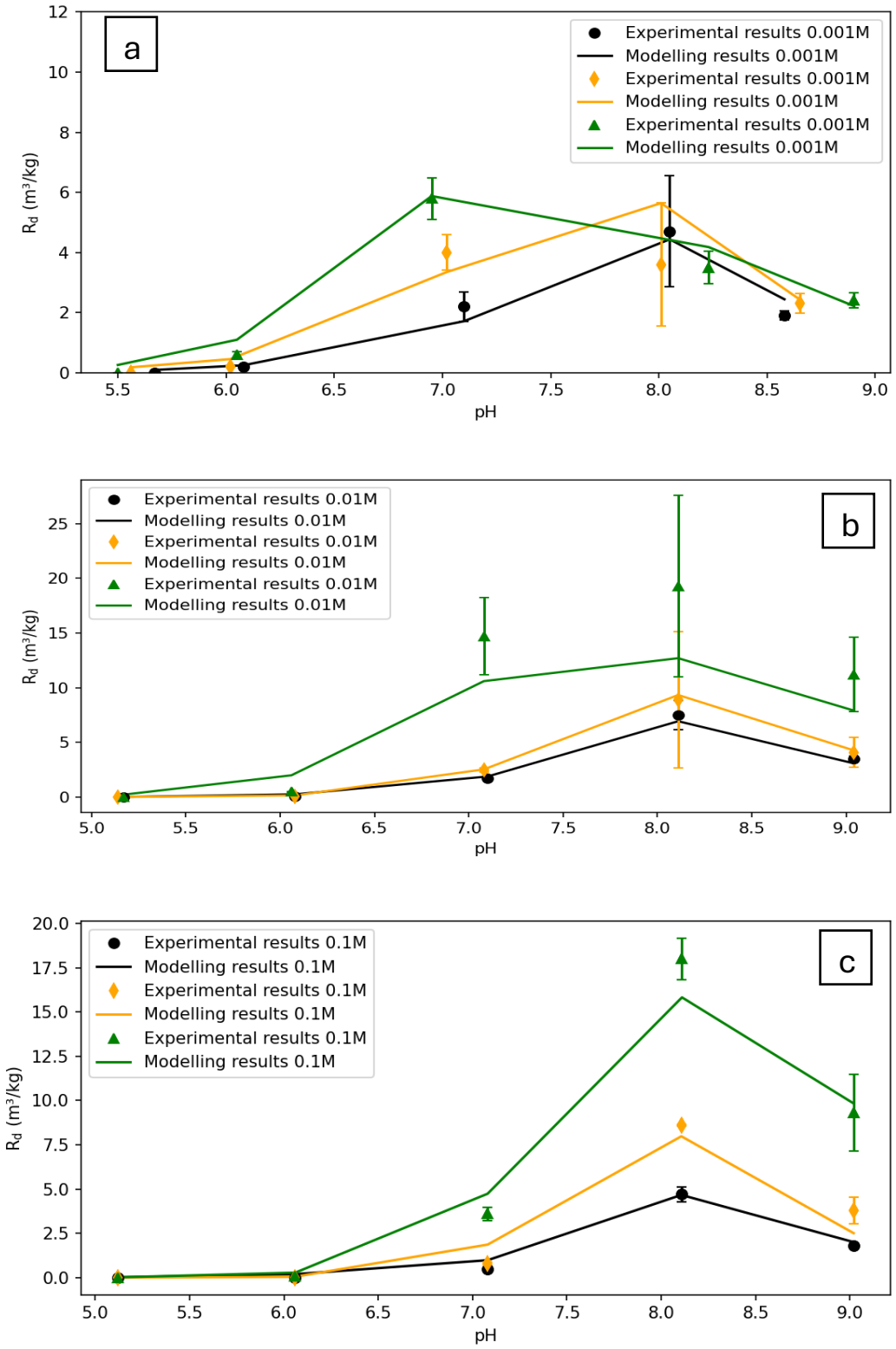

Figure 15: Cs sorption measurement (symbol) and modelling (continuous line) on biotite at 25 (Blank line), 40 (Yellow line), and 60 °C (Green line) in a) 0.001M, b) 0.01M and c) 0.1M $NaClO_4$ solution as a function of pH.

4.4 Europium

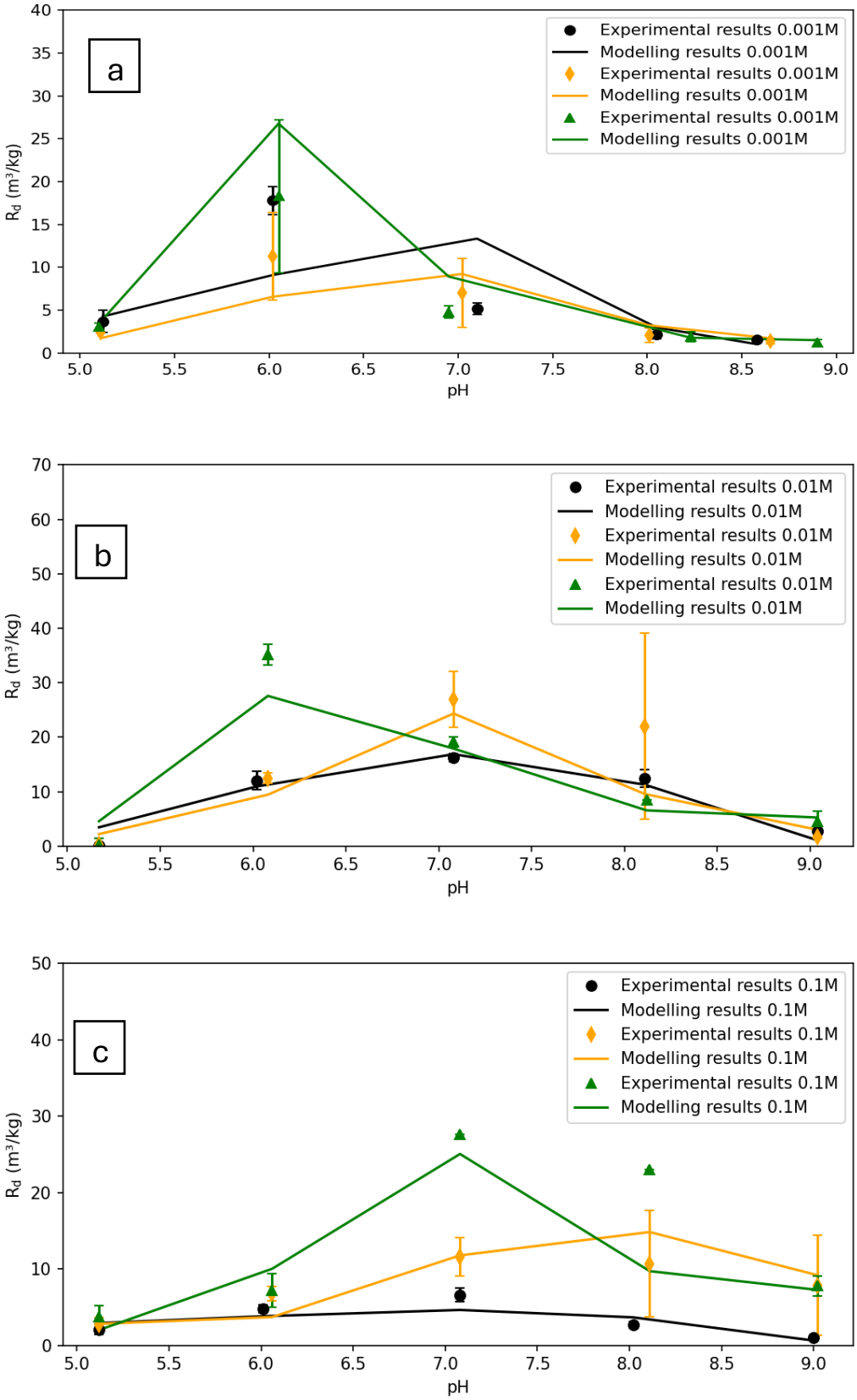

Figure 16: Cs sorption measurement (symbol) and modelling (continuous line) on biotite at 25 (Blank line), 40 (Yellow line), and 60 °C (Green line) in a) 0.001M, b) 0.01M and c) 0.1M $NaClO_4$ solution as a function of pH